

Politecnico di Torino

Department of Mechanical and Aerospace Engineering

Master's Degree in Automotive Engineering

Gullwing Door Post-Rollover Safety: Concept, Design and Numerical Validation of an Electromagnetic Hold-Down and Release Mechanism

Candidate
Agnese Besseghini

Supervisor
Prof. Andrea Tonoli

Company Tutor
Ing. Enrico Derivi

Academic Year 2025/2026

In collaboration with Pininfarina S.p.A.



Abstract

Gullwing doors, adopted on several high-performance vehicles, present a critical safety issue specifically in the case of rollover: roof frame deformation can misalign the hinge axis and generate friction locking forces that make the opening of the door impossible for a conventional electromechanical actuator. The only solution nowadays able to allow release under these conditions is the pyrotechnic hinge adopted, for example, on the Mercedes-Benz SLS AMG, which is untestable at the end-of-line, single-use and subject to stringent regulations on hazardous materials.

From a Systems Engineering analysis of gullwing doors in general, including functional analysis, feasibility checklist, target book and benchmarking of already existing gullwing solutions, it emerged that rollover management is today one of the biggest obstacles to the adoption of this kinematics among OEMs. The thesis focuses on the deepening of this critical aspect, with the main objective of developing an emergency release mechanism that is technologically and industrially more advantageous than the solutions available nowadays. The resulting HDRM-TCA concept separates the daily door kinematics (X-axis) from the emergency release (Z-axis), which is driven by an electromagnetic Thomson Coil Actuator (TCA) acting on a Cup-and-Cone interface secured by a shear ring. TCA and HDRM technologies, borrowed respectively from high-voltage engineering and aerospace release mechanisms, are here combined in an unprecedented automotive safety application. The electrical, electromagnetic and mechanical sizing is validated through an electromechanical Simscape 1D model, together with a sensitivity analysis of the main design parameters. A safety logic has also been designed (ASIL-D rollover detection via Sensor Fusion, cold-wiring architecture, and maintenance safety), inspired by the principles of ISO 26262 and UNECE R100.

Results show that the proposed system can replicate the force and timing performance of pyrotechnic devices, while remaining completely reversible, testable, and free of explosive charges, at the cost of adopting a high-voltage on-board network. The thesis concludes with a discussion of the model's limitations and the definition of the necessary future developments.

Questa tesi nasce da un piccolo capriccio progettuale: il desiderio di vedere più automobili con porte ad ala di gabbiano, così eleganti, leggere e sinuose, quasi ispirate alla natura e capaci di trasmettere un autentico senso di libertà.

Desidero ringraziare l'Ingegner Enrico Derivi per avermi proposto di lavorare a questo sistema e per avermi guidata durante questa esperienza, aiutandomi a trasformare un'idea in un progetto concreto.

Ringrazio il Professor Andrea Tonoli per la fiducia e la disponibilità che mi ha dimostrato, oltre che per la passione e la competenza con cui ha saputo coinvolgermi nei suoi corsi universitari.

Un sincero ringraziamento va a Pininfarina, per avermi offerto l'opportunità di lavorare in un ambiente nel quale forma, funzione e innovazione devono trovare ogni giorno un equilibrio reale. Ringrazio inoltre i miei colleghi, che mi hanno incoraggiata quotidianamente e il cui contributo è stato fondamentale durante la stesura e la preparazione di questa tesi.

Alla mia famiglia, per avermi lasciata libera di scegliere la mia strada e per avermi sostenuta in ogni modo, con la forza, la fiducia e i sacrifici concreti che mi hanno permesso di arrivare fin qui e di realizzare i miei obiettivi.

A Stefano, che mi supporta e mi sopporta costantemente — e devo ammettere che non è sempre stato facile! — grazie per essere rimasto al mio fianco e per aver creduto in me durante ogni momento di questo percorso.

Ai miei amici, ai colleghi dell'università e alle mie coinquiline — perché sì, di case ne ho cambiate tante — per aver condiviso con me questi anni, alleggerendo i momenti difficili e rendendo ancora più preziosi e indimenticabili quelli belli.

Infine, dedico questo traguardo alla persona che sono diventata. Non è stato un percorso semplice e la strada non è sempre stata in discesa; ora che ho raggiunto la vetta, però, posso dire che il panorama è mozzafiato. Sono fiera di me, della determinazione che ho dimostrato e della crescita che questo cammino mi ha regalato.

Questa tesi racchiude molti capitoli, ma quello più bello non è ancora stato scritto. Lo scriverò poco alla volta, vivendo pienamente la vita che mi aspetta.

"Above all, it must be beautiful."
— Battista "Pinin" Farina

Table of Contents

Abstract 5

List of Figures 12

List of Tables 14

1 Introduction 15
- 1.1 Historical and Market Context . . . 15
- 1.2 Objective of the Thesis . . . 17
- 1.3 Structure of the Thesis . . . 18

2 Systems Engineering Methodology 19
- 2.1 Introduction to the Methodological Approach . . . 19
- 2.2 Functional Analysis and Correlation Matrix . . . 20
  - 2.2.1 Identification of the Critical Architectural Node . . . 22
- 2.3 From Functions to Requirements: Target Book and Feasibility Checklist 23
- 2.4 Competitive Benchmark: Trade-offs in the State of the Art . . . 24
- 2.5 Case Study: the Pininfarina HK GT . . . 26
  - 2.5.1 Structural Integrity and Load Paths . . . 26
  - 2.5.2 Cantilever Mass and Hinge Stress . . . 27
  - 2.5.3 Thermodynamic and Actuation Limits . . . 27
  - 2.5.4 Kinematic Sweep and Packaging . . . 27
- 2.6 Identification of the Technological "Bottleneck": the Rollover Problem . . . 28

3 Rollover Problem and Limits of Existing Solutions 29
- 3.1 Binding in Rollover Conditions . . . 29
- 3.2 Cylindrical Hinge Structural Limits . . . 30
- 3.3 Industrial Reference: Pyrotechnic Hinge Release in the Mercedes-Benz SLS AMG . . . 31
- 3.4 State of the Art: Technologies from Other Domains . . . 33

3.4.1 Aerospace Hold-Down and Release Mechanisms 33
3.4.2 Thomson Coil Actuators in HVDC Systems 34
3.5 Synthesis: The Technological Gap 35

4 Proposed Architecture: HDRM-TCA System 37
4.1 General Concept and Advantages Over Pyrotechnic Systems 37
4.2 Complete Mechanical Layout 41
4.2.1 Base Plate and Dual-Axis Interface 42
4.2.2 Cup-and-Cone Interface 45
4.2.3 Shear Ring and TCA Cartridge 47
4.2.4 Ejection Spring and Ball Joints 49
4.3 Operating Sequence 51
4.4 Chapter Summary 52

5 Electric and Electromagnetic Design 53
5.1 Functioning Principle: Lorentz and Eddy-Current Forces 53
5.1.1 Lumped Parameter Model 54
5.2 Energy Balance and Capacitor Bank Design 54
5.3 DC-DC Boost Converter 56
5.4 Choice of the Switching Device: SCR vs IGBT 56
5.5 Coil Design 57
5.6 HV Routing and Shielding 58
5.7 Cold Wiring 60
5.8 Chapter Summary 61

6 Numerical Modelling and Robustness Assessment 63
6.1 Modelling Approach and Simulation Domains 63
6.2 Electric and Electromagnetic Transient 66
6.2.1 Analytical Cross-Check of the RLC Transient 66
6.2.2 Electromagnetic Force Transient 67
6.3 Pin Release Kinematics 68
6.4 Sensitivity Analysis under Degraded Rollover Conditions 69
6.5 End-of-Life Robustness Analysis 71
6.6 Low-Frequency Dynamics: Door Ejection 74
6.7 Chapter Summary 75

7 Functional Safety and Failure Analysis 77
7.1 Functional Safety Framing 77
7.2 Rollover Detection: Sensor Fusion Logic 78
7.3 Failure Mode and Effects Analysis of the HDRM-TCA System . . . 79
7.4 Electrical Risk Mitigation: Cold Wiring and Active Bleeding 82

7.5 Maintenance Safety and Manual Override 83
7.6 Chapter Summary 84

8 Discussion 85
8.1 Achievement of the Design Targets 85
8.2 Robustness under Degraded Rollover Conditions 86
8.3 Trade-offs with Respect to the Pyrotechnic Benchmark 86
8.4 Limitations of the Present Model 87
8.5 Generalization Beyond the Gullwing Case 88
8.6 Chapter Summary 88

9 Conclusions and Future Work 89
9.1 Conclusions Summary 89
9.2 Future Work 90

A Target Book 91

B Feasibility Checklist 97

Bibliography 103

List of Figures

1.1 Timeline of the main production vehicles that adopted gullwing doors. 16

2.1 Qualitative architectural benchmarking of representative upward-opening door systems across five engineering criteria. The scores are engineering assessments intended for architectural comparison and are not experimentally measured performance indices. 25

2.2 The Pininfarina HK GT concept, showing the full-length, B-pillar-free gullwing door. 26

3.1 Pyrotechnic gullwing-door hinge release mechanism of the Mercedes-Benz SLS AMG, showing the door hinge (1), pyrotechnic initiator (2) and hinge arm (3). Source: Mercedes-Benz rescue documentation [4]. 32

3.2 Autoliv pyrotechnic Pin-Pusher used as the actuator-level performance benchmark in this work. Source: Autoliv [5]. 32

3.3 Examples of aerospace Hold-Down and Release Mechanisms: (a) non-pyrotechnic REACT devices; (b) SSTL heritage HDRM showing the cup-cone retention architecture adopted as a mechanical reference in this work. Sources: ARQUIMEA [23] and Malavart et al. [24]. . 34

3.4 Operating principle of the Thomson Coil Actuator: a current pulse in the fixed pancake coil induces opposing eddy currents in the conductive disk, generating a repulsive electromagnetic force. Adapted from [25]. 35

4.1 Three-dimensional overview of the proposed HDRM-TCA hinge assembly. The upper view highlights the separation between the normal door-rotation axis (X-axis) and the emergency release direction (Z-axis), while the lower sectioned view identifies the main mechanical and electromagnetic components of the system. 40

4.2 Section view of the preliminary HDRM-TCA hinge assembly. Detail E highlights the main components involved in the emergency-release mechanism and their relative packaging. The indicated 15 mm stroke represents the required pin-release displacement. 42
4.3 Preliminary base-plate geometry and functional separation of the two main interfaces. The gooseneck hinge defines the normal door-rotation axis, while the cup-and-cone release interface acts along the vertical pin-release axis. 43
4.4 Preliminary geometry and assembled configuration of the cup-and-cone release interface. The 40° included cone angle corresponds to the adopted half-angle $\alpha = 20°$. 45
4.5 Preliminary dimensions of the sacrificial shear ring and Thomson-coil winding-pack envelope. The shear ring has an outer diameter of 16 mm, an inner diameter of 8.1 mm and a thickness of 2 mm. The preliminary winding-pack envelope has an outer diameter of 35 mm, an inner diameter of 10 mm and an axial thickness of 8 mm. 48

6.1 Simscape 1D model architecture, including the electrical discharge circuit, electromagnetic coupling block and mechanical release chain. 65
6.2 Coil current during the nominal discharge transient ($R = 0.03\,\Omega$, $L = 0.2\,\mathrm{mH}$, $C = 4.7\,\mathrm{mF}$ and $V_0 = 400\,\mathrm{V}$). 66
6.3 Electromagnetic force predicted during the nominal TCA discharge. The modeled peak is approximately 4.3 kN at about 0.7 ms. 68
6.4 Predicted pin displacement under nominal conditions. The prescribed 15 mm release position is reached within approximately 1–2 ms. 69
6.5 Pin-displacement sensitivity to the imposed equivalent radial load. Complete release is obtained for the 1, 5, 9 and 14 kN cases, while the 17.5, 18.5 and 20 kN cases do not reach the prescribed 15 mm release position within the investigated time window. 70
6.6 Discharge-current response for the investigated degraded EoL condition ($C = 4.0\,\mathrm{mF}$, $V_0 = 360\,\mathrm{V}$ and $R = 0.06\,\Omega$). 72
6.7 Pin-stroke response for the investigated degraded EoL electrical condition. The pin reaches the required 15 mm release position in the numerical model. 73
6.8 Low-frequency door-ejection response for the initial 800 N spring configuration. The door transiently exceeds the 150 mm displacement target but subsequently returns below it under the assumed inverted-vehicle condition. 74

List of Tables

2.1 Summary of system-level functions and associated risks 20
2.2 Macro-Correlation Matrix: Functional Categories vs. Physical Subsystems 22
2.3 Physical components with the highest connectivity in the Correlation Matrix 23

4.1 Multi-criteria comparison: Pyrotechnic emergency-release reference vs proposed HDRM-TCA architecture 38
4.2 Non-self-locking sensitivity matrix ($\alpha = 20°$) 46
4.3 Nominal operating sequence of the emergency-release mechanism . . 51

7.1 Failure mode and effects analysis of the HDRM-TCA emergency-release system. 79

Chapter 1

Introduction

For a long time, gullwing doors have been seen mainly as a style choice. The DeLorean DMC-12, known as the “time machine” of the *Back to the Future* trilogy, is one of the most recognizable examples of this door type in popular culture. However, while the gullwing-door architecture predates its most famous screen appearance, its fundamental engineering purposes have evolved considerably over the years.

1.1 Historical and Market Context

One of the earliest and most influential production examples of the modern gullwing door is the Mercedes-Benz 300-SL "Gullwing" of 1954, adopted primarily because of a structural constraint. The car’s tubular space-frame chassis occupied the height that a conventional door sill would normally use. Consequently, a top-hinged door was the most practical way to allow cabin access without compromising the load-bearing structure [1].

Seven decades later, the same top-hinged principle has been adopted for a different reason. Figure 1.1 presents the major production milestones of this door architecture on a timeline, from the 300-SL to the DeLorean DMC-12, the Mercedes-Benz SLS AMG, and the Tesla Model X. It highlights the shift in engineering motivations over time: from structural necessity and styling statement, to a packaging response driven by the specific constraints of modern electric-vehicle platforms.

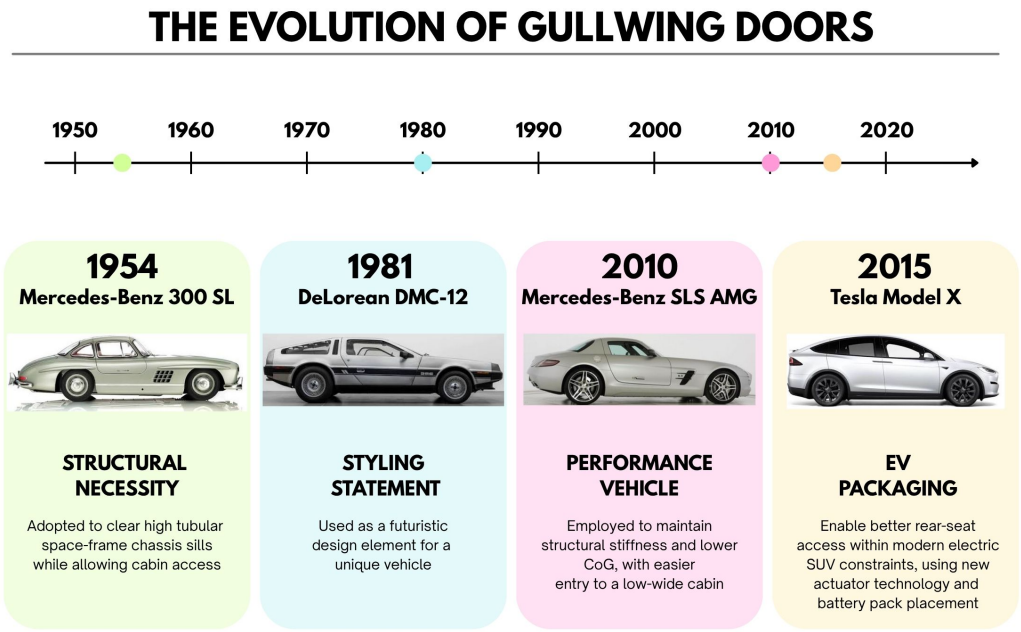


Figure 1.1: Timeline of the main production vehicles that adopted gullwing doors.

In the last two decades, this door architecture has also been used in modern supercars and high-end SUVs.

This renewed interest can be related to three main factors. First, the configuration of battery electric vehicle (BEV) platforms can raise the cabin floor and modify the relationship between sill height, seating position and door opening geometry. In some vehicle layouts, this can make an upward-opening solution attractive compared with a conventional outward-swinging door [2]. Second, opening upward requires less lateral clearance, which is useful in narrow parking spaces and facilitates ingress and egress in low, wide cabins; an increasingly common layout in performance and electric vehicles. Third, from a commercial perspective, gullwing doors provide manufacturers with an immediately recognizable means of signaling exclusivity. This partly explains their continued use on prestige and limited-production models.

However, the benchmarking also identifies engineering trade-offs associated with this architecture, including the mass distribution and centre of gravity (CoG) implications, structural stiffness and the thermal reliability of the hinge and actuation system. Among the engineering challenges associated with gullwing-door architectures, post-rollover occupant egress remains a particularly critical issue because structural deformation may compromise the mobility of the hinge interface.

Rollover crashes are disproportionately dangerous compared to other collision types; in the United States, they accounted for 28% of passenger-vehicle occupant fatalities in 2023 [3].

As explained in Chapter 3, roof deformation during a rollover can mechanically lock the door hinges, a phenomenon known as *binding*.

Among the production gullwing-door systems reviewed in this study, the Mercedes-Benz SLS AMG is the only vehicle identified in the literature with a dedicated pyrotechnic hinge-release function for post-rollover access [4]. The solution provides a documented automotive reference, but it is inherently single-use and introduces additional requirements associated with pyrotechnic components.

No directly comparable reusable production solution was identified in the sources reviewed for this work. The Mercedes-Benz SLS AMG is therefore used as the vehicle-level reference, while Autoliv's Pin-Pusher product data provide the actuator-level performance benchmark used for the quantitative comparison [5].

1.2 Objective of the Thesis

The main objective of this thesis is to design, develop and evaluate through numerical modelling an alternative architecture for the emergency release of gullwing doors. The proposed solution aims to replace pyrotechnic hinge actuation with a non-pyrotechnic electromagnetic release architecture while targeting comparable force and response characteristics and avoiding the use of energetic pyrotechnic material.

In this work, the proposed solution is called the HDRM-TCA architecture. It combines two technologies for which no integrated automotive application was identified in the sources reviewed for this thesis: a geometric anti-binding interface, adapted from the Hold-Down and Release Mechanisms (HDRM) used in aerospace applications, and an impulsive electromagnetic actuator, based on the Thomson Coil Actuator (TCA) used in HVDC systems.

To support this objective, the complete door system was first mapped at the functional and physical levels. This analysis identified post-rollover egress as the primary system bottleneck, rather than treating it as an initial assumption. The Systems Engineering methodology adopted for this analysis is described in Chapter 2.

The scope of the work is limited to concept-level engineering and numerical feasibility. No claim of vehicle homologation, production qualification, or experimental validation is made. The purpose of the study is to establish a coherent architecture, provide preliminary subsystem sizing and develop a numerical basis for the subsequent detailed-design and prototyping phase.

1.3 Structure of the Thesis

Chapter 2 presents the Systems Engineering methodology adopted for the development of the gullwing-door architecture. The chapter introduces the functional analysis, correlation matrix, Target Book, Feasibility Checklist and competitive benchmarking. The objective is to identify the functions and interfaces with the highest degree of system-level dependency and to determine the primary technological bottleneck addressed by the thesis.

Chapter 3 examines this problem from a physical point of view. It explains the binding phenomenon and the structural limits of a cylindrical hinge. It also reviews the industrial limitations of the existing pyrotechnic solution and introduces two non-automotive technologies, the aerospace Hold-Down and Release Mechanisms (HDRM) and the Thomson Coil Actuator (TCA), from which the proposed architecture is derived.

Chapter 4 describes the proposed HDRM-TCA architecture in detail. This includes the general concept, a comparison with the pyrotechnic benchmark, the complete mechanical layout (base plate, cup-and-cone interface, shear ring, and ejection spring) and the operating sequence that brings together all mechanical subsystems.

Chapter 5 develops the electrical and electromagnetic design of the TCA module. It covers the discharge circuit, power electronics and high-voltage wiring necessary to generate the forces assumed in the previous chapter.

Chapter 6 presents the numerical modelling and robustness assessment of the complete system, combining the electrical transient with the mechanical release response. It also includes a sensitivity analysis of the degraded load cases used to assess the robustness of the architecture.

Chapter 7 extends the functional safety analysis from Chapter 2 to the new architecture. It updates the relevant FMEA entries and analyzes the new failure modes introduced by the HDRM-TCA system, together with the proposed diagnostic and mitigation measures.

Chapter 8 discusses the results, compares the performance of the proposed system with the pyrotechnic benchmark and critically evaluates both the limitations of the work and the extent to which the proposed approach can be generalized beyond this specific case study.

Finally, **Chapter 9** summarizes the main results of the thesis and outlines the future work needed to bring the architecture from a concept-level numerical model to a tested physical prototype.

Chapter 2

Systems Engineering Methodology

2.1 Introduction to the Methodological Approach

Developing a gullwing automotive architecture is an engineering challenge that extends well beyond the geometric and aesthetic characteristics of the vehicle. Moving the hinge from the conventional lateral door pillars to the roof structure transforms the door from a simple closure panel into a highly integrated structural and dynamic subsystem. The development process therefore requires a system-level methodology able to identify interactions between functions, components, requirements and failure modes before detailed component design is performed.

For this reason, a Systems Engineering approach was adopted from the beginning of the project. The methodology was structured as an iterative process, starting from a macro-level description of the system and its attributes and then moving to functional and risk analyses, quantitative targets, a feasibility checklist and a validation plan.

The analysis was performed at two complementary levels. At the functional level, the complete door architecture was decomposed into elementary functions covering the main phases of the vehicle life cycle (normal operation, assembly, durability, service and crash-related conditions). At the physical level, these functions were correlated with the components and subsystems required to perform them.

This approach made it possible to identify not only individual component risk, but also highly interconnected architectural nodes. Particular attention was given to the hinge, roof-interface and actuation subsystems, where structural loads, kinematic constraints and safety functions converge.

The objective of this chapter is not to provide a complete vehicle homologation analysis, but to establish a traceable engineering framework from which the specific technological problem addressed by this thesis can be identified and then translated into quantitative design requirements.

2.2 Functional Analysis and Correlation Matrix

The aim of this methodological approach is to complement conventional component-oriented risk analysis with an initial function-oriented assessment. This was considered particularly useful during the concept phase, when the physical architecture had not yet been fully defined.

The first step involved an in-depth analysis of elementary functions, identifying 111 functions necessary for the correct operation of the door. These functions, intended to cover the entire vehicle life cycle and its operating conditions, were grouped into 10 macro-categories. In order to synthesize the extensive analysis without burdening the main text, Table 2.1 presents a condensed view of these categories, highlighting the primary system objectives, the most critical failure modes, and the key preventive actions. For the sake of document readability, the complete unabridged list of the 111 elementary functions is maintained as a digital annex in the project's Systems Engineering database.

Table 2.1: Summary of system-level functions and associated risks

Macro-Category	Main System Objectives	Critical Failure Modes	Key Preventive Actions
1. Appearance	Ensure surface continuity, prevent panel deformation ("oil canning") and guarantee trim alignment.	Visual mismatches, aerodynamic steps, metallic noise under closure, panel flutter.	Torsional rigidity (CAE), thermal aging simulation, paint-bake resistance.
2. Assembly	Guarantee correct hinge/striker tolerances, ensure proper clipping and harness routing.	Hinge/striker misalignment, excessive preload, hidden fixings, wire pinching.	Tolerance stack-up, DMU/Virtual build checks, operational effort limits.
3. Comfort	Guarantee NVH static/dynamic comfort and airtight sealing against water/wind.	Rattles/squeaks, harmonic resonance at certain speeds, seal lift-off, leaks.	Modal performance analysis, water management, seal flange stiffness.
4. Durability	Prevent corrosion, structural sagging and degradation due to thermal cycles.	Galvanic corrosion, fatigue failure of reinforcements, plastic embrittlement.	Corrosion resistance checks, fatigue CAE, material compatibility.
5. Ergonomics	Provide obstacle-free access, proper reachability of controls and roominess.	Insufficient overhead clearance, excessive opening effort, blind spots.	Ergonomic virtual assessment, swing clearance, operational load checks.

Continued on next page

Table 2.1 – continued from previous page

Macro-Category	Main System Objectives	Critical Failure Modes	Key Preventive Actions
6. Functionality	Ensure full vertical opening without clashes, correct latch preload and aero efficiency.	Asynchronous actuator motion, latch bounce, structural deflection under load.	Kinematics DMU, CFD for aero loads, end-stops dimensioning.
7. Homologation	Meet regulatory side-impact standards and ensure airbag compatibility.	Excessive intrusion into cabin, unwanted door opening, airbag blockage.	Crash CAE load cases, safety homologation requirements.
8. Logistics	Protect components during transport, shipment and workshop handling.	Scratches on Class-A surfaces, seal deformation, trim breakage.	Handling load CAE, proper packaging/handling points.
9. Safety	Prevent uncontrolled openings, sudden door drops and ensure crash behavior.	Door opens while driving, strut/actuator failure, hinge-roof joint detachment.	Inertial load-cases, door gas strut abuse load, obstacle sensors.
10. Service	Allow easy access for diagnostic checks and component replacement.	Hidden service points requiring teardown of unrelated modules.	Virtual build analysis, packaging DMU checks.

To quantify the impact of these elementary functions on the physical architecture, a correlation matrix was generated by cross-referencing the 111 functions with the 52 physical components assumed to make up the door system.

Instead of presenting the complete underlying dataset, the systemic connectivity is synthesized in Table 2.2. This macro-matrix aggregates the interactions between the 10 functional macro-categories and the 15 physical macro-subsystems. The values inside the matrix represent the number of direct dependencies: higher numbers indicate critical engineering bottlenecks where multiple functions rely on the same physical modules (e.g., the strong interdependence between Functionality, Safety and Structural Supports).

Table 2.2: Macro-Correlation Matrix: Functional Categories vs. Physical Subsystems

	Physical Subsystems (Macro-Groups)														
Functional Categories	Structural Supports	Outer Door Elements	Inner Door Structure	Sealing Elements	Locking System	Window System	User Interface	Finishing Components	Door Perimeter Interfaces	External Interfaces	Functional Interfaces	Electrical Interfaces	Sealing Interfaces	Aesthetic Interfaces	NVH Components
Appearance	0	18	0	10	0	4	0	15	14	10	0	0	0	18	0
Assembly	13	0	2	5	14	1	5	3	0	0	10	12	0	0	0
Comfort	0	17	11	24	0	7	1	18	12	6	0	0	18	0	9
Durability	4	7	3	17	2	0	4	12	0	0	1	4	1	6	0
Ergonomics	8	0	1	0	0	3	15	6	4	4	0	10	0	0	0
Functionality	27	4	7	14	16	4	19	4	8	1	15	0	8	0	0
Homologation	3	0	1	0	3	0	0	1	0	0	1	0	0	1	0
Logistics	0	2	0	2	0	1	0	2	0	0	0	2	0	2	0
Safety	27	4	10	0	35	0	9	5	0	7	16	7	0	4	0
Service	6	0	0	6	0	0	5	2	0	0	0	9	0	0	0

The mapping highlighted the degree of systemic connectivity by showing how many functions depended on each component. These nodes were subsequently considered priority areas for architectural analysis and risk assessment.

2.2.1 Identification of the Critical Architectural Node

The correlation matrix identified the gas-strut/electrical-actuation subsystem, the fixed/mobile door hinges and the upper roof hinge assembly as the physical elements with the highest functional connectivity, as summarized in Table 2.3.

Table 2.3: Physical components with the highest connectivity in the Correlation Matrix

Physical component	No. of functions
Gas strut/electrical actuator	35 functions
Fixed/mobile door hinges	34 functions
Upper roof hinge assembly	34 functions

The three components with the highest degree of interdependence belong to the hinge-roof interface node and its actuation system. Unlike a traditional door system, the components adopted in a gullwing vehicle must simultaneously guarantee structural frame stiffness, aerodynamic sealing, watertightness and complex lifting kinematics that operate against gravity.

The term *critical* is therefore used in this thesis according to a combined engineering criterion rather than according to connectivity alone. Identifying the hinge-roof interface as a critical architectural node does not imply that the existing hinge is inherently unsafe. It means that its failure or loss of mobility can affect several independent system functions at the same time, making it a priority for further analysis.

This is an important distinction because the 111 elementary functions are not equivalent to 111 failure modes. Failure modes are derived during subsequent risk analyses from the functions, architecture and operating conditions.

2.3 From Functions to Requirements: Target Book and Feasibility Checklist

The functions and associated system risks were subsequently translated into measurable engineering requirements. This conversion was formalized through the development of a Target Book (Appendix A) and a Feasibility Checklist (Appendix B).

The Target Book defines quantitative targets for the principal attributes of the door system, while the Feasibility Checklist associates the identified requirements with the corresponding virtual and physical verification activities.

For example, to ensure ergonomic consistency, regulatory checks were imposed on overall dimensions and visibility, in accordance with automotive standards (e.g., SAE J1100 [6], SAE J826 [7]). In parallel, for safety and structural resistance, FEM verifications were planned for concentrated roof loads with reference to the type of load case addressed by FMVSS 216 [8], and for lateral impact intrusion, in

accordance with ECE R95 [9] and FMVSS 214 [10].

These standards therefore provide reference conditions for the engineering development of the architecture; they do not constitute, by themselves, evidence that the proposed design has achieved formal homologation compliance. Among the main targets defined during the system analysis, a maximum door actuation time of 4 s and a maximum manual operating effort of 45 N were adopted for the normal-use condition. The environmental operating envelope was defined between −40 °C and +85 °C, with more specific temperature ranges applied to selected lifting components where appropriate.

2.4 Competitive Benchmark: Trade-offs in the State of the Art

To compare the defined objectives with existing market solutions, the preliminary system study was completed with an architectural benchmarking exercise.

The results were summarized in a radar chart comparing representative vehicles equipped with upward-opening door systems, including gullwing, falcon-wing and scissor-door configurations. The selected vehicles were Tesla Model X, Mercedes-Benz SLS AMG, Pagani Huayra, Lamborghini Aventador and DeLorean DMC-12. Although their door configurations differ, they share the main engineering trade-offs considered in this benchmark. Each vehicle was scored from 0 to 10 across five engineering axes – packaging (clearance & envelope), structural stiffness (roof crush), mass and CoG efficiency, thermal reliability, and ergonomic/actuation effort. The scores reported in this section are therefore qualitative engineering assessments based on a combination of published specifications, teardown/press reviews and the engineering interpretation developed within the project. They are intended for architectural comparison only and should not be interpreted as experimentally measured performance indices.

A sixth curve, "Project target", represents the desired profile for the proposed emergency-release architecture, with the objective of limiting adverse effects on the other five criteria.

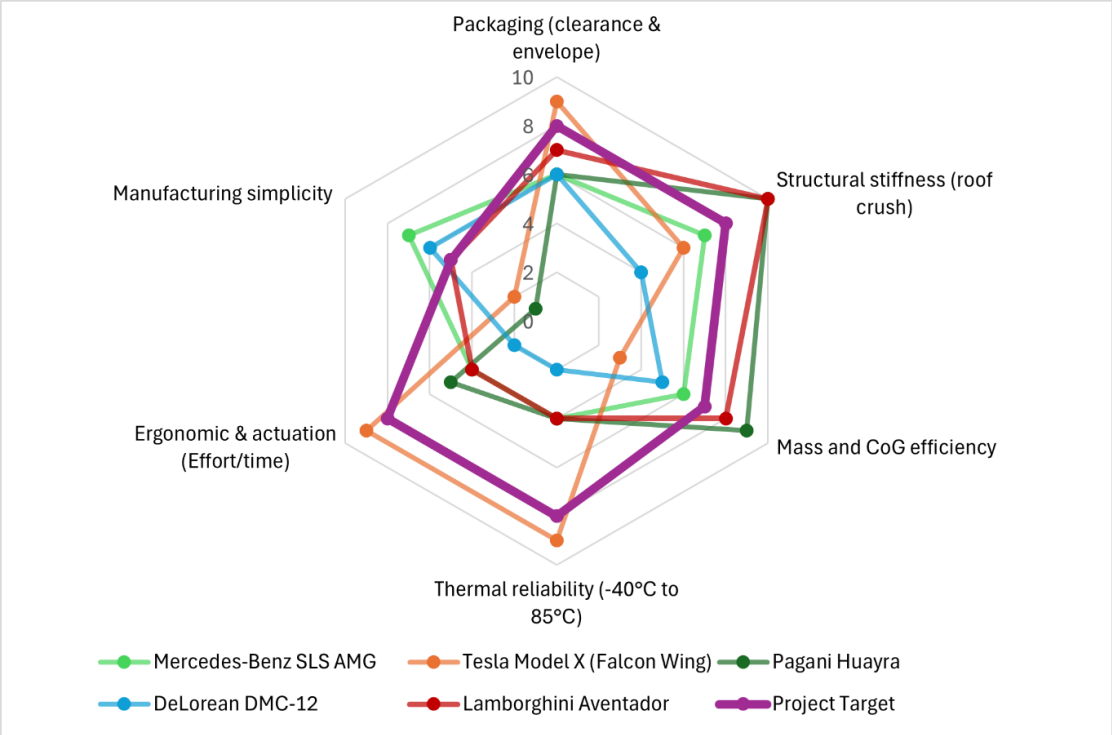


Figure 2.1: Qualitative architectural benchmarking of representative upward-opening door systems across five engineering criteria. The scores are engineering assessments intended for architectural comparison and are not experimentally measured performance indices.

The comparison indicates several engineering trade-offs associated with upward-opening door architecture:

- **Packaging vs. CoG**: Articulated architectures such as the one adopted by the Tesla Model X can reduce the required lateral clearance through motorized bi-fold kinematics [11]. However, roof-mounted actuators add mass above the vehicle floor and therefore introduce a potential penalty in terms of upper-body mass distribution [12].
- **Structural stiffness**: High-performance vehicles (such as Pagani and Lamborghini) compensate for the structural discontinuities of the roof by using a monocoque made of advanced composite materials [13] or a scissor-door architecture [14], providing high structural stiffness and favorable load-transfer characteristics, although at increased material and manufacturing complexity. To meet structural targets without relying exclusively on composite materials, some manufacturers use rearward-sloping roof architectures, which direct the structural load towards the rear roll cage [15].

- **Thermal reliability and ergonomics**: Gas-strut-assisted systems (historically used on the DeLorean DMC-12 and the Mercedes-Benz SLS AMG) are sensitive to temperature because gas pressure and seal behavior vary with operating conditions [16]. This can increase opening effort at low temperature and alter the assistance level at high temperature. Electromechanical assistance can therefore be used when a wider operating envelope or lower user effort is required.

2.5 Case Study: the Pininfarina HK GT

The trade-offs identified in Section 2.4 are not only a market-benchmarking exercise: they can be observed directly within Pininfarina's own design portfolio. The HK GT concept, unveiled at the 2018 Geneva Motor Show [17], is a Gran Turismo featuring a double-width gullwing door that spans the entire cabin length. By removing the B-pillar, it allows simultaneous access to both the front and rear seats. This concept is used as an internal case study to relate the general trade-offs identified above to a real Pininfarina vehicle architecture.

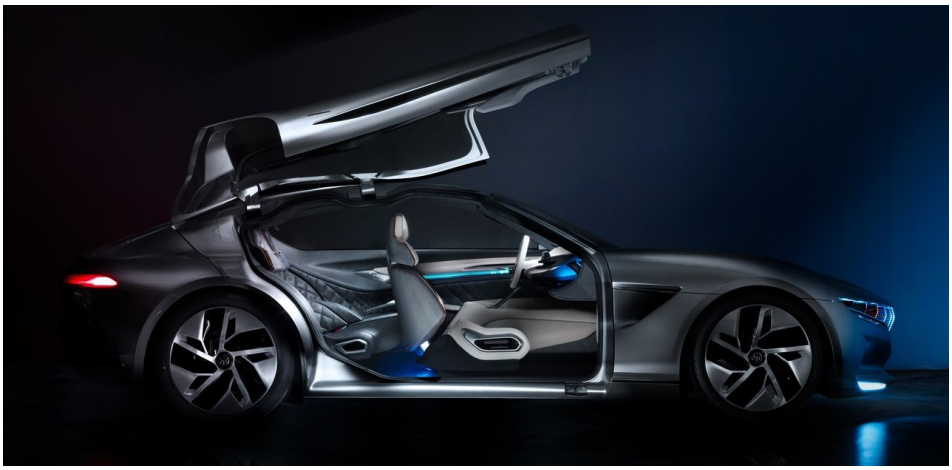


Figure 2.2: The Pininfarina HK GT concept, showing the full-length, B-pillar-free gullwing door.

2.5.1 Structural Integrity and Load Paths

The complete removal of the B-pillar interrupts one of the main vertical load paths useful for lateral crash protection (FMVSS 214 [10]) and reduces the overall torsional rigidity of the vehicle. Without the B-pillar, the roof structure becomes more vulnerable to crush loading (FMVSS 216 [8]). This is the same challenge already discussed in Section 2.4 for the general gullwing case. The available design

information indicates the use of a set-back Y-shaped roof frame [15] combined with heavily reinforced lower side structures, providing alternative load paths around the large door aperture.

2.5.2 Cantilever Mass and Hinge Stress

When fully open, the large HK GT door panel creates a pronounced cantilever effect, applying localized torque on the roof hinge. Over time, the dynamic load can cause structural sagging that misaligns the surface and compromises the weather-seal interface, precisely the fatigue and sagging failure mode that motivates the base-plate verification carried out for the HDRM-TCA hinge in Chapter 4. The available documentation indicates the use of reinforced structural and latching solutions aimed at mitigating the large door aperture and associated load paths.

2.5.3 Thermodynamic and Actuation Limits

Lifting a door panel of this size relies heavily on pneumatic gas struts. Gas struts sized around room-temperature conditions can provide a different assistance level at high and low temperature. High-temperature operation can increase the pull-down effort, while low-temperature operation can reduce the available lifting force. This reflects the same thermal-reliability trade-off identified in Section 2.4 for most vehicles in the sample. For a large door of this type, an electromechanical assist can reduce the user effort without placing a large linear actuator in the roof header. In the architecture considered here, a chassis-mounted tension-cable concept is treated as a possible solution for the normal closing function.

2.5.4 Kinematic Sweep and Packaging

During opening, a rigid door of this length sweeps a substantial lateral and vertical arc; opening the HK GT in a standard residential garage may create a risk of collision with the ceiling or with adjacent obstacles. Managing this dynamic envelope required a calibrated kinematic trajectory supported by an obstacle-detection sensor suite capable of halting or reversing the opening sequence: a system conceptually similar to the one adopted by Tesla [12].

Although the HK GT concept was not designed to address post-rollover egress specifically, its thermal, structural, and kinematic solutions are consistent with the packaging, stiffness, and actuation trade-offs identified in Section 2.4.

2.6 Identification of the Technological "Bottleneck": the Rollover Problem

The requirement mapping, risk analysis and target definition, identified post-rollover egress as the main unresolved issue selected for further development in this thesis. This issue is represented by function 102 in the functional analysis, relating to the prevention of door lock during a rollover, and by requirement 9.2.1 of the Target Book, concerning the availability of a post-rollover egress path.

Roof deformation and hinge misalignment during a rollover can restrict or prevent the motion of a conventional gullwing hinge. Among the production gullwing-door vehicles reviewed in this study, the Mercedes-Benz SLS AMG [18, 4] represents the main vehicle-level reference because it incorporates a dedicated pyrotechnic hinge-release system for post-rollover access. This solution presents several logistical, regulatory, and maintainability limitations related to the handling, replacement, diagnosis, and end-of-life management of pyrotechnic components.

Based on the results of the system-level analysis, the remainder of this thesis will focus on the development of an alternative release concept for this specific condition. The following chapters examine the hinge-locking phenomenon (known as *binding*) and use it to define a mechatronic release architecture. The proposed concept targets millisecond-scale pin actuation and repeatable electrical and mechanical checks, while retaining a replaceable sacrificial element in the release path.

Chapter 3

Rollover Problem and Limits of Existing Solutions

Chapter 2 identified the critical node of the gullwing system: the hinge-roof interface and its ability to provide an emergency egress path after a rollover event. This chapter analyses the physical cause of the problem in Sections 3.1 and 3.2. It then examines the operating characteristics and limitations of the documented automotive pyrotechnic reference represented by the Mercedes-Benz SLS AMG in Section 3.3. Finally, Section 3.4 reviews two technologies from non-automotive domains that form the theoretical basis of the architecture proposed in Chapter 4.

3.1 Binding in Rollover Conditions

In this thesis, *binding* refers to the loss of mobility of a mechanical joint due to structural deformation, geometric misalignment, and a subsequent increase in radial contact forces.

During a rollover event, the contact loads can be transferred to the roof frame, potentially deforming the pillars and the peripheral frame of the door. Under these degraded conditions, friction at the joint interface may generate a resisting force that exceeds the available force of a conventional electromechanical actuator. The resulting loss of mobility can prevent the door from being opened by the conventional actuation system, and corresponds to the failure mode described by function 102 in the preliminary FMEA (Section 2.2).

Several factors can worsen the phenomenon, making it more severe than a simple geometric misalignment. Because the release maneuver begins from a potentially jammed condition, the actuator force must first overcome the static friction threshold before sustained sliding can occur. Once motion begins, the resisting force may vary because of dynamic friction, stick-slip behavior, surface

damage and changes in the local contact geometry. Paint, corrosion products, or debris trapped at the interface during the impact can locally increase the resistance to motion. In addition, if the surrounding sheet-metal structure is deformed beyond its elastic limit, the resulting misalignment may become permanent rather than resolving through elastic springback. For these reasons, Section 3.2 represents the interface through a simplified degraded contact condition, while the release-mechanism sizing presented in Section 3.3 and Chapter 6 adopts a representative friction assumption.

3.2 Cylindrical Hinge Structural Limits

To understand the physical origin of the jamming event, consider a conventional cylindrical pin subjected to an axial extraction force F_a in the presence of a frame deformation. The component of the deformation load perpendicular to the pin axis generates an equivalent normal reaction N at the pin-hole interface. Under a simplified Coulomb-friction assumption, the resisting force is expressed as $F_f = \mu N$, where μ is the static or dynamic friction coefficient between the coupled materials. In severe rollover conditions, the radial reaction N is difficult to predict from the nominal geometry because it depends on the deformation of the surrounding structure, local contact conditions and load redistribution.

The main limitation of a cylindrical interface is that axial motion does not inherently reduce the radial interference. To complete disengagement, the pin must therefore slide along the deformed hole over the required extraction length. For the preliminary comparison developed in this thesis, this length is set to $s = 15\,\mathrm{mm}$, corresponding to the stroke of the selected actuator benchmark. Consequently, the friction force can remain significant throughout the ejection stroke. If the actuator does not provide sufficient force and impulse to overcome this resistance, the system may remain mechanically restrained.

This result has a clear consequence: increasing the actuator force may overcome the resistance, but it does not eliminate the geometric source of binding because contact may persist throughout the extraction stroke. An alternative approach is to use the interface geometry to reduce radial interference as axial disengagement begins, rather than relying only on a larger actuator force. This is the principle on which the aerospace release mechanisms discussed in Subsection 3.4.1 are based, and it forms the foundation of the cup-and-cone interface proposed in Chapter 4. For the idealized axisymmetric geometry considered here, defining α as the cone half-angle and x as the relative axial displacement, gives the following increase in the radial clearance:

$$g(x) = x \tan(\alpha) \tag{3.1}$$

Unlike the cylindrical case, a finite axial displacement progressively increases

the radial clearance and can therefore reduce the interference generated by a given radial misalignment. Binding is consequently addressed through the geometry of the interface rather than exclusively through an increase in actuator force. The selection of the angle α, the verification of the non-self-locking condition, and the complete dimensioning of the interface are discussed in Chapter 4.

3.3 Industrial Reference: Pyrotechnic Hinge Release in the Mercedes-Benz SLS AMG

The Mercedes-Benz SLS AMG provides a relevant automotive reference for emergency release of gullwing door hinges following a rollover event. The official Mercedes-Benz rescue documentation states that each door hinge contains a pyrotechnic initiator triggered by the restraint system's control unit when the vehicle comes to rest on its roof after an accident [4].

The actuator principle belongs to the family of pyrotechnic piston actuators used for rapid mechanical release applications. Autoliv, a specialist supplier of automotive safety systems, describes pyrotechnic piston actuators capable of performing functions such as push, pull, unlatching, piercing, and ejection, depending on the specific actuator configuration [5]. In this thesis, the Mercedes-Benz SLS AMG is therefore considered the vehicle-level reference, while Autoliv provides the relevant actuator technology reference associated with the pyrotechnic solution. The available Autoliv actuator data indicate a pushing force of approximately 1500 N over a stroke of 15 mm and a release time below 1 ms for the relevant actuator class [5]. These values provide an actuator-level reference for the order of magnitude of the force and response required by a rapid release device. They are not interpreted as a complete specification of the Mercedes-Benz SLS hinge, nor as a direct target validation for the proposed architecture. The quantitative requirements adopted for the HDRM-TCA system are instead derived from the mechanical and electromagnetic analysis developed in the subsequent chapters.

Functionally, pyrotechnic piston actuators use an electrically initiated pyrotechnic charge to generate the pressure required to drive a piston or pin over a short stroke [19]. Depending on the actuator design, the resulting motion can occur on a sub-millisecond timescale. The short response provides the temporal benchmark adopted for the preliminary comparison with the electromagnetic concept developed in Chapter 5 and Chapter 6.

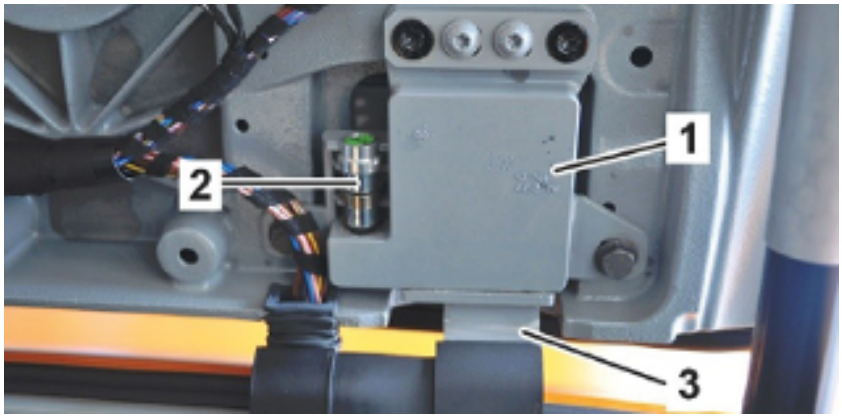


Figure 3.1: Pyrotechnic gullwing-door hinge release mechanism of the Mercedes-Benz SLS AMG, showing the door hinge (1), pyrotechnic initiator (2) and hinge arm (3). Source: Mercedes-Benz rescue documentation [4].



Figure 3.2: Autoliv pyrotechnic Pin-Pusher used as the actuator-level performance benchmark in this work. Source: Autoliv [5].

While the pyrotechnic principle provides a very rapid release event, it introduces characteristics that motivate the investigation of a non-pyrotechnic, electrically actuated alternative:

- **Irreversibility:** The complete pyrotechnic actuator is a single-use device and must be replaced after deployment.
- **Limited full-function testability:** As a single-use technology, a complete pyrotechnic deployment cannot be repeated on the same actuator. End-of-Line checks can verify the electrical and diagnostic chain, but not a full deployment without replacing the activated component.
- **False positive consequence:** An accidental deployment while the vehicle is travelling would compromise the integrity and functionality of the hinge-release system and would require inspection and replacement of the affected components.

- **Logistics and transport regulations:** Pyrotechnic safety devices may be subject to dangerous-goods classification and the corresponding transport, packaging, handling and documentation requirements [20]. This exact classification depends on the device design and applicable qualification route.
- **Post-crash safety:** Following activation, the state of the hinge-release assembly must be clearly understandable so that rescue personnel and service technicians can distinguish deployed components from undeployed ones. The corresponding handling requirements depend on the specific actuator design and applicable rescue procedures.

A practical advantage of the pyrotechnic reference is the low electrical energy required by the initiator and its compatibility with an airbag-control-unit triggering architecture [4]. By contrast, the proposed electromagnetic actuator requires a dedicated high-current discharge circuit, as discussed in Chapter 5.

3.4 State of the Art: Technologies from Other Domains

The review of existing solutions identified two technologies from different industrial domains that provide the main conceptual elements of the proposed architecture. The first is the Hold-Down and Release Mechanism (HDRM) used in aerospace applications. The second is the Thomson Coil Actuator (TCA) used for very high-speed electromagnetic actuation, including applications in HVDC switching equipment.

Neither technology, considered individually, directly solves the automotive rollover problem investigated in this thesis. Their combination provides the basis for the proposed HDRM-TCA architecture.

3.4.1 Aerospace Hold-Down and Release Mechanisms

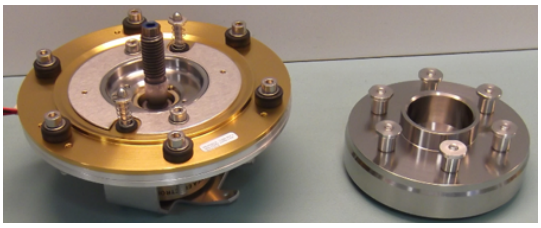
In the aerospace field, the Hold-Down and Release Mechanisms (HDRMs) are utilized to keep satellite appendages (e.g., solar panels, deployable antennas) securely attached during the critical launch phase, releasing them only once the correct orbit is reached [21]. Aerospace literature divides these into pyrotechnic devices (a mature technology but, as in the automotive field, single-use) and non-pyrotechnic alternatives, such as Non-Explosive Actuators (NEA, separable spool systems) and Shape Memory Alloys (SMA) [22]. The architecture proposed in this thesis adapts the cup-and-cone interface principle associated with this latter family of mechanisms. In cup-and-cone HDRM configurations, the retaining geometry can

be designed so that axial disengagement progressively creates a radial clearance. For a non-self-locking conical interface, the selected cone angle must be consistent with the friction conditions of the contacting materials [23].

As the actuator retracts the pin, the axial motion of the conical surface progressively creates radial clearance, reducing the normal contact force and the resulting frictional resistance. This is the same geometric principle described in Section 3.2 ($g(x) = x \tan \alpha$). This principle has been adopted in aerospace release applications where reliable separation is a critical functional requirement [24, 23].



(a) REACT family of non-pyrotechnic HDRMs.



(b) SSTL heritage HDRM with a cup-cone interface.

Figure 3.3: Examples of aerospace Hold-Down and Release Mechanisms: (a) non-pyrotechnic REACT devices; (b) SSTL heritage HDRM showing the cup-cone retention architecture adopted as a mechanical reference in this work. Sources: ARQUIMEA [23] and Malavart et al. [24].

3.4.2 Thomson Coil Actuators in HVDC Systems

In High-Voltage Direct-Current transmission networks (HVDC), **ultra-fast mechanical switches** are used as part of hybrid DC circuit-breaker architectures. Their operating time strongly influences the overall interruption sequence, which has motivated the development of high-speed electromagnetic actuation mechanisms [25, 26]. Among the most widely investigated solutions is the Thomson Coil Actuator (TCA). A high-current pulse in a fixed coil generates a rapidly varying magnetic field, inducing eddy currents in an adjacent conductive disk. The interaction between the coil field and the induced currents produces a repulsive electromagnetic force that accelerates the disk on a millisecond or sub-millisecond timescale [25].

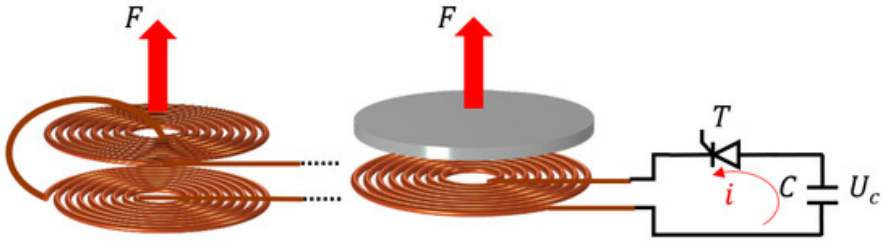


Figure 3.4: Operating principle of the Thomson Coil Actuator: a current pulse in the fixed pancake coil induces opposing eddy currents in the conductive disk, generating a repulsive electromagnetic force. Adapted from [25].

The TCA was chosen instead of a conventional solenoid because it can generate a short, high-magnitude repulsive force pulse during the first milliseconds of the discharge. This force-time characteristic is better suited to the rapid release event considered here than a conventional solenoid intended for slower sustained actuation. The electromagnetic details (Coil actuator dimensioning, capacitor bank, discharge mode) are developed in Chapter 5.

3.5 Synthesis: The Technological Gap

The reviewed solutions do not directly address all the requirements of the specific application considered here.

The pyrotechnic automotive reference provides very rapid release performance, but the technology is single-use and introduces additional requirements associated with energetic material.

The aerospace HDRM technology demonstrates how an appropriate mechanical interface can reduce sensitivity to radial interference by geometrically separating the retaining surfaces during release. However, it does not provide the high-speed electromagnetic force-generation capability required by the present application.

The TCA provides a mechanism for generating a high-speed electromagnetic impulse. Its industrial application demonstrates the feasibility of this actuation principle, but it has not been established as a complete solution for an automotive gullwing hinge subjected to crash-induced structural misalignment.

The technological concept developed in this thesis therefore combines the two principles:

- a **cup-and-cone HDRM interface** to reduce sensitivity to geometric binding;
- a **Thomson Coil Actuator** to provide the required high-speed release impulse.

No previously published application combining a cup-and-cone HDRM-inspired interface with a Thomson coil actuator for the post-rollover release of an automotive gullwing door was identified in the literature reviewed for this thesis.

The resulting HDRM-TCA architecture is developed and dimensioned in Chapter 4, while its electrical and electromagnetic characteristics are developed in Chapter 5 and its electromechanical performance is assessed numerically in Chapter 6.

Chapter 4

Proposed Architecture: HDRM-TCA System

This chapter describes the proposed HDRM-TCA architecture. Section 4.1 introduces the general concept and compares it against the pyrotechnic reference. Section 4.2 details the complete mechanical layout while Section 4.3 presents the operating sequence. The electrical and electromagnetic sizing that powers this layout follows in Chapter 5, and the numerical assessment is presented in Chapter 6.

4.1 General Concept and Advantages Over Pyrotechnic Systems

The decision to adopt a TCA is not solely guided by the kinematic requirements of the locking pin itself. Under nominal conditions, the required stroke is relatively short (15 mm) and can be achieved using various conventional technologies: electrical motors, solenoids, shape-memory actuators, or geared electromechanical latches.

The primary focus is not on easy pin retraction under nominal operating conditions. The release mechanism must function during a vehicle rollover, when severe structural deformation, unpredictable load paths and roof-door misalignment may occur (Chapter 3). Under these degraded conditions, stroke length is not the only constraint; the system must provide sufficient force and displacement to release the mechanical constraint within a short and repeatable time window under the assumed degraded conditions. Conventional electromechanical actuators may not provide the required combination of initial force, response time, and short-stroke impulse under the assumed binding conditions.

The HDRM-TCA architecture addresses these two requirements through two complementary mechanisms. First, the **cup-and-cone interface** provides a

geometrical means of reducing radial interference during axial pin extraction. The mechanism is intended to reduce the sensitivity to radial interference during pin extraction.

Second, the **TCA** provides a short-duration electromagnetic force impulse capable of initiating the pin motion rapidly. The proposed architecture is not intended to reproduce the operating principle of a pyrotechnic actuator. Instead, it combines a geometric anti-binding interface with a high-speed electrical actuator.

Table 4.1 summarizes a multi-criteria comparison between the pyrotechnic automotive reference represented by the Mercedes-Benz SLS AMG and associated Autoliv actuator technology, and the proposed HDRM-TCA architecture.

Table 4.1: Multi-criteria comparison: Pyrotechnic emergency-release reference vs proposed HDRM-TCA architecture

Criteria	**Pyrotechnic reference**	**Proposed HDRM-TCA architecture**
Principle	Rapid pyrotechnic actuation of the release element; single-use	Electromagnetic impulse followed by mechanical disengagement
Reversibility	Single-use deployment	Main actuator architecture is intended to be reusable; the sacrificial shear element needs replacement after deployment
Testability	Full deployment is destructive	The electrical discharge circuit and non-destructive diagnostic functions can be tested repeatedly. A complete release test requires replacement of the sacrificial shear ring
False positives	An unintended pyrotechnic deployment is irreversible and requires replacement of the activated actuator and associated components	An unintended electromagnetic activation would initiate the release sequence without destructive pyrotechnic effects; appropriate control logic, interlocks and fault detection are therefore required to prevent unintended deployment

continued on next page

(Table 4.1 continued)

Criteria	**Pyrotechnic system**	**Proposed HDRM-TCA architecture**
Regulations and logistics	Pyrotechnic safety devices may be subjected to dangerous-goods classification and the corresponding transport, packaging, handling and documentation requirements	The proposed architecture eliminates the energetic material and its associated pyrotechnic logistics, although the electronic components and high-voltage energy-storage system remain subject to their applicable automotive and environmental requirements
Post-crash electrical state	Low-voltage firing circuit	Dedicated capacitor-discharge circuit with controlled isolation and discharge of residual energy
Electrical complexity	Charge triggered at low current on a 12 V network	The proposed concept assumes a 400 V capacitor-discharge circuit. This introduces additional requirements for insulation, protection against direct contact, isolation monitoring, controlled residual-energy discharge and crash-safe cable routing. The detailed regulatory classification depends on the final electrical architecture and is assessed in Chapter 5

To provide an overall understanding of the proposed HDRM-TCA architecture before discussing the individual subsystems in detail, Figure 4.1 shows a three-dimensional overview of the complete hinge assembly. The representation highlights the functional separation between the normal door-rotation axis and the emergency release direction, together with the main mechanical and electromagnetic components of the proposed system.

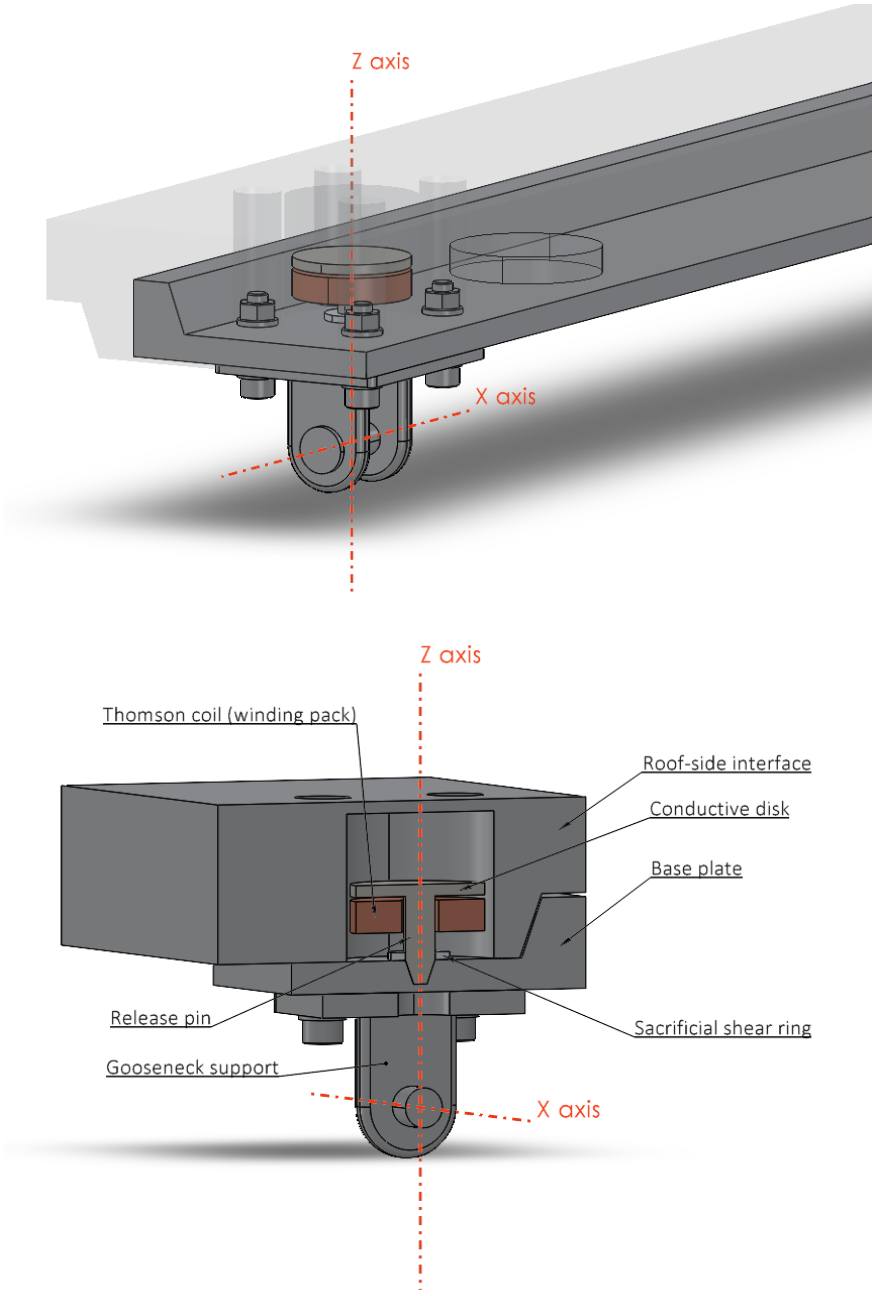
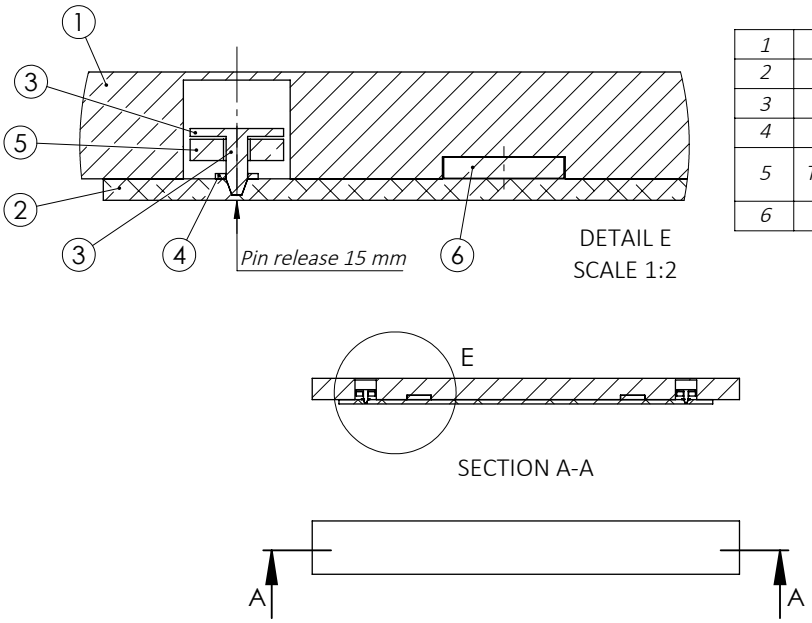


Figure 4.1: Three-dimensional overview of the proposed HDRM-TCA hinge assembly. The upper view highlights the separation between the normal door-rotation axis (X-axis) and the emergency release direction (Z-axis), while the lower sectioned view identifies the main mechanical and electromagnetic components of the system.

4.2 Complete Mechanical Layout

The architecture comprises two door-level assemblies, one for each gullwing door. Each assembly uses a common structural baseplate supporting two HDRM-TCA hinge modules. Each module incorporates two mechanically distinct functional interfaces: everyday opening kinematics (X axis) and emergency release (Z axis). This functional separation is one of the main principles of the proposed layout. The normal-opening and emergency-release functions use mechanically distinct local interfaces, although both ultimately transfer load through the common base plate.

Distributing the release function across four independent hinges, rather than concentrating it in a single centralized actuator, is itself a deliberate design choice. Since the roof deformation that causes binding is unpredictable in location and magnitude (Section 3.1), each HDRM-TCA module is intended to address the local misalignment at its respective roof corner. The consequences of a failed individual release channel are considered separately in the function-safety analysis of Chapter 7; successful door ejection with one hinge remaining engaged is not assumed in the present mechanical model. The following sections describe and size each subsystem of the hinge module individually.



1	Roof-side interface
2	Base plate
3	Conductive disk
4	Sacrificial shear ring
5	Thomson coil (winding pack)
6	Ejection spring

Figure 4.2: Section view of the preliminary HDRM-TCA hinge assembly. Detail E highlights the main components involved in the emergency-release mechanism and their relative packaging. The indicated 15 mm stroke represents the required pin-release displacement.

4.2.1 Base Plate and Dual-Axis Interface

The base plate is the central element of the roof header and door interface. The current concept assumes an EN AW-7075-T6 aluminum alloy [27] base-plate profile, 700 mm long and 8 mm thick, with a folded lip flange along one edge that brings the overall width envelope to 80 mm. A channel-type cross-section was selected over a flat bar specifically to raise flexural stiffness without adding excessive mass.

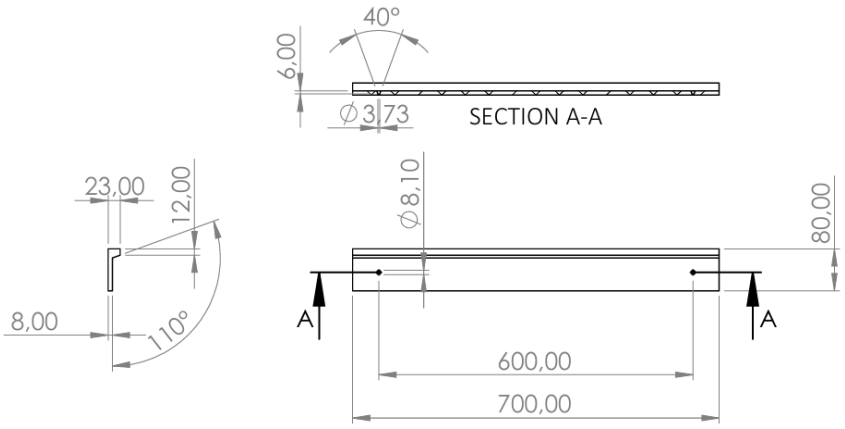
The base plate simultaneously performs three functions:

1. *Load distribution*: under rollover conditions, it is intended to distribute loads between the two gullwing hinge regions and contribute to the stiffness of the roof-hinge structure.

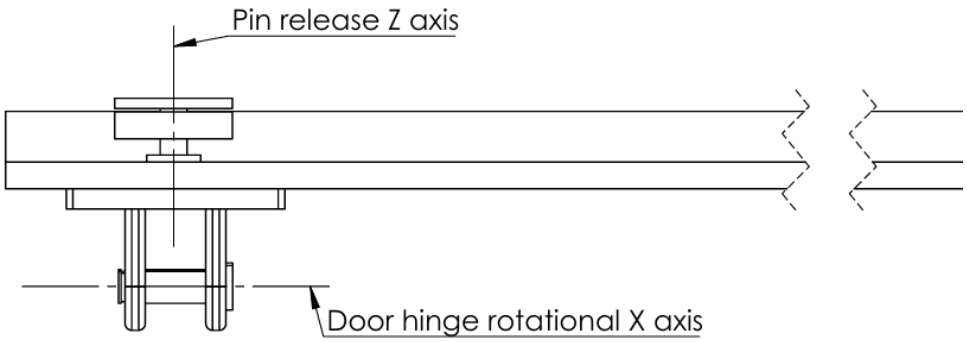
2. *HDRM alignment*: its flexural stiffness is intended to reduce relative misalignment between the conical housings when the surrounding roof structure deforms.

3. *Everyday hinge support*: the gooseneck hinge [28], which provides the normal door rotation about the X-axis, is mounted to the lower face.

Utilizing a single continuous plate for both hinges, rather than separate plates, provides a continuous structural connection between the two hinge regions and may reduce localized load concentration compared with separate mounting plates.



(a) Dimensioned geometry of the base plate.



(b) Separation of the normal-rotation and release axes.

Figure 4.3: Preliminary base-plate geometry and functional separation of the two main interfaces. The gooseneck hinge defines the normal door-rotation axis, while the cup-and-cone release interface acts along the vertical pin-release axis.

Preliminary structural stress screening. The following calculation is retained as a preliminary structural stress screening, rather than as a fatigue verification.

The proposed base plate has a folded channel geometry. For a first-order calculation, the local region around the gooseneck mounting interface is approximated

as a solid rectangular cross-section ($b = 50\,\text{mm}$, $t = 8\,\text{mm}$).

Although the center of the conical seat is aligned with the gooseneck's mounting axis to eliminate planar eccentricity, the gooseneck geometry introduces a lever arm l between the anchoring plane and the actual rotation axis of the door. Consequently, the weight of the door applied at this axis generates a local bending moment on the plate.

Assuming a preliminary door mass $m = 30\,\text{kg}$ (estimated to safely encompass the weight of complex door systems like those found on the Tesla Model X, Mercedes-Benz SLS AMG, and Pagani Huayra), a dynamic load factor $k = 2$ (vibrations, potholes, forceful closures), and a lever arm $l = 50\,\text{mm}$, the resulting equivalent force and the corresponding bending moment are:

$$F = m\,g\,k = 30 \times 9.81 \times 2 \approx 590\,\text{N} \tag{4.1}$$

$$M = F\,l = 590 \times 0.05 = 29.5\,\text{Nm} \tag{4.2}$$

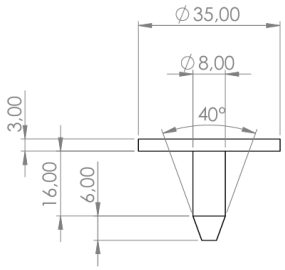
Idealizing the loaded cross-section as the solid rectangle above gives a nominal bending stress of $\sigma_{\text{nom}} = 6M/(b\,t^2) \approx 55\,\text{MPa}$. This value is retained only as a first-order stress indicator. A fatigue safety factor is not assigned at this stage because the local stress concentration, load spectrum, mean stress, surface condition and actual folded-section geometry have not yet been established.

However, this calculation does not represent a final structural verification. On the one hand, the folded lip flange increases the section's second moment of area relative to the flat idealization used above; for pure bending about the axis the flange is designed to stiffen, this would tend to lower the real stress below the $55\,\text{MPa}$ nominal value calculated here. On the other hand, the same lip flange makes the plate an open thin-walled cross-section. Such sections generally provide much lower torsional rigidity than closed sections of comparable envelope and can also exhibit local warping. Since the lever arm l that generates the bending moment M also introduces a torque about the plate's longitudinal axis wherever the gooseneck mounting is not perfectly centered on the section's shear center, the actual stress state at the hinge interface may include bending, torsion and local warping effects that are not represented by the simplified calculation.

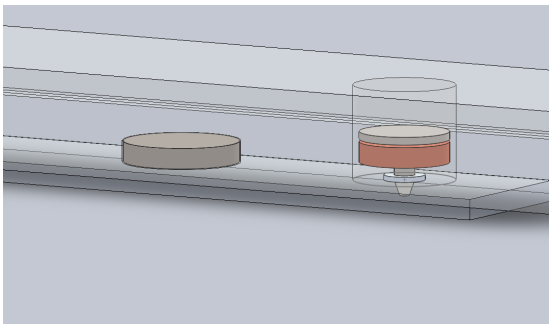
The blind hole for the truncated-cone seat further introduces a stress concentration factor K_t [29] (such that $\sigma_{\max} = K_t\,\sigma_{\text{nom}}$) that is likewise not captured here. Definitive validation is accordingly deferred, as already planned, to a 3D FEM analysis during the detailed design phase (Chapter 9). This analysis will explicitly model the true folded-channel geometry under a combined bending-torsion-warping load case once the commercial hinge component's exact specifications are available.

4.2.2 Cup-and-Cone Interface

The conical seat (cup) is machined into the upper face of the plate, with a half-angle $\alpha = 20°$ and an insertion depth of approximately 5–6 mm. The conical pin (cone), made of 17-4PH stainless steel [30], has a nominal diameter of 8 mm and a total length of 25 mm.



(a) Conical release pin and conductive disk.



(b) Local assembled HDRM–TCA interface.

Figure 4.4: Preliminary geometry and assembled configuration of the cup-and-cone release interface. The 40° included cone angle corresponds to the adopted half-angle $\alpha = 20°$.

The purpose of the geometry is to convert a relatively small axial displacement into a radial separation between the mating surfaces. The idealized clearance is $g(x) = x \tan \alpha$.

For a radial deformation or interference δ, the axial displacement required to generate an equivalent clearance is therefore

$$x_{\text{clear}} = \frac{\delta}{\tan \alpha}. \tag{4·3}$$

For the design conditions $\delta = 5\,\text{mm}$ and $\alpha = 20°$, the required displacement is

$$x_{\text{clear}} = \frac{5\,\text{mm}}{\tan 20°} = 13.7\,\text{mm}. \tag{4·4}$$

In this simplified geometric screening, δ represents the prescribed relative radial offset between the cup and cone axes. It does not directly represent the total deformation of the vehicle roof.

With the adopted 15 mm release stroke, the resulting geometrical margin is approximately

$$15\,\text{mm} - 13.7\,\text{mm} = 1.3\,\text{mm}. \tag{4.5}$$

This result is particularly relevant because it shows that the selected 15 mm stroke is not only inherited from the actuator benchmark, but it is also geometrically sufficient, within the idealized model, to accommodate the selected 5 mm relative radial-offset case.

The exact relationship between crash-induced structural deformation and local interface interference must nevertheless be established through full-vehicle or body-in-white structural analysis.

Non-Self-Locking Verification. An important design requirement is to avoid self-locking of the conical interface under the assumed friction conditions. In the mechanics of conical joints, a system is self-locking if the geometric angle of the profile is smaller than the material's friction angle. Under the simplified wedge-friction model adopted here, the preliminary non-self-locking condition $\alpha > \varphi$ must be met [31], where $\varphi = \arctan\mu$ is the static friction limit angle. Table 4.2 maps the safety margin for several tribological pairings plausible in the automotive sector, given the selected cone angle of $\alpha = 20°$.

Table 4.2: Non-self-locking sensitivity matrix ($\alpha = 20°$)

μ	$\varphi = \arctan\mu$	Safety condition
0.10	5.7°	Satisfied, margin 14.3°
0.15	8.5°	Satisfied, margin 11.5°
0.20	11.3°	Satisfied, margin 8.7°
0.30	16.7°	Satisfied, margin 3.3°

The selected cone angle (20°) satisfies the non-self-locking criterion for all friction coefficients considered in the preliminary sensitivity analysis. The margin decreases as the effective coefficient of friction increases, but the condition remains satisfied up to $\mu = 0.30$. This result supports non-self-locking behavior of the geometric interface under the simplified friction model; experimental verification is still required.

Structural Verification of the Pin Under Radial Shear. The 8 mm pin diameter, selected primarily from packaging considerations, must withstand the radial shear loads associated with crash-induced misalignments. Using the preliminary allowable shear strength adopted for the 17-4PH pin [30] $\tau_{\text{allow}} \approx 500\,\text{MPa}$, the idealized single-shear area is

$$A = \frac{\pi d^2}{4} = \frac{\pi(8)^2}{4} = 50.26\,\text{mm}^2. \tag{4.6}$$

The corresponding idealized shear capacity is therefore

$$F_{\text{shear,ind}} = A\,\tau_{\text{allow}} \approx 50.26 \times 500 \approx 25.1\,\text{kN}. \tag{4.7}$$

This value exceeds the highest radial-load case for which the electromechanical release model predicts successful disengagement, namely 14 kN in the sensitivity analysis presented in Chapter 6. This comparison is retained only as a preliminary structural screening. It does not represent a pin strength verification because the actual stress state can include local bearing, bending, contact concentration and non-uniform load transfer through the cup-and-cone interface. In addition, the two hinge modules on one door are not assumed to share the crash-induced load equally. A detailed 3D contact and structural analysis is therefore required before the pin geometry can be considered finalized.

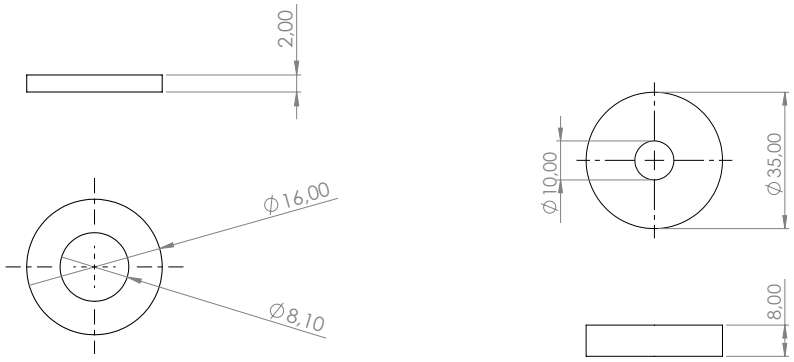
4.2.3 Shear Ring and TCA Cartridge

A safety requirement identified in the FMEA calls for preventing accidental release triggered by harsh NVH inputs or high lateral accelerations (2–3 g). Therefore, the pin is rigidly constrained within its seat by a **sacrificial shear ring**, a principle inspired by sacrificial release elements used in aerospace mechanisms (Subsection 3.4.1). The ring is intended to remain intact during normal loading and to undergo controlled shear failure when the TCA impulse exceeds the selected release threshold. The final break-load window must satisfy $F_{\text{vehicle,max}} < F_{\text{break}} < F_{\text{TCA,available}}$ and requires experimental qualification.

Preliminary structural stress screening. The shear ring is made of a lightweight aluminum alloy EN AW-6060-T6 [32] adopted as a preliminary material assumption for the concept model. The exact alloy, temper and allowable shear stress must be finalized together with the final ring geometry before qualification. The ring is intended to fail by controlled shear rather than by brittle fracture, and its release threshold must be established experimentally.

The TCA cartridge is housed entirely within the roof and comprises: an EN AW-7075-T6 [27] mobile armature disk (⌀ 35 mm); a preliminary Thomson-coil

winding pack (designed as "pancake" type, to minimize the inductance, Chapter 5); a 1 mm insulating air gap; the conical pin rigidly attached to the disk; and a preloaded ejection spring (Subsection 4.2.4). The preliminary assembly occupies an axial envelope of approximately 40 mm, which is considered compatible with the available roof-header packaging at concept level. Final packaging remains subject to detailed CAD and structural verification.



(a) Sacrificial shear ring.

(b) Preliminary Thomson-coil winding-pack envelope.

Figure 4.5: Preliminary dimensions of the sacrificial shear ring and Thomson-coil winding-pack envelope. The shear ring has an outer diameter of 16 mm, an inner diameter of 8.1 mm and a thickness of 2 mm. The preliminary winding-pack envelope has an outer diameter of 35 mm, an inner diameter of 10 mm and an axial thickness of 8 mm.

Mobile Mass Estimate. The actuator's moving assembly comprises the aluminum disk and the conical pin rigidly attached to it. For the disk geometry adopted here (⌀ 35 mm, 3 mm thickness, EN AW-7075-T6 [27], $\rho \approx 2.81\,\mathrm{g/cm^3}$) the estimated disk mass is ≈ 8.4 g. For preliminary inertia sizing, the pin is conservatively approximated as a full cylindrical volume with ⌀ 8 mm, 25 mm length. Using a 17-4PH [30] stainless steel density $\rho \approx 7.8\,\mathrm{g/cm^3}$ this gives an upper-bound geometric mass of approximately 9.8 g. The actual conical pin mass is slightly lower because part of the cylindrical envelope is removed by the tapered geometry. The resulting moving-mass estimate is therefore of the order of 18 g. This value is lower than the total mass of commercial aerospace pin-puller HDRMs, whose reported actuator masses include the housing, triggering hardware and additional structural components [33]. To stress-test the architecture against this uncertainty, the mobile mass adopted in the Simscape model of Chapter 6 is fixed at 0.05 kg, nearly three times the estimated 18 g, thereby imposing a deliberately higher inertial load than the preliminary moving-mass estimate.

4.2.4 Ejection Spring and Ball Joints

Once the TCA module retracts the conical pin, the main roof-side mechanical constraint is released. However, the door does not necessarily move away from the vehicle spontaneously because, in an inverted condition, gravity opposes the initial separation and additional resistance may be introduced by the door seals, residual structural deformation and the normal-opening support hardware.

For this reason, a passive ejection mechanism is introduced as a preliminary functional feature. Drawing inspiration from passive deployment systems used in aerospace release mechanisms, the present concept uses preloaded compression springs integrated into the hinge region.

The preliminary spring-sizing target adopts a door mass of 30 kg, a nominal ejection stroke of 150 mm and a combined peak spring force of approximately 1200 N. The selected peak force is approximately 4.1 times the static weight of the assumed door:

$$\frac{1200}{30 \times 9.81} \approx 4.1. \tag{4.8}$$

This force level is used as a preliminary concept assumption intended to provide margin against gravity, seal adhesion and other low-frequency resistances. The contribution of the door seals, residual roof deformation and the normal-opening hardware has not been experimentally characterized in this work.

Assuming that the spring force decreases approximately linearly from 1200 N to zero over the complete 150 mm stroke gives

$$k = \frac{\Delta F}{\Delta x} = \frac{1200\,\mathrm{N}}{150\,\mathrm{mm}} = 8\,\mathrm{N/mm}, \tag{4.9}$$

$$E_{\mathrm{elastic}} = \tfrac{1}{2} k\,\Delta x^2 = \tfrac{1}{2} \times 8 \times 150^2 = 90\,\mathrm{J}. \tag{4.10}$$

The corresponding gravitational potential-energy increase associated with raising a 30 kg door by 150 mm is approximately

$$E_g = mgh = 30 \times 9.81 \times 0.15 \approx 44\,\mathrm{J}. \tag{4.11}$$

The remaining nominal spring energy can in principle contribute to overcoming seal adhesion, friction and other resisting effects, although these contributions have not been fully characterized.

The adopted packaging concept distributes the required energy between two springs, one at each hinge module, corresponding to approximately 45 J per spring and an initial force of approximately 600 N per spring if the load is shared symmetrically.

The present spring definition must therefore be interpreted as a preliminary functional sizing and packaging envelope rather than as a complete physical spring design. Wire diameter, mean coil diameter, number of active coils, solid height, buckling, fatigue life and mounting details remain to be developed and verified experimentally.

The residual connection provided by the normal-opening gas struts must also be considered after the hinge-release event. In the current concept, the gas struts are assumed to be connected through ball-joint interfaces representative of automotive lift supports [34, 16].

The adopted 150 mm ejection stroke is treated as a preliminary packaging and kinematic target rather than as a demonstrated ball-joint disengagement distance. Exceeding the nominal angular operating range of a ball joint does not by itself prove that the joint will disengage in a predictable or repeatable way.

The behaviour of the gas-strut end connections under combined lateral displacement, angular loading and post-crash deformation has not been validated in this work. A dedicated detachable interface, or an experimentally characterized ball-joint release mechanism, may therefore be required during the detailed-design phase.

4.3 Operating Sequence

Table 4.3 summarizes the nominal emergency-release sequence, integrating the mechanical subsystems described in this chapter with the power electronics developed in Chapter 5. The reported times correspond to the electromechanical model and should not be interpreted as experimentally validated system-level response times.

Table 4.3: Nominal operating sequence of the emergency-release mechanism

Time	Event
$t = 0\,\mathrm{ms}$	The rollover-detection logic issues the emergency-release command. The same event is assumed to trigger the main electronic door latch and the SCR-based discharge circuits of the four HDRM–TCA modules.
$t \gtrsim 0\,\mathrm{ms}$	The capacitor-discharge circuit is triggered and the 400 V capacitor bank begins to discharge through the Thomson coil. The rapidly increasing coil current induces eddy currents in the conductive disk and generates the repulsive electromagnetic force pulse.
$t \approx 0.7\,\mathrm{ms}$	The numerical model predicts a nominal electromagnetic-force peak of approximately 4.3 kN. If the calibrated release threshold of the sacrificial shear element is exceeded, the moving disk and pin assembly begins its axial motion.
$t \approx 1.3\,\mathrm{ms}$	The model predicts completion of the prescribed 15 mm pin-release stroke. As the conical surfaces separate, the radial clearance progressively increases and the contact associated with geometric interference is reduced. At this stage the roof-side mechanical retention provided by the cup-and-cone interface is released.
After pin release	Following release of the main hinge constraint, the preloaded ejection springs provide the passive door-separation impulse. The lower-frequency door-ejection dynamics are treated separately in Chapter 6; therefore, no complete door-opening time is claimed from the millisecond-scale TCA model.

4.4 Chapter Summary

This chapter presented the preliminary mechanical architecture of the proposed HDRM-TCA release system. The concept combines a common structural base plate, a cup-and-cone interface intended to reduce sensitivity to radial interference, a Thomson coil actuator for rapid short-stroke actuation, and a sacrificial shear element that defines the release threshold.

The cup-and-cone geometry was assessed through a preliminary clearance calculation and a simplified non-self-locking criterion. The conical pin and base plate were evaluated using first-order structural screening calculations. These results support the concept-level feasibility of the selected dimensions but do not constitute final structural, fatigue, or release-reliability verification.

The proposed architecture is partially reusable. Following deployment, the electromagnetic actuator and main mechanical assembly are intended to be retained, while the sacrificial shear ring must be replaced and the release mechanism must be inspected and reset. The feasibility of repeated electrical discharge, component reset, and post-deployment servicing requires experimental validation.

The electrical and electromagnetic design of the TCA is developed in Chapter 5, while the predicted force, displacement, and response time are assessed numerically in Chapter 6.

Chapter 5

Electric and Electromagnetic Design

Chapter 4 introduced the mechanical layout of the HDRM-TCA system and its emergency-release sequence. The purpose of this chapter is to define the electrical architecture needed to drive the actuator. The discussion starts from the electromagnetic operating principle and the energy needed for the release event (Section 5.1). It then develops the capacitor bank (Section 5.2), the power electronics (Sections 5.3 and 5.4), the preliminary coil design (Section 5.5), the high-voltage routing and shielding (Section 5.6) and the cold-wiring strategy (Section 5.7). Its numerical assessment follows in Chapter 6.

5.1 Functioning Principle: Lorentz and Eddy-Current Forces

As discussed in Section 4.1, the release event requires a short and intense force pulse during the first milliseconds of actuation. For this reason, a Thomson Coil Actuator was considered suitable for the present application.

Its operation can be divided into three main steps:

1. **Capacitor discharge:** The capacitor bank discharges a very high current pulse (thousands of Amperes in a few milliseconds) into a fixed flat coil (Thomson coil).

2. **Electromagnetic induction:** The variation of the current generates a time-varying magnetic field $B(t)$, which passes through the movable disk. According to Faraday's law and Lenz's law, opposing eddy currents are induced in the disk [25].

3. **Electromagnetic repulsion:** The two opposing magnetic fields generate a repulsive Lorentz force that accelerates the disk and initiates the pin-release motion.

The discharge circuit is represented as an underdamped series RLC network comprising the capacitor bank, the SCR, the total series resistance and the Thomson-coil inductance. The numerical implementation is described in Chapter 6.

5.1.1 Lumped Parameter Model

For the preliminary design phase, the electromagnetic force is represented through

$$F(t) = k(x)i(t)^2, \tag{5.1}$$

where k is a lumped coefficient describing the electromagnetic coupling between the coil and the conductive disk.

Published results from comparable flat-coil actuators give an order of magnitude of 20 kN at 2 kA, giving an initial coefficient of about

$$k_0 = \frac{20\,000}{2000^2} \approx 0.005\,\mathrm{N/A^2} \tag{5.2}$$

[25, 35, 36].

Targeting a peak force of 2 kN, the required static current is:

$$I_{\mathrm{screen}} = \sqrt{\frac{2000}{0.005}} \approx 632\,\mathrm{A}. \tag{5.3}$$

This value is not a strict release-current threshold. The actual actuator response depends on the complete RLC transient and on the reduction of $k(x)$ as the disk-to-coil gap increases. A more accurate determination of the position-dependent electromagnetic coupling would require a dedicated 2D or 3D FEM model including the real coil geometry disk conductivity and skin-effect phenomena.

5.2 Energy Balance and Capacitor Bank Design

A preliminary energy screen can be obtained by assuming an average mechanical release force of 2000 N acting over a 15 mm stroke:

$$W_{\mathrm{mech}} = F_{\mathrm{mean}}\, s = 2000 \times 0.015 = 30\,\mathrm{J}. \tag{5.4}$$

Reported TCA efficiencies depend strongly on actuator geometry and operating conditions and generally fall between 3% and 14% [37]. For the preliminary sizing,

an 8% conversion efficiency is adopted and so the total electrical-energy estimate per hinge is:

$$E_{\text{required}} = \frac{30\,\text{J}}{0.08} = 375\,\text{J}. \tag{5.5}$$

For the selected commercial capacitor, $C = 4.7\,\text{mF}$ and $V = 400\,\text{V}$, the nominal stored energy per capacitor is

$$E = \frac{1}{2}CV^2 = \frac{1}{2} \times 0.0047 \times 400^2 \approx 376\,\text{J}. \tag{5.6}$$

Therefore, one 4.7 mF capacitor provides approximately 376 J nominally at 400 V.

For the two-capacitor door-level module,

$$C_{\text{door}} = 9.4\,\text{mF}, \tag{5.7}$$

and therefore

$$E_{\text{door}} = \frac{1}{2}C_{\text{door}}V^2 = \frac{1}{2} \times 0.0094 \times 400^2 \approx 752\,\text{J}. \tag{5.8}$$

Commercial Capacitor Selection. The selected capacitor family is the TDK EPCOS B43725 series [38]. A 4.7 mF, 400 V DC variant provides the capacitance and voltage rating required by the nominal single-hinge equivalent model.

The exact ordering code, ESR and mechanical envelope must be finalized together with the packaging design because different variants within the family are available.

The physical architecture provides one power module per vehicle side (i.e., per door), serving the two hinges of that door. Each module consists of two 4.7 mF capacitors connected in parallel, providing an equivalent nominal capacitance of approximately 9.4 mF. At 400 V, this corresponds to a stored electrical energy of approximately 752 J for the complete power module. The 4.7 mF capacitance used in the Simscape model of Chapter 6 represents the equivalent capacitance associated with a single hinge actuation channel. The physical two-capacitor-per-door architecture therefore provides the required energy at vehicle level while remaining consistent with the single-hinge equivalent model adopted for the electromechanical analysis.

Including assembly tolerances, the M6 threaded studs, and the galvanic/mechanical enclosure, a preliminary packaging envelope of approximately $155 \times 80 \times 120$ mm, corresponding to about 1.5 L, is assumed for the complete door-level power module. Possible installation locations include the boxed cross-member behind the rear seats, the lower pillar region and the door-sill area. The final position remains dependent on the vehicle packaging study.

End-of-life Thermal Reliability. The selected component is rated for an operating temperature range of −40 to 85 °C, with a maximum permissible temperature of up to 105 °C under the specified conditions [38]. In the proposed architecture, the capacitor bank is maintained at the required standby voltage while remaining essentially free of continuous high ripple current. Consequently, continuous ohmic self-heating due to ripple current is expected to be negligible during standby operation. The actual capacitor temperature, however, remains dependent on the local ambient temperature, thermal conduction through the mounting structure, enclosure conditions, and any transient losses associated with charging and actuation.

The nominal stored energy of a single 4.7 mF capacitor at 400 V is approximately 376 J, while the two-capacitor parallel configuration provides approximately 752 J per door. The previously calculated value of 375 J is therefore treated as a preliminary energy-sizing screen rather than as a guaranteed end-of-life energy requirement. Since capacitance and ESR may vary with ageing and operating conditions, the degraded parameter set adopted for the EoL study is explicitly investigated in Chapter 6.

5.3 DC-DC Boost Converter

The emergency system is assumed to interface with a local low-voltage vehicle supply, typically in the 12 V (ICE powertrains) or 48 V (mild-hybrid) range depending on the vehicle electrical architecture, while the local pulse-power capacitor bank operates at 400 V. A galvanically isolated DC-DC converter is therefore used to charge the capacitor bank. The isolation separates the low-voltage control electronics from the pulse-power domain and limits the propagation of electrical faults between the two domains.

This choice is treated as a system-level safety measure rather than as a direct requirement of ISO 26262 [39].

Once the capacitor bank reaches its standby voltage, the converter only needs to compensate for capacitor leakage and other standby losses until a discharge command is issued.

5.4 Choice of the Switching Device: SCR vs IGBT

Although the power transistor, specifically the IGBT, is the industry standard for automotive inverters, its application in impulsive power circuitry is highly critical due to Safe Operating Area (SOA) limitations. When an IGBT is crossed by a

current far above its rated range, it enters the linear region and desaturates. This causes a drastic increase in the collector-emitter voltage that generates a power dissipation destructive for the semiconductor [40, 41].

The solution adopted is the SCR (Silicon Controlled Rectifier) thyristor, chosen for two properties:

- **Transient current capability:** The datasheets of leading manufacturers (Infineon, Vishay) report maximum currents for pulse thyristors above 5000 A for 10 ms [42]. The predicted nominal current peak of approximately 1.73 kA is therefore within the order of magnitude of available devices. Final selection must still consider I^2t, di/dt, junction temperature, gate-drive requirements and automotive qualification.
- **Natural current-zero commutation:** Once it receives the trigger signal from the airbag ACU, the SCR enters deep conduction and does not require a turn-off command. In the underdamped discharge considered here, conduction terminates when the current reaches its first natural zero crossing. This simplifies the switching strategy compared with a fully gate-controlled device, although the final SCR selection must still address fault behavior, I^2t, di/dt, junction temperature and gate-drive reliability [25].

Natural current-zero commutation is therefore an architectural advantage, but it is not considered an intrinsically fail-safe feature.

5.5 Coil Design

To meet the total circuit resistance budget imposed by the Simscape model (0.030 Ω) and an inductance of 0.2 mH, the actuator was designed as a flat coil (pancake coil) with **96 turns** as a preliminary layout investigated using Wheeler's approximation [43]. The resulting inductance is of the same order as the 0.2 mH target adopted in the numerical model.

The CAD winding-pack envelope has an outer diameter of approximately 35 mm, an inner diameter of approximately 10 mm and an axial thickness of 8 mm. The corresponding radial winding width is

$$w_r = \frac{35 - 10}{2} = 12.5\,\text{mm}, \tag{5.9}$$

giving a gross winding-window section of approximately

$$A_{\text{window}} = 12.5 \times 8 \approx 100\,\text{mm}^2. \tag{5.10}$$

This packaging constraint limits the conductor cross-section that can be assigned to each turn. Consequently, the previously considered $10\,\mathrm{mm}^2$ equivalent conductor bundle is not retained as a final winding definition. The detailed conductor size and strand arrangement must be selected jointly with the final turn count, fill factor, resistance and thermal constraints.

The present 96-turn geometry is therefore retained as a preliminary inductance-sizing reference consistent with the concept-level model, while the final winding resistance and conductor arrangement remain part of the detailed electromagnetic optimization.

Why Multiple Parallel Conductors. The final winding may use multiple smaller conductors in parallel rather than a single large conductor. This can be useful during a fast discharge because the AC resistance can become higher than the corresponding DC value.

- **Skin effect:** The rapidly varying current tends to become concentrated toward the outer region of the conductor, reducing the effective conducting area [44].
- **Proximity effect:** The magnetic field produced by adjacent turns further modifies the current distribution within each conductor and can increase the effective resistance [44].

Using multiple smaller conductors in parallel may reduce these effects, but the final strand size and arrangement must be verified once the winding geometry is fixed.

5.6 HV Routing and Shielding

Transferring the energy pulse (400 V, approximately 1.73 kA peak) from the capacitor bank to the TCA module requires dedicated routing, sized both electrically and in terms of safety.

Cable cross-section. The thermal severity of the discharge pulse is firstly evaluated through the current-squared-time integral. For the nominal discharge waveform

$$I^2t \approx 800\,\mathrm{A}^2\mathrm{s}. \tag{5.11}$$

Using the standard adiabatic form

$$I^2 t \leq k^2 S^2, \tag{5.12}$$

with copper thermal coefficient $k = 143$ [45] and a preliminary conductor cross-section $S = 10\,\mathrm{mm}^2$, gives

$$k^2 S^2 = 143^2 \times 10^2 \approx 2.0 \times 10^6\,\mathrm{A}^2\mathrm{s}. \tag{5.13}$$

The pulse-heating requirement is therefore far below the adiabatic short-circuit thermal capability of the conductor. This comparison does not size the cable completely, because connector inductance, resistance, pulse-current capability and mechanical routing remain relevant. For a flexible automotive HV cable of class 5–6 with a nominal 10 mm² cross-section (resistance 1.91 mΩ/m at 20 °C according to IEC 60228 [46]), with a total routing length per door of about 1.5 m thanks to the decentralized packaging of the power module, the wiring resistance is $R_{\mathrm{wiring}} = 1.91\,\mathrm{m\Omega/m} \times 1.5\,\mathrm{m} \approx 2.86\,\mathrm{m\Omega}$. – the value used in the resistive budget of Section 5.5.

EMC and Shielding Considerations. The high current transient from 0 to 1.73 kA within about a millisecond can generate conducted and radiated electromagnetic disturbances, so the connection between the power module and the actuator requires dedicated EMC consideration.

Shielded automotive HV cables conforming to ISO 19642-9 requirements [47] is therefore considered as a preliminary routing solution (e.g. Coroplast or Huber+Suhner RADOX).

The cable shield mainly reduces electric-field and high-frequency electromagnetic coupling. The local magnetic field generated by the Thomson coil requires a separate assessment.

Additional local magnetic-flux management may be required around the TCA cartridge. High-permeability materials such as Mu-metal may be investigated as one possible shielding approach; however, placing magnetic material close to the actuator can modify the useful electromagnetic coupling and may affect the generated force [48, 49].

For this reason, the magnetic shield is not considered as a finalized design and must be evaluated with the detailed electromagnetic model.

5.7 Cold Wiring

One objective of the electrical architecture is to reduce permanently energized high-voltage wiring in the roof and pillar regions, where large structural deformation may occur during a crash.

For this reason, the DC-DC boost converter and capacitor bank are located in a local power module at the lower part of the body structure. The roof-side discharge cable is positioned downstream of the SCR and remains nominally de-energized during normal vehicle operation.

It is energized only during the short emergency discharge. This arrangement is referred to here as a *cold-wiring* architecture and reduces the amount of continuously energized HV routing in structurally vulnerable areas. The low-voltage supply required to charge and control the system must remain available during the relevant crash condition. Its post-crash availability is therefore treated as a functional requirement of the final vehicle architecture rather than as an assumed property of every 12/48 V network.

Residual-energy discharge. Each door-level power module includes a controlled bleed path for post-event and service conditions. For the complete door-level capacitance

$$C_{\text{door}} = 9.4\,\text{mF}, \tag{5.14}$$

a target time constant of approximately 5 s gives

$$R_{\text{bleed}} = \frac{\tau}{C} = \frac{5}{9.4 \times 10^{-3}} \approx 532\,\Omega. \tag{5.15}$$

Starting from 400 V, the voltage after 10 s is

$$V(10) = 400\,e^{-10/(RC)} \approx 54\,\text{V}. \tag{5.16}$$

The selected resistance therefore brings the nominal capacitor-bank voltage below the adopted 60 V target within approximately 9.5 s. The initial resistor power is

$$P_0 = \frac{V_0^2}{R} = \frac{400^2}{532} \approx 301\,\text{W}, \tag{5.17}$$

but this value decays exponentially and should be interpreted as the initial transient power rather than as a continuous resistor rating. The resistor and switching element must ultimately be selected from their pulse-energy capability.

5.8 Chapter Summary

The electrical architecture developed in this chapter combines a 400 V pulse-power domain with a 4.7 mF single-hinge-equivalent capacitance and a 9.4 mF door-level capacitor bank. The nominal door-level stored energy is approximately 752 J.

The discharge path is represented by target lumped parameters of $L \approx 0.2\,\mathrm{mH}$ and $R \approx 0.03\,\Omega$, together with an SCR-based switching architecture. Preliminary analytical checks were used to assess capacitor energy, conductor pulse-heating capability, wiring resistance, winding-pack feasibility and residual-energy discharge.

The detailed coil conductor arrangement and vehicle-level EMC performance remain open design items requiring electromagnetic FEM and hardware validation. The electrical parameters established here are the inputs adopted in the numerical release model developed in Chapter 6.

Chapter 6

Numerical Modelling and Robustness Assessment

This chapter integrates the mechanical layout developed in Chapter 4 and the electrical sizing from Chapter 5 into a single electromechanical model implemented in the Simscape 1D environment. The primary objective is to assess the proposed concept numerically against the industrial pyrotechnic benchmark (Autoliv pyrotechnic pin-pusher, 1500 N over 15 mm, release time $<$ 1 ms) [5] and to evaluate its response under the degraded rollover load cases defined in this thesis.

Section 6.1 describes the simulation architecture. Section 6.2 shows the electric and electromagnetic transients, while Section 6.3 presents the resulting mechanical kinematics of the pin. Section 6.4 extends the numerical assessment through a parametric sensitivity analysis covering degraded rollover load cases. Finally, Section 6.5 investigates the robustness of the system at the end of the vehicle's service life, and Section 6.6 discusses the distinct low-frequency dynamics governing the final door-ejection.

6.1 Modelling Approach and Simulation Domains

The transient generated by the TCA operates on two drastically different time scales: the electromagnetic release happens in the order of a few milliseconds, while the mechanical door ejection takes hundreds of milliseconds after the hinge is freed.

Solving both phenomena within a single solver would necessitate an inefficiently small time step across a long simulation window. Therefore, a decoupled approach was adopted: the fast electromagnetic release (0-20 ms) is simulated numerically in the Simscape 1D environment, while the low-frequency door-ejection response is treated separately through a preliminary mechanical and energy-based assessment.

A 1D lumped-parameter environment such as Simscape was preferred over a

full 3D FEM/Multiphysics tool (e.g. Ansys Maxwell coupled to a structural solver) for this concept-assessment phase for three practical reasons. First, it allows the electrical, electromagnetic-coupling and mechanical domains to be assembled and iterated rapidly as the design parameters of Chapters 4 and 5 evolved. Second, it keeps the position-dependent force law $k(x)$ explicit, rather than hidden inside a mesh-dependent field solution, which is valuable when the goal is to build engineering intuition about the release transient. Third, it allows rapid iteration of the investigated scenarios with a much lower computational cost than a coupled 3D multiphysics model. The trade-off, already acknowledged in Section 5.1.1, is that the position-dependent coefficient $k(x)$ derives from literature data rather than a first-principles field solution specific to this actuator's geometry. As stated previously, the 2D/3D FEM refinement remains a planned future step (Chapter 8).

The Simscape model reproduces the discharge circuit and the mechanical release chain through three interacting domains, as shown in Figure 6.1:

- **Electrical domain:** A 400 V DC source charges the single-hinge-equivalent capacitor (4.7 mF). An ideal switch simulates the SCR trigger closing the discharge path through the Thomson coil, characterized by an inductance of 0.2 mH and a total resistive budget of 0.03 Ω (as defined in Sections 5.5 and 5.6).

- **Electromagnetic coupling:** A MATLAB Function block converts the instantaneous coil current and disk position into the electromagnetic Force. It uses the lumped relation

$$F(t) = k(x)i(t)^2. \tag{6.1}$$

  The pin position x is read from the mechanical domain and used to update the coupling coefficient through the look-up table $k(x)$. In this way, the model accounts for the reduction in electromagnetic coupling as the disk-to-coil gap increases.

- **Mechanical domain:** An ideal force source applies the computed electromagnetic force to a translational mass of 0.05 kg. This value is higher than the approximately 18 g moving mass estimated in Subsection 4.2.3, providing a conservative inertia assumption. The motion is opposed by the prescribed resistive-load model and limited by a mechanical hard stop at the 15 mm release position.

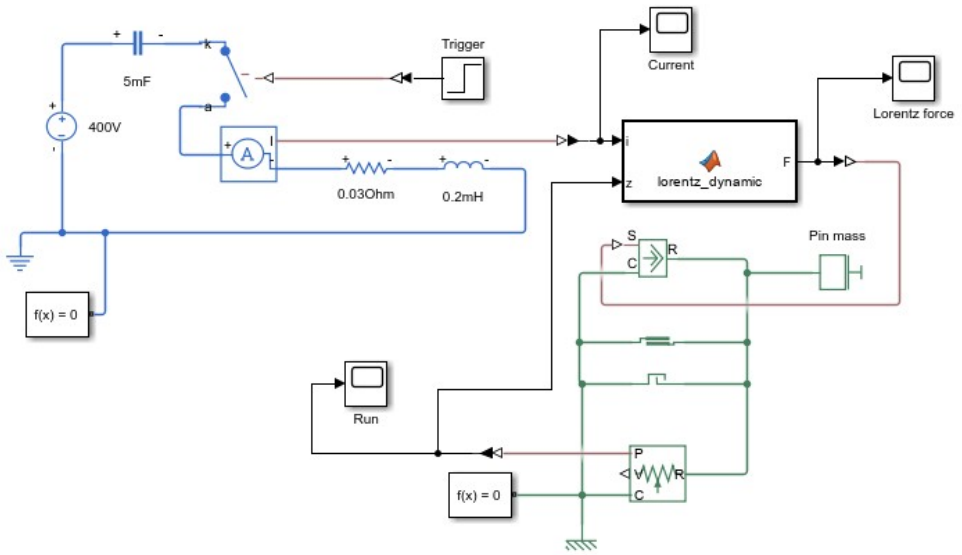


Figure 6.1: Simscape 1D model architecture, including the electrical discharge circuit, electromagnetic coupling block and mechanical release chain.

The simulation utilized an ideal, bidirectional switch rather than a unidirectional SCR model. This methodological choice was made to observe the oscillatory RLC response over several cycles (Section 6.2). In the physical hardware, the SCR blocks any reverse current at the first zero crossing ($t \approx 3ms$) [25]; so, only the initial current and force peaks are functionally relevant for the release mechanism.

6.2 Electric and Electromagnetic Transient

Figure 6.2 shows the current delivered by the capacitor bank into the pancake coil under nominal conditions. The circuit exhibits a classic underdamped RLC response, peaking at $\approx 1.73\,\mathrm{kA}$ around $t \approx 1.5\,\mathrm{ms}$, followed by a decaying oscillation.

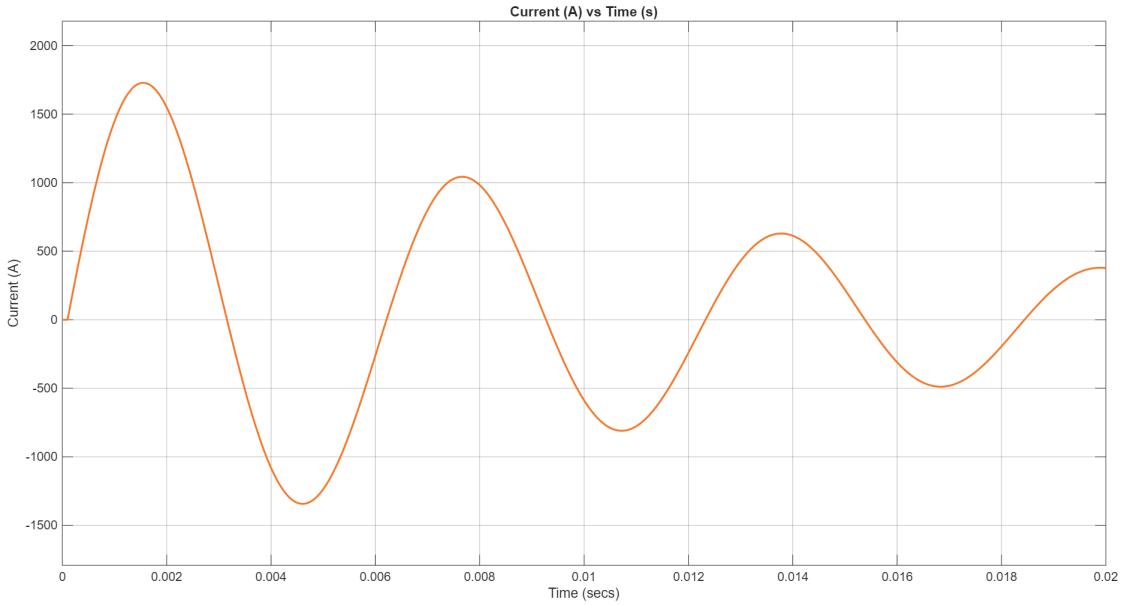


Figure 6.2: Coil current during the nominal discharge transient ($R = 0.03\,\Omega$, $L = 0.2\,\mathrm{mH}$, $C = 4.7\,\mathrm{mF}$ and $V_0 = 400\,\mathrm{V}$).

6.2.1 Analytical Cross-Check of the RLC Transient

To ensure numerical reliability, the simulated waveform can be verified independently via the standard series-RLC discharge solution. Using the parameters established in Chapter 5, the undamped natural frequency (ω_0) and the damping attenuation (α) of the circuit are:

$$\omega_0 = \frac{1}{\sqrt{LC}} \approx 1.03 \times 10^3\,\mathrm{rad/s}, \qquad f_0 \approx 164\,\mathrm{Hz}, \qquad T_0 \approx 6.1\,\mathrm{ms}, \tag{6.2}$$

$$\alpha = \frac{R}{2L} \approx 75\,\mathrm{s}^{-1}, \qquad \tau = \frac{1}{\alpha} \approx 13.3\,\mathrm{ms}. \tag{6.3}$$

The resulting damping ratio $\xi = \alpha/\omega_0 \approx 0.073$ confirms that the circuit is only lightly damped. The corresponding damped natural frequency is approximately $1029\,\mathrm{rad/s}$, giving a first-current-peak time of about 1.46 ms. The analytical peak-current estimate is therefore:

$$i_{\text{peak}} \approx \frac{V_0}{\omega_d L} \exp(-\alpha t_{\text{peak}}) \approx 1.74\,\text{kA}. \tag{6.4}$$

This analytical cross-check is consistent with the approximately 1.73 kA first peak visible in the Simscape result. The comparison supports the internal consistency of the lumped RLC model, but it is not an experimental validation of the physical actuator.

6.2.2 Electromagnetic Force Transient

Figure 6.3 shows the electromagnetic force predicted by the position-dependent lumped model. Under nominal conditions, the force reaches a peak of approximately 4.3 kN at about 0.7 ms, before the current reaches its first maximum. A similar offset between force and current has been reported in the TCA literature [50, 51]. In the present model, it is mainly associated with the position dependence of the electromagnetic coupling coefficient $k(x)$. During the first part of the discharge, the current rises rapidly while the conductive disk is still close to the coil. As the disk begins to move and the air gap increases, the coupling coefficient decreases. The force can therefore reach its maximum before the current reaches its own peak.

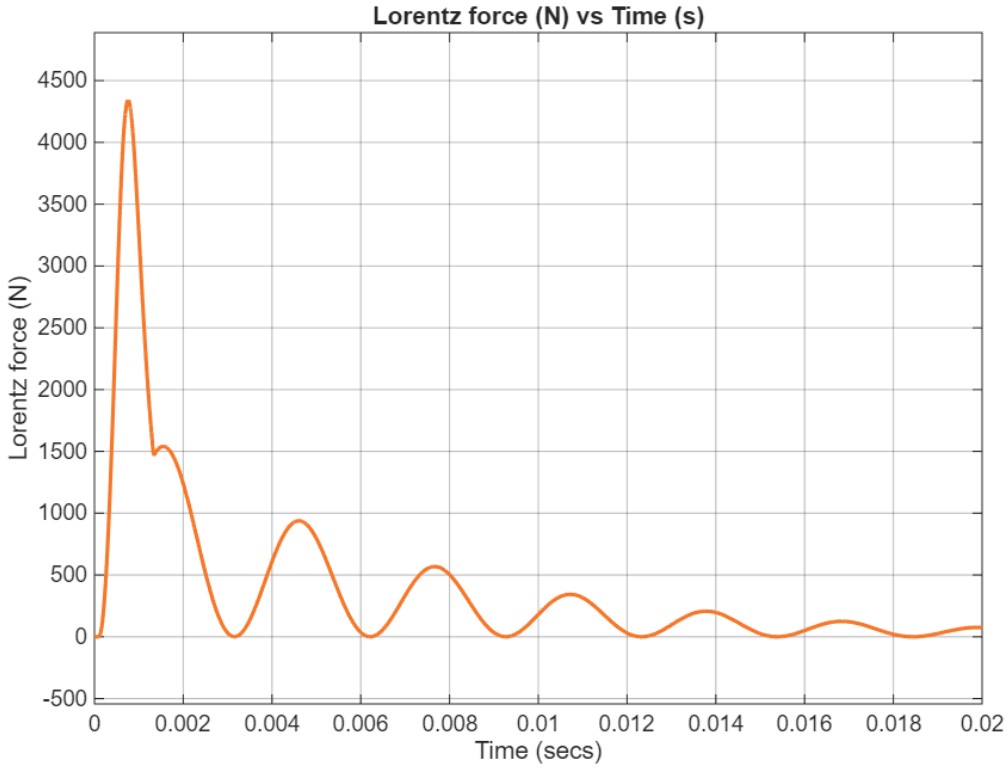


Figure 6.3: Electromagnetic force predicted during the nominal TCA discharge. The modeled peak is approximately 4.3 kN at about 0.7 ms.

Because the force peak occurs while the disk is still close to the coil, the initial value of the lumped coefficient k remains a useful order-of-magnitude check. Using a current of roughly 0.9 kA around the force-peak region gives a force of the order of 4 kN from $F = ki^2$, consistent in magnitude with the 4.3 kN predicted by the position-dependent Simscape model. The comparison is used as an internal consistency check rather than as an independent validation.

This early force peak provides the principal impulsive load available to the release interface and is the value used as a preliminary design reference for the shear-ring assessment in Subsection 4.2.3.

6.3 Pin Release Kinematics

Figure 6.4 shows the resulting pin displacement under nominal conditions as a function of time. The impulsive Lorentz force acts on the 0.05 kg moving mass while the nominal resistive load opposes the motion.

In the numerical model, the pin reaches the prescribed 15 mm release position within approximately 1–2 ms. The mechanical hard stop then limits any further

displacement. This result shows that, under the nominal model assumptions, the predicted electromagnetic transient is compatible with the required short-stroke release time.

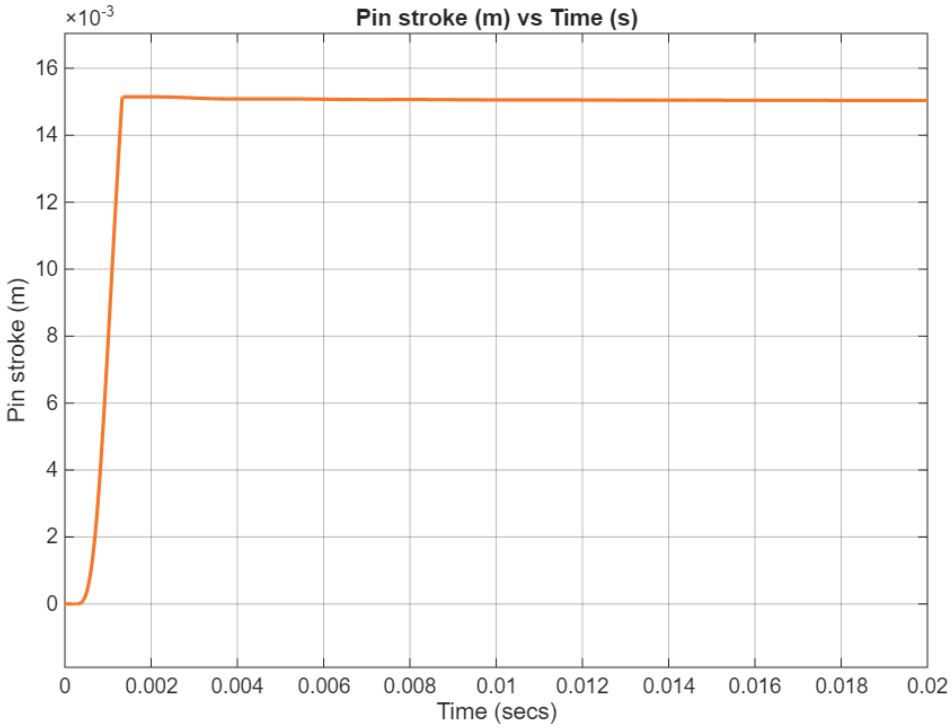


Figure 6.4: Predicted pin displacement under nominal conditions. The prescribed 15 mm release position is reached within approximately 1–2 ms.

6.4 Sensitivity Analysis under Degraded Rollover Conditions

A release mechanism intended to operate after a rollover should not be assessed only under nominal conditions. Its response must also be examined under increased mechanical resistance associated with crash-induced misalignment.

To represent this effect, seven values of equivalent radial contact load were defined:

$$F_{\text{rad}} = \{1,\ 5,\ 9,\ 14,\ 17.5,\ 18.5,\ 20\}\,\text{kN} \tag{6.5}$$

The effect of crash-induced misalignment is represented through an equivalent radial contact load F_{rad}. Under the simplified Coulomb-friction assumption adopted in the model, the corresponding opposing force is

$$F_C = \mu F_{rad} \tag{6.6}$$

where μ is the effective friction coefficient used in the model. For the present sensitivity sweep, a representative value of $\mu = 0.30$ was adopted.

Figure 6.5 overlays the resulting pin-stroke curves over the 20 ms simulation window.

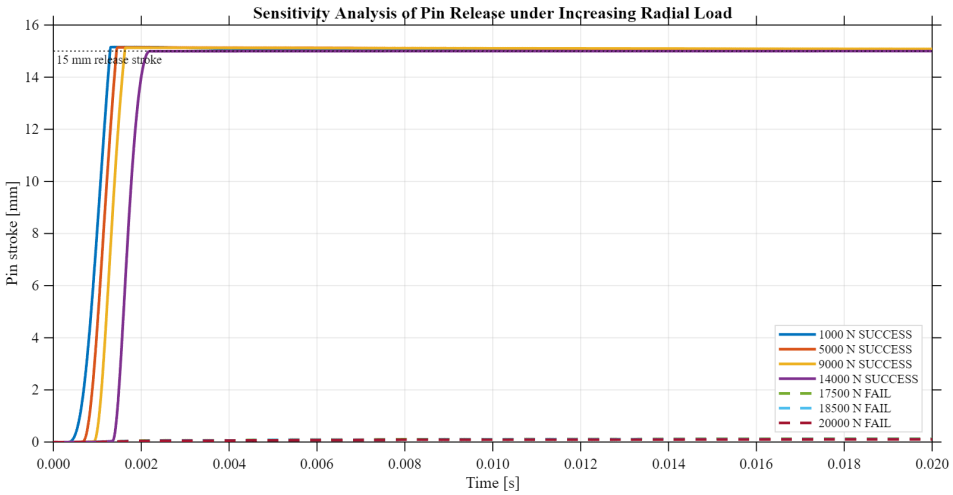


Figure 6.5: Pin-displacement sensitivity to the imposed equivalent radial load. Complete release is obtained for the 1, 5, 9 and 14 kN cases, while the 17.5, 18.5 and 20 kN cases do not reach the prescribed 15 mm release position within the investigated time window.

The discrete sweep shows a transition between complete and incomplete release. For equivalent radial loads of 1, 5, 9 and 14 kN, the pin reaches the 15 mm release stroke. Increasing the imposed load progressively delays the extraction. At 17.5 kN and above, the pin no longer completes the required stroke and the simulated displacement remains close to its initial position.

The present discrete sweep places the numerical loss-of-function boundary between 14 and 17.5 kN,

$$14\,\text{kN} < F_{rad,lim} < 17.5\,\text{kN} \tag{6.7}$$

This interval represents the transition obtained from the adopted one-dimensional equivalent-load model and should not be interpreted as a vehicle-level structural limit or certified safety factor. The highest investigated load case for which complete release is obtained is 14 kN, retained here only as a numerical robustness reference.

The analysis also simplifies the evolution of the cup-and-cone contact during disengagement. As discussed in Subsection 4.2.2, axial pin displacement progressively opens the radial clearance according to $g(x) = x\tan(\alpha)$, reducing contact interaction as disengagement proceeds. The one-dimensional sensitivity model does not reproduce the complete three-dimensional evolution of contact pressure, local deformation and friction as the conical surface separates. The load sweep is therefore interpreted as a parametric robustness assessment of the actuator rather than as a vehicle-specific rollover structural simulation. A coupled structural finite-element and contact analysis would be required to establish the corresponding physical deformation limit for the complete hinge assembly.

6.5 End-of-Life Robustness Analysis

In addition to the nominal operating condition, a degraded electrical scenario was investigated to assess the sensitivity of the release mechanism to a simultaneous reduction in stored energy and increase in series resistance. This analysis is intended as an End-of-Life (EoL) robustness case rather than as a prediction of capacitor ageing over a specified vehicle lifetime.

The nominal single-hinge equivalent model uses a capacitance of 4.7 mF charged to 400 V with a total lumped series resistance of 0.03 Ω. For the degraded case, the model parameters were changed to

$$C_{\mathrm{EoL}} = 4.0\,\mathrm{mF}, \qquad V_{\mathrm{EoL}} = 360\,\mathrm{V}, \qquad R_{\mathrm{EoL}} = 0.06\,\Omega, \tag{6.8}$$

while the inductance was maintained at 0.2 mH. The corresponding initial electrical energy is

$$E_{\mathrm{EoL}} = \frac{1}{2}C_{\mathrm{EoL}}V_{\mathrm{EoL}}^2 = \frac{1}{2}(4.0\times10^{-3})(360)^2 \approx 259\,\mathrm{J}. \tag{6.9}$$

For comparison, the nominal 4.7 mF, 400 V equivalent channel stores

$$E_{\mathrm{nom}} = \frac{1}{2}(4.7\times10^{-3})(400)^2 \approx 376\,\mathrm{J}. \tag{6.10}$$

The investigated degraded condition therefore corresponds to an approximately 31% reduction in initial stored energy, together with a doubling of the lumped series resistance. It represents a deliberately degraded electrical operating point used to evaluate the robustness of the numerical release model.

Figure 6.6 compares the resulting current response with the reduced electrical parameters.

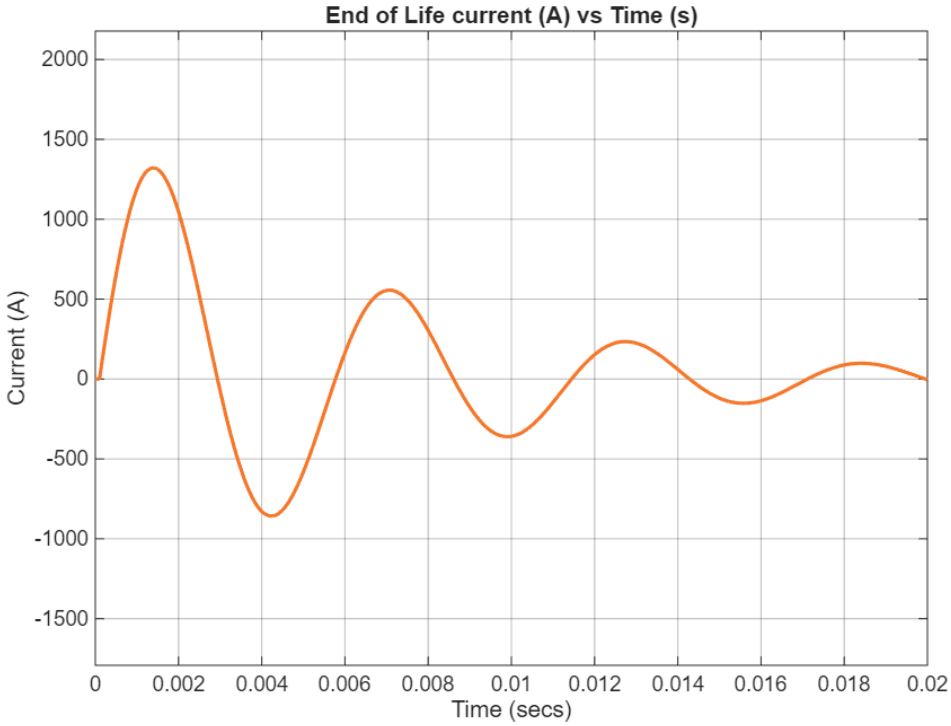


Figure 6.6: Discharge-current response for the investigated degraded EoL condition ($C = 4.0\,\text{mF}$, $V_0 = 360\,\text{V}$ and $R = 0.06\,\Omega$).

The degraded electrical parameters reduce the first current peak to approximately 1.3 kA, compared with approximately 1.73 kA in the nominal 4.7 mF model. The increased series resistance also produces stronger damping of the oscillatory discharge. Despite this reduction in current amplitude and available electrical energy, the simulated mechanical response still completes the required pin extraction, as shown in Figure 6.7.

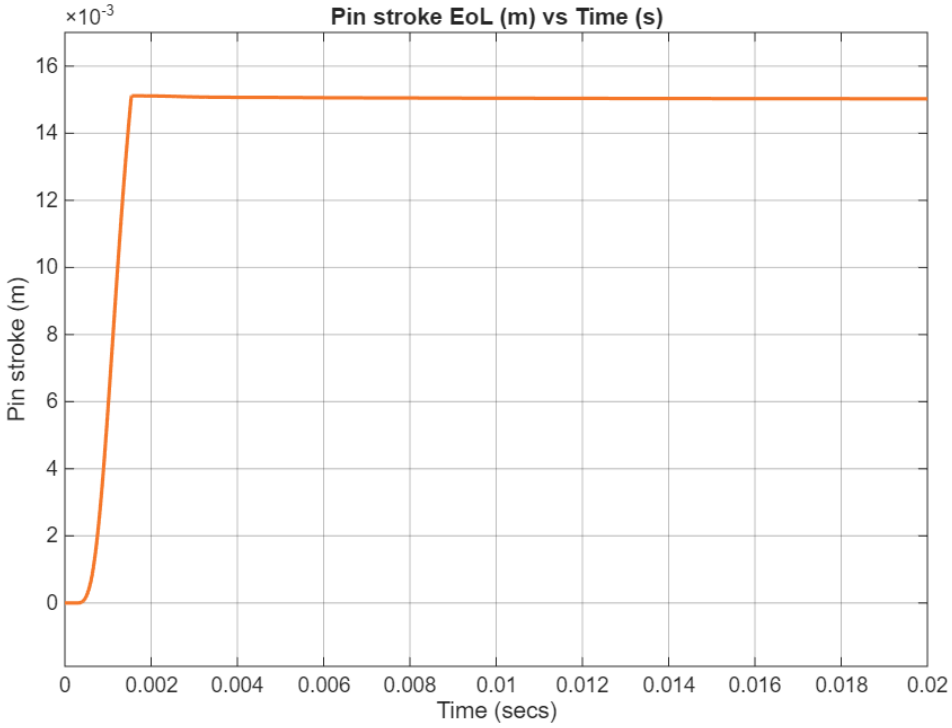


Figure 6.7: Pin-stroke response for the investigated degraded EoL electrical condition. The pin reaches the required 15 mm release position in the numerical model.

The EoL simulation therefore indicates that successful release is retained for the investigated degraded electrical condition. This result should be interpreted as a numerical robustness check rather than as a certified lifetime capability. In particular, the selected values of capacitance, initial voltage and series resistance are imposed degraded parameters; establishing their relationship with a specified service life would require component ageing data, temperature-dependent degradation models and experimental validation.

The result also clarifies the role of the preliminary energy sizing presented in Section 5.2. The previously calculated 375 J value is a first-order sizing estimate based on assumed mechanical work and conversion efficiency, rather than a strict minimum-energy threshold for successful actuation. The present simulation predicts complete release even though the degraded equivalent channel initially stores approximately 259 J. This does not invalidate the preliminary energy calculation; instead, it shows that the detailed transient model and the preliminary energy-screening calculation serve different purposes and should not be interpreted as equivalent validation criteria.

6.6 Low-Frequency Dynamics: Door Ejection

As explained in Section 6.1, the lower-frequency door-ejection response was assessed separately via the energy balances in Subsection 4.2.4 (spring stiffness $k = 8\,\mathrm{N/mm}$, stored energy 90 J, peak force 1200 N). This preliminary spring target was informed by an earlier simulation using a softer spring (5.3 N/mm, peak force 800 N). As shown in Figure 6.8, the door reaches a peak displacement of approximately 183 mm at $t \approx 0.2\,\mathrm{s}$. However, gravity, acting under the assumed upside-down vehicle condition, subsequently causes the displacement to decrease towards approximately 80 mm. Since the adopted concept-level target is a door displacement of 150 mm, the initial configuration was considered inadequate despite its transient overshoot beyond this value. This result motivated the adoption of the higher preliminary spring target ($k = 8\,\mathrm{N/mm}$, peak force 1200 N and approximately 90 J of stored energy) presented in Subsection 4.2.4. The low-frequency analysis therefore provides a preliminary dynamic check supporting the selected ejection-system requirements, while detailed spring design and vehicle-level door-ejection validation remain outside the scope of the present concept study.

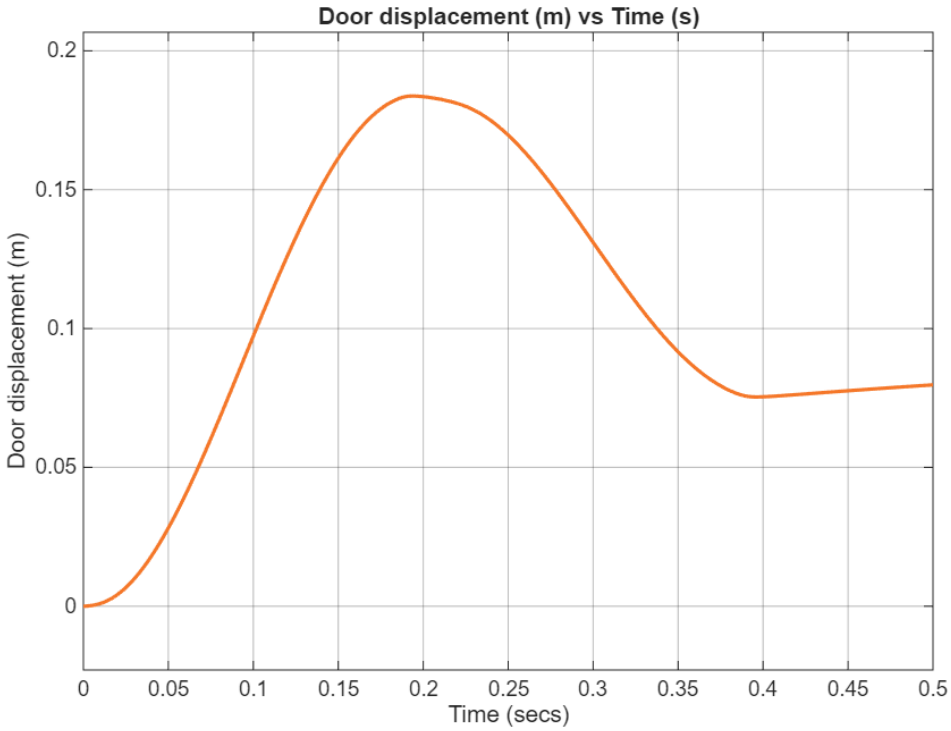


Figure 6.8: Low-frequency door-ejection response for the initial 800 N spring configuration. The door transiently exceeds the 150 mm displacement target but subsequently returns below it under the assumed inverted-vehicle condition.

6.7 Chapter Summary

The Simscape 1D model provides a concept-level assessment of the electrical transient and release kinematics. Under the nominal parameter set, the first current peak is approximately 1.73 kA, the predicted electromagnetic-force peak is approximately 4.3 kN, and the modeled pin reaches the 15 mm release stroke at approximately 1–2 ms.

The sensitivity analysis predicts complete release for the investigated equivalent radial-load cases up to 14 kN and incomplete release for the investigated cases from 17.5 kN upward.

Furthermore, the investigated degraded End-of-Life condition ($C = 4.0\,\mathrm{mF}$, $V_0 = 360\,\mathrm{V}$ and $R = 0.06\,\Omega$) also retains successful pin release in the numerical model, providing a robustness check against simultaneous energy reduction and increased series resistance.

The results therefore support the concept-level feasibility of the HDRM-TCA release architecture under the assumptions adopted in the model. They do not replace geometry-specific electromagnetic, structural and experimental verification, which remains part of the future development described in Chapter 9.

Chapter 7

Functional Safety and Failure Analysis

The System Engineering analysis of Chapter 2 identified post-rollover egress as a critical function of the gullwing architecture. Chapters 4– 6 subsequently developed the HDRM-TCA concept and assessed its predicted release performance numerically.

The introduction of a high-voltage electromagnetic release device also creates failure modes that are not present in a conventional mechanical hinge. These failure modes must therefore be considered before the proposed solution architecture can be compared with a production pyrotechnic solution from a functional-safety perspective.

This chapter extends the function-level FMEA of Chapter 2 to the component and control-logic level of the HDRM-TCA system. Section 7.1 frames the functional-safety context; Section 7.2 develops the rollover-detection Sensor Fusion Logic that authorizes deployment; Section 7.3 presents the FMEA of the new hardware failure modes and their mitigations; Section 7.4 details the electrical risk-mitigation architecture; Section 7.5 covers maintenance safety protocols and manual override procedures; Section 7.6 provides a summary of the Chapter.

7.1 Functional Safety Framing

According to ISO 26262 [39], vehicle-level hazards are assessed through a Hazard Analysis and Risk Assessment (HARA), considering severity, exposure and controllability.

An unintended release of a gullwing-door hinge during normal driving could have severe consequences because it can cause a sudden change in the door state. For this reason, the present concept treats the release-control path as an ASIL-D-oriented design target. A formal HARA assignment is not made in this thesis,

since this would require a complete vehicle-level HARA and safety concept.

Modifying the actuator technology does not remove the underlying hazard, so the release authorization logic and its failure modes must be designed accordingly. The electrical hazards of the 400 V pulse domain are addressed separately from the functional safety classification.

7.2 Rollover Detection: Sensor Fusion Logic

A single sensor is not enough to authorize the emergency release. For example, a basic accelerometer cannot easily tell the difference between a real, unrecoverable rollover and a temporary loss of gravity. This temporary effect can happen during an aggressive jump, a severe curb strike, or when driving fast over a steep hill. In these situations, the car might seem upside down to the sensor for a moment, even if it is not.

The present concept therefore uses a multi-sensor safing approach based on independent physical quantities. Candidate information channels include:

- Primary trigger: Vehicle attitude and roll rate: A 3-axis MEMS gyroscope provides the roll-rate information. Together with accelerometer data, this signal can be used to estimate the vehicle attitude and identify a developing rollover condition. Established estimation approaches include filtering techniques based on 6-DOF IMU data [52].

- Secondary trigger: Suspension and vertical-dynamics information: Suspension travel and vertical/lateral acceleration provide additional info on wheel unloading and vehicle inversion. These signals can help distinguish a rollover from short airborne events such as jumps or severe road inputs.

- Vehicle-motion cross-check: Wheel-speed signals and other chassis-dynamics information can provide additional confirmation of wheel unloading or vehicle inversion. At concept level, these signals are treated as supplementary inputs rather than as a finalized trigger condition.

At concept level, deployment is authorized only when the available sensing channels provide mutually consistent evidence of an unrecoverable rollover. The exact threshold, voting logic, timing windows and diagnostic coverage are not frozen in this thesis and must be defined during the formal vehicle-level safety-development process.

This sensor-fusion approach is intended to reduce susceptibility to single-sensor false activation while avoiding reliance on a single measurement channel.

7.3 Failure Mode and Effects Analysis of the HDRM-TCA System

Table 7.1 extends the function-level FMEA of Chapter 2 to the specific hardware and control-logic failure modes introduced by the TCA release mechanism, together with the design countermeasure adopted against each. Several of these countermeasures were already introduced in Chapter 4 and 5 for functional reasons; they are collected and cross-referenced here as a single safety-oriented view of architecture.

Table 7.1: Failure mode and effects analysis of the HDRM-TCA emergency-release system.

Failure mode	**Potential cause**	**Effect if unmitigated**	**Design countermeasure**
Unwanted/accidental pin release	High lateral acceleration (2–3 g), road vibration, NVH loading over vehicle life	Door unintentionally disengages during ordinary driving	Aluminum sacrificial shear ring (Subsection 4.2.3): provides mechanical retention under normal operating conditions. The final break-load window and material selection require experimental calibration.

continued on next page

Table 7.1 – *continued from previous page*

Failure mode	**Potential cause**	**Effect if unmitigated**	**Design countermeasure**
Capacitor energy degradation/self discharge	Dielectric self-discharge over long periods of vehicle inactivity; thermal ageing of the electrolyte over the vehicle lifetime	Insufficient stored energy at the moment of an actual rollover	Continuous standby charging and capacitor-voltage monitoring; diagnostic estimation of capacitance, ESR or series-path degradation may be added in the detailed implementation. The degraded electrical case is assessed in Section 6.5
Electromagnetic interference	Rapid current transient, with a peak of approximately 1.73 kA, generating conducted and radiated electromagnetic disturbances	Corruption or damage to vehicle electronics	Shielded HV routing according to the preliminary architecture of Section 5.6, followed by vehicle-level EMC verification. Additional magnetic-flux management around the TCA may be required and must be evaluated together with the final electromagnetic design.

continued on next page

Table 7.1 – *continued from previous page*

Failure mode	**Potential cause**	**Effect if unmitigated**	**Design countermeasure**
False-positive activation while driving	Single-sensor misinterpretation of potholes, curb strikes or jumps as a rollover	Door ejects at speed: sudden structural failure at cruising speed	Multi-sensor safing architecture (Section 7.2) using independent vehicle-dynamics signals and diagnostic checks before release authorization.
Service/maintenance misuse	Technician works on a hinge with the capacitor bank still charged	Accidental firing during disassembly; risk of injury	Lock-Out Tag-Out procedure and physical Manual Service Disconnect (Sections 7.4 and 7.5)
Propagation of an HV fault into the LV logic domain	Insulation failure or short circuit in the 400 V wiring	Corruption of the vehicle's low-voltage control and sensing logic	Galvanically isolated DC-DC boost converter (Section 5.3), separating the Sensor Fusion logic network from the 400 V power domain.

continued on next page

Table 7.1 – *continued from previous page*

Failure mode	**Potential cause**	**Effect if unmitigated**	**Design countermeasure**
Loss of residual post-crash electrical safety	Capacitor bank retains stored energy after the crash event	Electrocution risk for occupants or rescue personnel during extrication	Cold-wiring architecture and active bleed circuit (Section 5.7, Section 7.4): roof-side HV routing is normally de-energized during normal vehicle operation and energized only during the commanded discharge. Residual capacitor energy is removed through the controlled bleed path.
Single-point failure of the SCR trigger path	Gate-driver fault or SCR failure to fire on a given hinge	Non-deployment of one of the four hinges in a genuine rollover	Not resolved at concept level in this thesis; identified as an open item for the detailed-design phase (redundant trigger path or continuous self-test), see Chapter 8.

7.4 Electrical Risk Mitigation: Cold Wiring and Active Bleeding

The presence of class B (> 60 V DC) potential close to the passenger cell requires dedicated measures to reduce electrical-shock risk for occupants, first responders and maintenance personnel. These measures operate independently of, and in addition to, the logic-control safeguards detailed in Section 7.2. Two complementary mechanisms, already introduced for their electrical rationale in Section 5.7, are summarised here from a functional-safety perspective.

- Cold wiring: The DC-DC boost converter, capacitor bank and the SCR are integrated into the lower power module. The roof-side discharge cable is positioned downstream of the SCR and is therefore normally de-energized during ordinary vehicle operation. It is energized only during the short release pulse. This arrangement reduces the duration and spatial extent of possible HV exposure in the pillar and roof regions.
- Active bleeding: Each door power module consists of two 4.7 mF capacitors in parallel, corresponding to 9.4 mF, approximately 752 J at 400 V. For the preliminary bleed resistance $R_{\text{bleed}} \approx 532\,\Omega$, the time constant is approximately 5 s and the ideal RC discharge reaches 60 V after approximately 9.5 s. The resistor and switching path must be selected according to their pulse-power and pulse-energy capability [53, 54].

Together, these mechanisms are intended to reduce post-crash exposure to energized conductors and residual capacitor energy. Their effectiveness must be verified against the final vehicle architecture and the applicable post-crash electrical-safety requirements.

7.5 Maintenance Safety and Manual Override

Beyond the automatic bleed circuit, workshop-level safety requires the system to be positively de-energized before work is carried out on the hinge or power module.

The detailed-design architecture should include a physically removable Manual Service Disconnect (MSD). Removing the MSD mechanically opens the upstream HV circuit and can also initiate the bleed-resistor discharge path, preventing normal recharging and actuator firing while the system is in the service configuration.

This hardware safeguard is complemented by a software-level Lock-Out Tag-Out (LOTO) service mode that disables capacitor charging for the duration of a maintenance operation.

The pyrotechnic benchmark also provides a manual emergency-release path in motorsport applications. On the SLS AMG GT3 variant, an external pull-ring at the base of the windscreen allows rescue marshals to detonate the pyrotechnic hinges from outside the vehicle, while a centre-console switch gives the driver the same capability, in order to meet FIA homologation requirements on rollover and fire-related extraction speed [55, 56].

A similar function could be considered for the HDRM-TCA architecture, for example through an external rescue command or a dedicated emergency switch.

Unlike a pyrotechnic actuator, the electromagnetic one itself does not consume an energetic charge during activation. However, a complete deployment of the present concept is not fully reversible because the sacrificial shear ring must be replaced and the release mechanism should be inspected and reset before the vehicle is returned to service.

7.6 Chapter Summary

This chapter extended the function-level FMEA of Chapter 2 to the hardware and control-logic level of the HDRM-TCA system. A multi-sensor safing concept was introduced to reduce susceptibility to single-sensor false positives, while the component-level FMEA identified the principal failure modes associated with the actuator, capacitor bank, switching path, HV routing and post-crash residual energy. The resulting mitigation concept includes sacrificial mechanical retention, capacitor-state monitoring, galvanic isolation, shielded HV routing, normally de-energized roof-side wiring, controlled residual-energy discharge and service lockout provisions. These measures constitute concept-level safety requirements rather than a completed ISO 26262 safety case.

A potential single-point failure in the SCR trigger path remains unresolved at this stage and is carried forward as an explicit design item requiring diagnostic coverage or redundancy during detailed development.

Chapter 8

Discussion

The previous chapters developed the HDRM-TCA architecture (Chapter 4), its electrical and electromagnetic dimensioning (Chapter 5), its numerical assessment (Chapter 6) and its functional-safety architecture (Chapter 7).

This chapter synthesizes the results obtained throughout the thesis to evaluate the proposed HDRM-TCA architecture against the primary objective defined in Chapter 1: engineering an emergency release mechanism that provides millisecond-scale actuation and a force level comparable with the pyrotechnic actuator reference, while avoiding irreversible pyrotechnic deployment.

Section 8.1 assesses the achievement of the initial design targets. Section 8.2 discusses the system's robustness under degraded structural conditions. Section 8.3 analyzes the engineering trade-offs associated with replacing the pyrotechnic baseline. Finally, Section 8.4 examines the limitations of the current numerical models, and Section 8.5 discusses the potential application of the proposed mechatronic approach beyond the specific gullwing door application.

8.1 Achievement of the Design Targets

The qualitative comparison of Table 4.1 can now be considered together with the quantitative results of Chapter 6. Against the Autoliv actuator-level reference of 1500 N over a 15 mm stroke (Section 3.3), the nominal HDRM-TCA model predicts a peak electromagnetic force of $\approx 4.3kN$ and reaches the prescribed 15 mm pin-release position within approximately $1 - 2$ ms.

The predicted force level also provides the basis for the degraded-load sensitivity analysis discussed in Section 6.4. Unlike a pyrotechnic actuator, the electromagnetic actuator itself is not consumed during activation. However, the complete system release is not fully reusable after deployment because the sacrificial shear ring must be replaced.

8.2 Robustness under Degraded Rollover Conditions

The sensitivity analysis of Section 6.4 directly addresses the effect of increased mechanical resistance associated with crash-induced misalignment. The adopted 1D model represents this condition through an equivalent radial load combined with a Coulomb friction coefficient of $\mu = 0.30$.

Complete release is obtained for the investigated radial-load cases up to 14 kN, while incomplete release occurs for the investigated cases from 17.5 kN upwards. The discrete numerical transition is therefore

$$14\,\mathrm{kN} < F_{\mathrm{rad,lim}} < 17.5\,\mathrm{kN}. \tag{8.1}$$

This result provides a numerical robustness indication for the actuator, but it should not be interpreted as a vehicle-level structural limit. The one-dimensional model does not reproduce the complete evolution of contact pressure, local deformation and friction within the cup-and-cone interface.

The End-of-Life analysis of Section 6.5 extends this robustness assessment to degraded electrical parameters. In the investigated case, the capacitance is reduced from 4.7 to 4.0 mF, the initial voltage from 400 to 360 V, and the total series resistance is increased from 0.03 to 0.06 Ω.

These changes reduce the initial stored energy from approximately 376 J to 259 J, corresponding to a reduction of about 31%. The numerical model still predicts complete pin release under this parameter set. This result should be interpreted as a robustness check, rather than as a prediction of component ageing over a specified vehicle lifetime.

8.3 Trade-offs with Respect to the Pyrotechnic Benchmark

The performance characteristics discussed above are obtained at the cost of a more complex electrical architecture. As anticipated in Table 4.1 and quantified in Chapter 5 the proposed system requires a 400 V capacitor domain together with appropriate insulation, HV routing, electrical protection and EMC measures.

This introduces additional packaging, routing and safety requirements compared with the low-energy firing circuit used by a conventional pyrotechnic actuator.

For the hypercar and supercar segment considered in this thesis, this additional complexity may be compatible with the available vehicle architecture and packaging constraints. In vehicles already equipped with high-voltage electrical systems, some of the required insulation, routing and protection practices may also be shared with the existing HV architecture. The trade-off would need to be reassessed for vehicles without an existing high-voltage network.

8.4 Limitations of the Present Model

Several simplifications were adopted throughout this work to keep the concept-design phase tractable. They are collected here as an explicit account of the model limitations and are consistent with the future-work items already identified in Chapters 4 and 6.

- Lumped Electromagnetic Model: The electromagnetic force is computed from a scalar coefficient k, corrected only through a one-dimensional look-up table $k(x)$ built from published literature data (Section 5.1.1 and 6.2.2), rather than from a position-and-geometry resolved electromagnetic field solution. The analytical checks provide internal consistency at concept level, but they do not finalize the coil geometry. A detailed 2D/3D FEM analysis (e.g. Ansys Maxwell) accounting for the actual disk conductivity and skin depth is required before the detailed-design phase.
- Simplified structural friction model: The sensitivity analysis of Section 6.4 represents crash-induced misalignment through an equivalent radial load and a simplified Coulomb friction relationship. This provides a parametric robustness representation, but it is not a substitute for a coupled structural and contact analysis of the roof, hinge region and cup-and-cone interface during a rollover event.
- Preliminary structural verifications: The base-plate bending assessment (Chapter 4) and the pin shear assessment (Subsection 4.2.2) are first-order analytical checks. They do not include the complete 3D stress state, local contact effects or final load-transfer conditions. Detailed structural FEM and experimental verification are therefore required during the detailed-design phase.
- Degraded electrical parameter set: The EoL case of Section 6.5 combines reduced capacitance and initial voltage with increased series resistance. These values are imposed degraded parameters rather than the output of a component-specific automotive ageing model. Their relationship with a defined service life would require qualified ageing data and experimental testing.
- Single-point failure not resolved: Chapter 7 (Table 7.1) identifies a potential single-point failure in the SCR trigger path of an individual hinge but does not propose or evaluate a redundant triggering architecture; this remains open for the functional-safety design phase.
- No experimental validation: All results presented in this thesis are numerical or analytical. The predicted millisecond-scale release response and degraded-condition robustness have not yet been demonstrated on physical hardware. Prototype testing and Hardware-in-the-Loop activities are therefore required before the numerical results can be experimentally validated.

8.5 Generalization Beyond the Gullwing Case

Although this thesis addresses the specific case of a gullwing-door hinge, the combination of geometric anti-binding release and impulsive electrical actuation may also be relevant to other mechanisms subjected to structural misalignment. No comparable automotive application combining the two principles was identified in the literature reviewed for this thesis.

Other pillarless or partially pillarless roof-hinged architectures, such as butterfly or canopy doors, and scissor-door hinges mounted on deformable body structures may present similar release requirements. Related principles may also be applicable to non-hinge systems, such as emergency battery-disconnect mechanisms, where rapid mechanical separation under abnormal loading can be required.

In this sense, the contribution of this thesis can be interpreted as a concept-level assessment of how two established technologies can be combined into a candidate automotive release architecture. Broader applicability remains to be demonstrated for other vehicle mechanisms.

8.6 Chapter Summary

The numerical results of Chapter 6, considered together with the functional-safety architecture of Chapter 7, support the concept-level feasibility of the proposed HDRM-TCA system.

The analyses indicate that the proposed architecture can achieve the required millisecond-scale release while retaining functionality under the investigated degraded electrical and mechanical conditions. At the same time, the sensitivity studies identify the operational limits of the current one-dimensional model.

These results are obtained at the cost of a more complex high-voltage pulse-power architecture compared with the pyrotechnic reference. The present work nevertheless remains a concept-level numerical study. Its electromagnetic, structural, ageing and functional-safety simplifications, together with the absence of physical testing, define the scope of the conclusions and the future work presented in Chapter 9.

Chapter 9

Conclusions and Future Work

9.1 Conclusions Summary

This thesis addresses the engineering challenge of emergency egress after a rollover event in vehicles equipped with gullwing doors. As identified in Chapter 2 through the Systems Engineering analysis, post-rollover egress represents one of the main limitations considered. The reviewed automotive reference addresses it through an irreversible pyrotechnic hinge-release mechanism.

Starting from the analysis of the binding phenomenon developed in Chapter 3, and drawing inspiration from two technologies used outside conventional automotive hinge systems (aerospace HDRMs and TCAs adopted in fast electrical switching applications), this work proposes and develops the HDRM-TCA architecture: an electrically actuated release concept combining a cup-and-cone anti-binding interface with a short-duration electromagnetic force pulse.

The mechanical layout, presented in Chapter 4, and the electrical design developed in Chapter 5, were assessed through the numerical model of Chapter 6. Under nominal conditions, the model predicts a peak electromagnetic force of approximately 4.3 kN and reaches the prescribed 15 mm pin-release position within approximately 1–2 ms.

The sensitivity and degraded-electrical analyses also show that complete pin release is retained for the investigated parameter sets within the assumptions of the numerical model. The functional safety analysis of Chapter 7 identifies the main failure modes and the corresponding concept-level mitigation measures.

Overall, the results support the feasibility of an electrically actuated alternative operating on the same millisecond time scale as the pyrotechnic reference, without requiring an energetic pyrotechnic charge for actuation. The electromagnetic actuator itself is reusable; however, after a complete deployment, the sacrificial shear element must be replaced and the mechanism inspected and reset before returning to service.

9.2 Future Work

Future research and development should proceed in three main directions to advance the proposed architecture toward a detailed design and physical validation.

First, the preliminary structural checks outlined in Chapter 4 should be extended through detailed 3D FEM analysis of the base plate, the cup-and-cone interface and the sacrificial shear ring. These analyses should include the final geometry, material properties, contact conditions and representative structural load cases.

In parallel, a geometry-specific transient electromagnetic FEM analysis is also required to refine the coil design, the position-dependent force characteristic and the influence of the final winding and shielding geometry.

Second, the numerical results of Chapter 6 should be verified experimentally on a physical prototype of the HDRM-TCA module. The test should measure the discharge current, electromagnetic force and pin-release time under representative manufacturing tolerances, friction conditions and material behaviour.

Third, once a functional physical prototype is available, a Hardware-in-the-Loop test campaign, as anticipated in Chapter 7, should be carried out to assess the rollover-detection logic, diagnostics, trigger path and fault-handling strategy under representative electrical and thermal conditions. Particular attention should also be given to the unresolved single-point failure of the SCR trigger path identified in the same chapter.

The subsequent development phase should then extend the assessment to vehicle-level testing, including the complete hinge-release sequence and the door-ejection behavior under representative rollover conditions.

Appendix A

Target Book

The Target Book defines the quantitative engineering targets adopted for the gullwing-door system developed in this thesis. It translates the principal functional, ergonomic, structural, thermal, and safety requirements into measurable design criteria, providing a common reference framework for the subsequent design and assessment activities.

The document includes the main dimensional constraints, operating efforts, environmental conditions, structural limits, and safety-related targets considered during the development of the proposed door architecture.

The complete Target Book is reproduced on the following pages.

Gullwing Door - Target Book

N.	Attribute/Test cases	Metrics	PF Virtual validation/check [Y/N]	PF Physical validation [Y/N]	Test method	Test condition/Note	Limit	Target value	Status (VIRTUAL)	Status (PHYSICAL)
1 PACKAGING & ERGONOMICS										
1.1 Dimensions										
1.1.1	W103: Overall width excluding mirrors	[mm]	Y(CAD)	N	SAE J1100	Vehicle dimensions definition	Nom	Package protected (CAD)		
1.1.2	W144: Overall width including mirrors	[mm]	Y(CAD)	N	SAE J1100	Vehicle dimensions definition	Nom	Package protected (CAD)		
1.1.3	W145: Overall width mirrors folded	[mm]	Y(CAD)	N	SAE J1100	Vehicle dimensions definition	Nom	Package protected (CAD)		
1.1.4	H101: Vehicle height ready to drive	[mm]	Y(CAD)	N	SAE J1100	Baseline roof height	Nom	Package protected (CAD)		
1.1.5	Max vehicle height - Door open (Z-axis)	[mm]	Y(CAD)	N	Standard garage clearance	Standard garage clearance; must include gas strut over-travel/expansion at high temperatures	Max	2100 mm		
1.1.6	W120: Vehicle width, doors open	[mm]	Y(CAD)	N	SAE J1100	Max lateral distance between the widest point on the doors when the doors are in the max hold-open position	Max	≤ standard parking stall width		
1.1.7	A125: Door open angle	[deg]	Y(CAD)	N	SAE J1100	Angle of the door between its closed position and its max hold-open position, measured along the hinge axis	Max	Package protected (CAD)		
1.2 Roominess										
1.2.1	H-point to ground (SgRP) (H70)	[mm]	Y(CAD)	N	SAE J1100	Seating reference point	Nom	Ergonomically defined		
1.2.2	Max effective headroom front (H62-1)	[mm]	Y(CAD)	N	SAE J1100		Nom	Ergonomically defined		
1.2.3	95th percentile min head clearance lateral (W35)	[mm]	Y(CAD)	N	SAE J1100		Nom	Ergonomically defined		
1.2.4	95th percentile min head clearance vertical (H35)	[mm]	Y(CAD)	N	SAE J1100		Nom	Ergonomically defined		
1.2.5	H125-1: Door opening angle (Vertical)	[deg]	Y(CAD)	N	SAE J1100		Nom	Ergonomically defined		
1.3 Visibility										
1.3.1	A1-L: Pillar lateralization - front visibility	[deg]	Y(CAD)	N	SAE J1100		Nom	Package protected (CAD)		
1.3.2	A2-L: Front pillar obstruction	[deg]	Y(CAD)	N	SAE J1100		Nom	Package protected (CAD)		
1.4 Ingress/Egress										
1.4.1	Height of sill to ground (H130-1-M1)	[mm]	Y(CAD)	N	SAE J1100	Determines step-in difficulties	Nom	Package protected (CAD)		
1.4.2	Step over width (W18)	[mm]	Y(CAD)	N	SAE J1101	Determines how far the occupant must stretch their leg to clear the sill	Nom	Package protected (CAD)		
1.4.3	Entrance height RML H-Pt to upper trim	[mm]	Y(CAD)	N	SAE J1100			Package protected (CAD)		
1.4.4	Upper body opening height to ground (H50-1-M1)	[mm]	Y(CAD)	N	SAE J1100	Determines lateral head clearance during exit	Nom	Package protected (CAD)		
1.4.5	Lower door edge to ground - Door open	[mm]	Y(CAD)	N	SAE J1100	Head strike prevention. Ensures a 95th percentile adult can stand comfortably under the open door edge	Nom	> 95th percentile male height + clearance		
1.5 Packaging & ergonomics (SUBJECTIVE)										
1.5.1	Accessibility - Passenger compartment	Rate	NA	Y	9T0060EN	Defines the percentage of the population that can ingress/egress without severe ergonomic penalty	Min	0.95		
1.5.2	Visibility	Rate	NA	Y	9T0060EN	Front up/down, side, rear vision. Visibility night evaluation	Min	Specific project target		
1.5.3	Ergonomics while driving	Rate	NA	Y	9T0059EN	Overall seat comfort, roominess, pedal feeling, visibility and device visibility while driving	Min	Specific project target		
1.6 Reachability/Usability (SUBJECTIVE)										
1.6.1	Exterior devices	Rate	NA	Y	9T0060EN	Defines the percentage of the population that can ingress/egress without severe ergonomic penalty	Min	0.95		
1.6.2	Interior devices - Driver	Rate	NA	Y	9T0060EN	Defines the percentage of the population that can ingress/egress without severe ergonomic penalty	Min	0.95		
1.7 Reachability/Usability (OBJECTIVE)										
1.7.1	Operational effort load - Lift up	[N]	N	Y	9T0058EN	Ergonomic limit for unassisted manual lifting. Critical target because gas struts lose internal pressure in extreme cold (-40°C)	Max	30 N		
1.7.2	Operational effort load - Pull down	[N]	N	Y	9T0058EN	Ergonomic limit for reaching up and pulling the door closed from a seated position	Max	45 N		
1.7.3	Pull-down reachability (Z-axis)	[mm]	Y (CAD)	Y	OEM guidelines	Max reach distance from SgRP. Ensures a 5th percentile female can reach the handle from a seated position	Max	≤ max 5th percentile arm span from H-point		
1.7.4	Anti-pinch force	[N]	N	Y	FMVSS 118	If power-assisted: safety requirement for obstacle detection and auto-reverse	Max	100 N		
1.7.5	Actuation time (if power-assist engaged)	[s]	N	Y	EN 16005	If power-assisted: max time allowed for full automated opening/closing sequence	Max	4 s		

N.	Attribute/Test cases	Metrics	PF Virtual validation/check [Y/N]	PF Physical validation [Y/N]	Test method	Test condition/Note	Limit	Target value	Status (VIRTUAL)	Status (PHYSICAL)
1.7.6	Obstacle detection/Anti-collision (Z-axis)	Pass/Fail	N	Y	UN ECE R21	If power-assisted: detects overhead obstacles and stops actuation to prevent damage	Min	0 contact		
1.7.7	Emergency manual release effort	[N]	N	Y	UN/ECE R11 FMVSS 206	Max effort to manually unlatch the door from inside in case of total power loss	Max	Max ergonomic effort		
2 WEIGHT & CLEARANCE										
2.1 Vehicle mass impacts										
2.1.1	Base curb mass	[kg]	N	Y	9T0052EN		Max	Specific project mass book		
2.1.2	Centre of gravity height (Z-axis)	[mm]	Y(CAE)	Y	OEM guidelines	≤ target because the gullwing door raises the CG so it must be kept as low as possible	Max	Specific project mass book		
2.2 Macro system (component weights)										
2.2.1	Body structure + BIW + Closures	[kg]	Y	Y	9T0052EN	Program mass distribution target	Max	Specific project target		
2.2.2	Interior trim	[kg]	Y	Y	9T0052EN	Program mass distribution target	Max	Specific project target		
2.2.3	Door system mass	[kg]	Y (CAD/CAE)	Y	OEM guidelines	Mass of system to be recorded on calibrated scales. Directly affects required strut lifting force	Max	Specific project target		
2.2.3a	BIW door mass	[kg]	Y (CAD/CAE)	Y	OEM guidelines	Tracks the structural mass efficiency	Max	Specific project target		
2.2.3b	Glazing mass	[kg]	Y (CAD/CAE)	Y	OEM guidelines		Max	Specific project target		
2.2.4	Door hinge mass	[kg]	Y (CAD/CAE)	Y	OEM guidelines	Record hinge mass using calibrated scales. Hinges are at the highest point of the car, reducing this mass helps maintain a low CoG	Max	Specific project target		
2.2.5	Electrical (Actuators & sensors)	[kg]	N	N	OEM guidelines	Program mass distribution target	Max	Specific project target		
2.2.6	Gas strut/Actuator mass	[kg]	N	N	OEM guidelines	Tracks the weight penalty of the lifting mechanism required for the gullwing architecture	Max	Specific project target		
3 AERODYNAMICS & SEALING										
3.1	Aero load at V-max (permanent deformation)	[mm]	N	Y	OEM guidelines	Drive at V-max for 10 min + pre/post gap-flush inspection Ensures no bend of the door or hinges	Max	0 mm		
3.2	Seal lift-off (aero load)	[mm]	Y (CAE)	Y	OEM guidelines	Apply pressure load (0.0045 MPa if aero at 300 km/h not available)	Max	Seal tolerance		
3.3	Aero load at V-max (elastic deflection)	[mm]	N	Y	OEM guidelines	Drive at V-max for 10 min Max allowed temporary bowing of the door under aero suction at top speed	Max	Dynamic flushness tolerance		
3.4	Drag coefficient	[-]	Y (CFD)	Y	9T0087EN	Evaluation of drag penalty due to roof cutlines, gap and flushes with respect to ideal drag target. Physical test is conducted at a reference speed into the wind tunnel	Max	0.003		
4 THERMAL MANAGEMENT										
4.1 Door system										
4.1.1	Max usable temperature - door actuation	[°C]	N	Y	Solar soak requirement	Ensures actuator/struts function without binding or failure after extreme heat exposure	Max	85 °C		
4.1.2	Min usable temperature - door actuation	[°C]	N	Y	Cold climate chamber	Ensures actuators/struts have sufficient force to lift the door in extreme cold	Min	-40 °C		
4.1.3	Thermal exposure	[mm]	N	Y	Thermal cycling (-40°C to +85°C)	No visible distortion, crazing, cracking, dimensional changes.	Max	0 mm		
4.1.4	Sun simulation	[mm]	N	Y	9H0010EN	Test under artificial sunlight without UV, representing approximately the radiation during a summer day at the Equator (1050 W/m2), for a defined number of cycles alternating non-exposure and exposure.	Max	No deformations [mm] after a min of 12 h with the car in ambient conditions		
4.1.5	Thermal exposure (elastic displacement)	[mm]	Y (CAE)	Y	OEM guidelines	Apply regulated thermal cycles and then visual inspection CAE: displacement < target TEST: no visible distortion, crazing, cracking or dimensional changes	Max	Package clearance limit		
5 VEHICLE DYNAMICS										
5.1 Handling (SUBJECTIVE)										
5.1.1	Body roll behavior	Rate	N	N	SAE J1441 (slalom/lane change @80km/h)	Evaluates if the high-mounted door mass negatively impacts perceived roll stiffness	Min	8		
5.1.2	Roll centre height variation	Rate	N	N	OEM guidelines	The high mass of the gullwing hinges/struts must not cause the roll centre to migrate excessively under load	Max	0.05		
5.2 Handling (OBJECTIVE) - No objective evaluations considered										
6 NVH										
6.1 NVH (SUBJECTIVE)										

N.	Attribute/Test cases	Metrics	PF Virtual validation/check [Y/N]	PF Physical validation [Y/N]	Test method	Test condition/Note	Limit	Target value	Status (VIRTUAL)	Status (PHYSICAL)
6.1.1	Wind noise @ reference speed	Rate	N	Y	ISO 9921/ANSI S3.5	(@130 km/h) Ensures passengers can converse comfortably despite potential turbulence near the roof hinge seam	Min	0.75		
6.2 NVH (OBJECTIVE)										
6.2.1	Modal analysis	-	-	-	-	-	-	-	-	-
6.2.1.1	BIW torsion mode	[Hz]	Y	N	9T0022EN	Primary structural frequency; door design must not compromise this baseline target	Min	Specific project base target		
6.2.1.2	BIW bending mode	[Hz]	Y	N	9T0022EN	Primary structural frequency; door design must not compromise this baseline target	Min	Specific project base target		
6.2.1.3	Wind noise @ reference speed	[Sone]	N	Y	ISO 9921/ANSI S3.5	(@130 km/h) Ensures passengers can converse comfortably despite potential turbulence near the roof hinge seam	Min	0.75		
6.2.1.4	Door closing sound quality ("slam")-loudness	[Sone]	N	Y	ISO 532-1	(2.5 m/s closing velocity) Replaces subjective rating with objective acoustic energy measurements	Max	20 Sone		
6.2.1.5	Door closing sound quality ("slam")-sharpness	[Acum]	N	Y	DIN 45692	(2.5 m/s closing velocity) Limits high-frequency noises to ensure a premium, solid closing sound	Max	1.5		
6.2.1.6	Modal performance	[Hz]	Y	N	9T0022EN	The first natural frequency of the door system must be greater than or equal to the programmed target. For physical testing, an NVH assessor must deem the modal performance acceptable relative to the alignment chart	Min	Programmed target (first natural frequency of suspension system)		
6.2.1.7	Roof seam wind noise	[dB]	Y(CFD)	Y	OEM guidelines	Aero acoustic wind tunnel testing with internal microphones at driver/passenger ear level	Max	65 dB @130 km/h		
7 STRENGTH										
7.1 BIW (static strength)										
7.1.1	Torsional static stiffness	[kNm/deg]	Y	N	OEM guidelines	Primary structural baseline. The underbody must compensate for the lack of shear stiffness across the roof opening	Min	Specific project target		
7.1.2	Bending static stiffness	[kN/mm]	Y	N	OEM guidelines		Min	Specific project target		
7.2 Gullwing door structure & actuation										
7.2.1	Gullwing door buckling stiffness	[N/mm]	Y(CAE)	Y	OEM guidelines	Apply compressive load along the door profile; measure displacement and identify buckling point	Min	Target (no buckling under 400 N load)		
7.2.2	Roof flexural stiffness (snow load)	[N/mm]	Y(CAE)	N	9T0079EN	Evenly distribute previously evaluated sand bags over roof marked area. Leave the roof load for 15 min and record max deformation under load. Remove bags and record permanent deformation immediately after load removal and after 30min.	Max	1000 N/mm		
7.2.3	Gas strut/Actuator mounting stiffness	[N/mm]	Y(CAE)	N	OEM guidelines	Apply maximum extended/compressed strut force to the mounting bracket	Max	1000 N/mm		
7.2.4	Rollover/Roof crush strength	[SWR]	Y(CAE)	Y	FMVSS 216a	Roof must withstand 3x the vehicle's unloaded weight	Min	3 SWR		
7.2.5	Open overload (Z-axis upward load)	[mm]	N	Y	OEM guidelines	Apply 225N upward load at latch location; door rotation shall not exceed target and no permanent set shall appear	Max	0° plastic deformation		
7.2.6	Sag test	[mm]	N	Y	9T0068EN	Apply a 200 N load to the latch hook and maintain it for 10 s; remove the load and let the door settle for about 60 s. Repeat the procedure in 200 N increments up to 1000 N to measure vertical stiffness.	Max	Latch catch limit		
7.2.7	Torsional rigidity (latch torque)	[Nm]	Y	Y	OEM guidelines	±271 Nm torque at latch connected via pivot joint; door must withstand torque at latch with deflection below target at front and rear lower corners	Max	Seal tolerance		
7.2.8	Door gas strut abuse load	Pass/Fail	N	Y	OEM guidelines	Apply axial force while strut is locked out	Max	Permanent set at strut mount ≤ target		
7.2.9	Hinge separation loads	Pass/Fail	N	Y	UN /ECE R 11 FMVSS 206	Apply loads as specified by the regulations. Hinges must not separate under 11000 N longitudinal or 9000 N transverse loads.	Min	Hinges must not separate under 11000 N longitudinal, 9000 N vertical or 9000 N transverse loads		
7.2.10	Ultimate strength	[MPa]	Y (CAE)	N	UN /ECE R 11 FMVSS 207	±2g acceleration/brake; ±2g lateral; 4g bump Door must remain below target yield strength under peak vehicle loads	Max	Material yield strength		
7.2.11	Glass seal flange	[mm]	Y (CAE)	Y	OEM guidelines	100 N outboard Y load applied at ¼ ½ ¾ length of flange		Flange deflection must not exceed target		
7.2.12	Exterior handle mounting stiffness	[mm]	N	Y	OEM guidelines	180 N release load + 500 N abuse load tangent to control travel; Deflection < target under release load; no permanent set under abuse load	Max	Zero permanent set		
7.2.13	Trim mounting stiffness	[mm]	Y	Y	OEM guidelines	50 N normal load applied sequentially to points Each trim point must not exceed target displacement	Max	Zero permanent set		
7.2.14	Airbag mounting stiffness/strength	[mm]	N	Y	UN/ECE R95 FMVSS 214	100 N then 500 N upward Z-load at airbag points; 100 N load: disp < target; 500 N load: Von Mises stress < target	Max	Airbag supplier specification		
7.2.15	Seal flange stiffness	[mm]	Y	Y	OEM guidelines	80 N /100 mm distributed load on critical perimeters Meet deflection and permanent deformation targets under seal pressure	Max	Zero permanent set		
7.2.16	Pre-load limit	[N]	N	Y	OEM guidelines	Apply combined Z-Y load until skin is flush; limits the required force to make the skin flush prior to latching at 20°C	Max	Max closing operational effort		
7.2.17	Hinge friction	[Nm]	N	Y	OEM guidelines	Remove gas strut; open/close and record torque at hinges	Max	Max limit given by supplier		
7.2.18	Hinge friction (cold at -20°C)	[Nm]	N	Y	OEM guidelines	Remove gas strut; open/close and record torque at hinges after cold soak at -20°C. Lubricant stiffening check	Max	Max limit given by supplier		

N.	Attribute/Test cases	Metrics	PF Virtual validation/check [Y/N]	PF Physical validation [Y/N]	Test method	Test condition/Note	Limit	Target value	Status (VIRTUAL)	Status (PHYSICAL)
7.2.19	Hinge free play variability	[mm]	N	Y	OEM guidelines	Fix body leaf; move door leaf vertically/radially and record displacement Vertical and radial free play < target; no variability introduced	Max	Zero perceived play		
7.2.20	Handling load panel deflection	[mm]	Y (CAE)	Y	OEM guidelines	Panel modeled with shells; test replicates CAE deflection on 3 lowest points Panel deflection under worst-case handling loads must remain < target	Max	Clash clearance		
7.2.21	Wind gust resistance (open state)	Pass/Fail	Y (CAE)	Y	OEM guidelines	Door fully open. Expose to 80 km/h - 100 km/h lateral wind gust. Door must not close unexpectedly and hinges must not yield	Max	0 yield		
7.2.22	Abuse slam cycle	Pass/Fail	N	Y	9B3011EN	Determine the door opening necessary for 14 J slam energy with the spring attached from the door inner panel to the opposite side of the body. Slam the door to 25000 cycles (some cycles at room T, some at 70°C and some at -30°C)	-	No paint chipping and wear through the weatherstrip section		
7.2.23	Abuse check cycle	Pass/Fail	N	Y	OEM guidelines	Perform check events at 2.5 m/s and inspect the door	-	No paint chipping; door must not contact body during check up to 2.5 m/s		
7.3 Outer panel integrity										
7.3.2	Denting (resistance to dents)	[mm]	N	Y	9T0066EN	Incrementally load up to 80 N via a 1 inch steel half sphere contactor perpendicularly to surface under test and then slightly decrease the load back to zero	-	0 defects, deflections, cracks, distortions		
7.3.3	Oil canning (flexural stiffness)	[mm]	N	Y	9T0066EN	Incrementally load up to 156 N via a 75 mm wooden disk perpendicularly to surface under test and then slightly decrease the load back to zero	-	0 defects, deflections, cracks, distortions		
8 SOLIDITY - S&R;										
8.1 Static										
8.1.1	Gullwing door closing solidity impression	Rate	N	Y	9T0061EN	Subjective	Min	8 (1-10)		
8.1.2	Body leakage	[cm2]	N	Y	9T0020EN	Set the blower fan speed to index 10, switch on the blower unit, and increase the fan speed until the internal pressure gauge reaches the reference pressure of 1.5 mbar ± 0.05. Evaluate total body air leakage in [cm2].	Max	Specific project target		
8.2 Dynamic										
8.2.1	Solidity on 4-poster rig	Rate	N	Y	9T0061EN	S&R; evaluation along the CREST on 4-poster rig. To be performed at new and at steps of 25% of the durability test (performance decay evaluation)	Min	8 (1-10)		
8.2.2	Solidity on track	Rate	N	Y	9T0061EN	Straight drive 1st gear creeping mode on cobblestones	Min	8 (1-10)		
9 PASSIVE SAFETY										
9.1 Side impact										
9.1.1	Side impact FMVSS214 50th%ile pole	Pass/Fail	Y(CAE)	Y	FMVSS214	Full vehicle crash test per FMVSS 214 protocols		Pass (meet all dummy injury limits)		
9.1.2	Side impact FMVSS214 5th%ile pole	Pass/Fail	Y(CAE)	Y	FMVSS214	Full vehicle crash test per FMVSS 214 protocols		Pass (meet all dummy injury limits)		
9.1.3	Side impact FMVSS214 barrier	Pass/Fail	Y(CAE)	Y	FMVSS214	Full vehicle crash test per FMVSS 214 protocols		Pass (meet all dummy injury limits)		
9.1.4	Side impact Euro NCAP pole (UN R135)	Pass/Fail	Y(CAE)	Y	UN R135	Full vehicle crash test per Euro NCAP/UN R135 protocols at 32 km/h		Pass		
9.2 Rear impact										
9.2.1	Post-Rollover egress (misuse & abuse)	Pass/Fail	Y(CAE)	Y	FMVSS216	Invert vehicle; apply 500 N max effort to open, or trigger emergency release pyrotechnics		Doors must be openable without tools		
9.2.2	Body - roof crush (FMVSS216)	Pass/Fail	Y	N	FMVSS216					
10 DURABILITY & AGEING										
10.1 Closures durability										
10.1.1	Open/Close cycle durability (Small series)	Pass/Fail	N	Y	9T0065EN	25000 cycles, 14 J load over range of -40°C to 82°C	Min	25000 cycles		
10.1.2	Durability-vehicle level (CREST)	Pass/Fail	N	Y	9T0062EN	Follow durability standards, verify fastener torque pre/post		No squeaks/rattles after physical validation (CREST)		
11 SEALING TIGHTNESS										
11.1 Water tightness - Parking										
11.1.1	Heavy rain during parking with different gradient (40')	[L/min]	NA	Y	9T0051EN	Simulation of uphill/downhill (8.5°), side-angled parking (left/right, 7°), and twisted parking (front/rear left/right wheel up, 200 mm). Each test lasts 5 min and the water flow is 110-115 mm/min/m2.	Max	0 L/min		
11.2 Car wash										
11.2.1	Water test with high pressure jet spray	[L/min]	NA	Y	9T0051EN	130-150 bar @ 0.5 m distance. Guarantees commercial car wash jets will not penetrate the complex roof hinge seals	Max	0 L/min		

N.	Attribute/Test cases	Metrics	PF Virtual validation/check [Y/N]	PF Physical validation [Y/N]	Test method	Test condition/Note	Limit	Target value	Status (VIRTUAL)	Status (PHYSICAL)
11.2.2	Freezing resistance (car wash + freeze)	N	N	Y	OEM guidelines	(-20°C post-water sprays) Simulate car wash, freeze, perform open/close, measure efforts	Max	150 N		
11.3 Others										
11.3.1	Water run-off	[L]	N	Y	9T0051EN	Wait 10 s after the water flow stops, open the door, and check whether water seeps into the passenger compartment.	Max	0 L		
11.3.2	Water ingress resistance (roof hinge)	[L/min]	N	Y	OEM guidelines	Apply high-pressure water spray (80-100 bar) directly at roof-hinge seam for 3 minutes	Max	0 L/min		
11.3.3	Dust ingress resistance	[g]	N	Y	Arizona dust test protocol	Ensures the complex roof seals keep fine particulates out of the cabin and hinge mechanism	Max	0 g		
11.3.4	Snow/ice spilling prevention	Pass/Fail	N	Y	9T0079EN	Simulate 50 mm of snow/ice load on the roof. Perform kinematic opening.	Max	No snow/ice must slide into the cabin or onto seats		
12 HOMOLOGATION										
12.1 Body related homologation										
12.1.1	Door latches and hinges	Pass/Fail	Y	NA	UN reg. No 11 FMVSS Std No 206 (UN R11)	Both the latch and the roof hinges must be tested and certified as primary occupant retention devices	Min	Pass		
12.1.2	External projections	Pass/Fail	Y	NA	UN reg. No 26	Any exposed hinge mechanism or roof panel gaps must maintain a min radius of 2.5 mm to protect pedestrians	Min	2.5 mm		
12.1.3	Forward and side direct vision	Pass/Fail	Y	Y	ECE R125/FMVSS 111	The A-pillar and roof structure required to support the gullwing hinges must not obscure the driver's binocular vision targets	Min	Pass		
12.1.4	Flammability	Pass/Fail	N	Y	FMVSS 302	Burn rate B = 60 x (D/T)	Max	100 mm/min		
12.1.5	Ejection mitigation	Pass/Fail	N	Y	FMVSS 226 UN/ECE R11	A 100 mm impactor must not pass through the side window aperture during a rollover. Heavy roof hinges can warp frames during crashes, risking seal/glass failure	Max	100 mm		
13 MATERIAL & CORROSION										
13.1 Corrosion resistance										
13.1.1	Accelerated corrosion resistance (salt spray)	[mm]	N	Y	EN ISO 9227	Max allowed corrosion creep from a scribe line. Assesses the water drainage paths around the roof hinges	Max	2 mm		
13.1.2	Galvanic corrosion prevention	Pass/Fail	N	Y	EN ISO 9227	Joints between the steel hinges and Al/composite door panels must show zero degradation after accelerated environmental cycling	Max	0 visual		
13.2	Resistance to paint bake cycle	Pass/Fail	N	Y	OEM guidelines	Perform paint shop bake cycle and inspect coatings	Max	0 visual		
13.3	Environmental seal ageing (UV/Ozone)	Pass/Fail	N	Y	EN ISO 4892	Roof seals are exposed to direct, intense UV light. They must not crack, chalk, or lose compression set over the vehicle's lifespan	Min	Pass		
14 PERCEIVED QUALITY										
14.1	Static gap tolerance (roof & fenders)	[mm]	Y(CAD)	N	OEM guidelines	Dimensional control target. Ensures visual uniformity across the roof and A-pillar seams. Gaps wider than target risk wind noise; tighter gaps risk panel clashes	±0.5	3.5 mm		
14.2	Static flush tolerance (step)	[mm]	Y(CAD)	N	OEM guidelines	Ensures the door sits perfectly flush with adjacent panels. A positive flush (door sticking out) creates severe aero drag and wind noise	±1.0	0 mm		
14.3	Dynamic flush variation	[mm]	Y(CAD)	N	OEM guidelines	(@130 km/h) The aerodynamic lift over the roof tends to pull the gullwing door outward. Flushness must be maintained at speed to prevent sudden cabin noise.	Max	1.5 mm		
14.4	Kinematic smoothness (judder)	Pass/Fail	Y(CAD)	N	OEM guidelines	The door must rise and fall perfectly smoothly. Zero visual judder, stuttering, or "stick-slip" from the gas struts or hinges, which feels cheap to the customer	Max	0 visual		
14.5	Hardware concealment	Pass/Fail	Y(CAD)	N	OEM guidelines	When the door is fully raised, the gas struts, wiring harnesses, and inner hinges must be covered by premium trim. No exposed raw body-in-white or messy wiring	Min	Pass		
14.6	Class-A read-through	Pass/Fail	N	Y	OEM guidelines	NVH team assesses read-through under controlled lighting post-paint	Max	No objectionable read-through visible on Class-A surfaces		

Appendix B

Feasibility Checklist

The Feasibility Checklist provides a structured overview of the verification activities associated with the engineering targets defined in the Target Book. It relates the principal requirements to the corresponding assessment methods, including virtual design evaluations, CAD/CAE analyses, numerical simulations, and physical verification activities where applicable.

The checklist supports a systematic assessment of the proposed gullwing-door architecture and distinguishes between requirements addressed within the scope of this thesis and those requiring further experimental or vehicle-level validation.

The complete Feasibility Checklist is reproduced on the following pages.

Feasibility Checklist - Gullwing Door

Section / Component	Feasibility check	Applicable standard	Status	Justification (from FMEA)
PHASE 0				
Volume door	Compatibility with window movement check	FMVSS 118		Standard architectural packaging
	Belt-line height vs R-point check	SAE J1100-H25 SAE J826		Standard ergonomic packaging
	Side visibility and greenhouse geometry check	SAE J941		Proper side visibility and no blind spots
	Elbow and leg clearance vs inner door panel check			Proper elbow/leg clearance and no cramped feeling
	Roof hinge footprint and structural package check	ECE R11/FMVSS 206		Definition of the primary load-bearing node volume
	Footprint anti-intrusion bar check (min clearance 5 mm)	ECE R95/FMVSS 214		Standard safety packaging
	Min dimension mirror base check	ECE R46/FMVSS 111		Standard architectural packaging
	Belt-line flange dimension for window scraper			Standard architectural packaging
	Footprint window lift device front door check	FMVSS 118		Standard architectural packaging
	Door max length vs open door overall width and height	SAE J1100-W/H120-1		Standard ergonomic packaging
	Z-axis garage clearance check			Max vertical operational limit
	Y-Z swept volume and overswing clearance check			Full swing envelope including extreme overswing
	Head clearance during ingress/egress check	SAE J1052		Easy entry/exit and no contact with rising door
	Roof kinematics interference check			No interference with roof or hinge arms
	Roof hinge geometry and overhead clearance check			Enough opening clearance above the user
	Obstacle detection and standing zone trajectory mapping	ISO 26262		Obstacle detection and no closure when the user is standing in the door opening zone
PHASE 1				
PH0 CHECKS UPDATE				
Installation window lifts	Window regulator guide definition (helical trajectory)			Standard architectural packaging
	Kinematics vs exterior hard points			Standard architectural packaging
	Compatibility with mirror base and A pillar obstruction	ECE R46/FMVSS 111		Standard architectural packaging
	Window footprint vs front door body profile check			Standard architectural packaging
	Window descent vs rear door body profile check			Standard architectural packaging
	Window descent vs door lock check			Standard architectural packaging
	Window descent vs anti-intrusion bars check	ECE R95/FMVSS 214		Standard architectural packaging
	Clearance of window-guide sliders toward crossbeams and door frame (10 mm) check			Standard architectural packaging
	Window descent vs door handle check			Standard architectural packaging
	Window descent vs door latch check			Standard architectural packaging
	Carrier module disassemblability through door plane			Standard architectural packaging
	Anti-pinch device presence check (sistema antipizzicamento)	ECE R21/FMVSS 118		Standard architectural packaging
	Min distance (10 mm) between lower fixings (rails) and door body profile check			Standard architectural packaging
	Compatibility with safety-belt anchorage areas	ECE R14/FMVSS 210		Standard architectural packaging
	Compatibility with lamella bag			Standard architectural packaging

Section / Component	Feasibility check	Applicable standard	Status	Justification (from FMEA)
	Compatibility with window regulator volume			Standard architectural packaging
	Check with cut door cut line on A pillar section			Standard architectural packaging
	Check with cut door cut line on B pillar section			Standard architectural packaging
	Check with cut door cut line on roof section			Standard architectural packaging
	Check with cut door cut line on rocker section			Standard architectural packaging
	B-pillar constant-section drop for anti-pinch clearance	FMVSS 118		Standard architectural packaging
	Vertical down position vs belt line			Standard architectural packaging
	Compatibility with sealing solution			Standard architectural packaging
	Compatibility with key latch position			Standard architectural packaging
	Glass centre-of-gravity and mass compatibility	ECE R43/FMVSS 205		Standard architectural packaging
	Glass installation trajectory			Standard architectural packaging
	Correct push-force application point			Standard architectural packaging
	Min Y distance vs belt line sealing			Standard architectural packaging
	Window short-drop synchronization vs door unlatching time check			Standard architectural packaging
	Window-descent deviations for pinch prevention check			Standard architectural packaging
Molding	Draft angles external panel check			Standard platic/molding requirements
	Draft angles door structure check			Standard platic/molding requirements
	Molding OPT bezels seat check			Standard platic/molding requirements
	Molding handle compartment			Standard platic/molding requirements
Gas spring for wing door	Dead point calculation			Kinematic standards
	Close force calculation			Kinematic standards
	Wind load stability and hold-open check			Stable door position when fully open
	Actuator synchronization and stroke coordination check			Prevent asynchronous motion and twinsting loads on hinges
	Hold-open force check at extreme temperatures (-30°C to +80°C)	ISO 16750-4		Account for fluid viscosity changes that could make the door drop or difficult to open
	Overall door-assembly CoG trajectory vs. gas-strut force-curve mapping			
	End-stops limit and actuator torque/overheating check			Reliable end-stops preventing high load on actuators
	Gas strut/actuator dynamic clearance check			Acceptable opening/closing efforts
Installation components	Installation hinges, fixings accessibility (screwdrivers)			Standard architectural packaging
	Installation door lock and fixing accessibility (screwdrivers)			Standard architectural packaging
	Door lock 90° orientation vs door rotation			Standard architectural packaging
	Striker installation (footprint screwdrivers)			Standard architectural packaging
	Courtesy-light installation installation on chassis			Standard architectural packaging
	Passage for lamp maintenance door body profile check			Standard architectural packaging
	Installation conduit for electric functions			Standard architectural packaging
	Height anti-intrusion bar vs lateral barrier check	ECE R95/FMVSS 214		Standard architectural packaging
	Ground height check and bezels check vs overall width			Standard architectural packaging
	Hi-Fi speaker installation			Standard architectural packaging
	Compatibility with kick plate and side skirts			Standard architectural packaging

Section / Component	Feasibility check	Applicable standard	Status	Justification (from FMEA)
	Antitheft protection bracket installation			Standard architectural packaging
	Compatibility with electrical lay out accessibility			Standard architectural packaging
	Lamella bag fixing point definition			Standard architectural packaging
	Fixing definition for inner door trim panel installation			Standard architectural packaging
	Exterior door frame bezel installation on B-pillar			Standard architectural packaging
	Rollover emergency release system packaging	ECE R11/FMVSS 216a		Rescue access
	Roof hinge harness routing, connection, calibration check			Correct routing of wiring through the roof hinge area
	Obstacle detection sensor positioning check	ISO 26262		Obstacle detection and automatic stop
Coupling with interface elements	Compatibility body side			Standard interface checks
	Compatibility with front fender			Standard interface checks
	Compatibility with rear fender			Standard interface checks
	Compatibility with headliner			Standard interface checks
	Compatibility with side skirt and longitudinal beam (longitudinal beam)			Standard interface checks
	Compatibility with OPT bezels mounting			Standard interface checks
	Compatibility with seal sections			Standard interface checks
Profile P-P1 points	Definition of minimum sections for spot-welding tool access			Standard structural and aesthetic checks
	Dimension vs ergonomic constraints check			Standard structural and aesthetic checks
	Window plane constancy for frameless windows check			Standard structural and aesthetic checks
	Door profiles stamping angle vs exterior split lines check			Standard structural and aesthetic checks
	Compatibility with structure elements			Standard structural and aesthetic checks
	Definition of beat track on orthogonal door structure P-P1			Standard structural and aesthetic checks
	Aesthetic care with style of the profile P-P1 check			Standard structural and aesthetic checks
Handle	Ergonomic finger clearance for handle operation with gloves	SAE J833		Standard operational checks
	Ergonomic ground clearance			Standard operational checks
	Position door latch vs door handle and lock check	ECE R11/FMVSS 206		Standard operational checks
	Footprint switch for window drop down system check			Standard operational checks
	Position and accessibility fixings (screwdriver) check			Standard operational checks
	Footprint handle vs window and moving door check			Standard operational checks
	Opening force calculation			Standard operational checks
	Vane rotation with respect to external panel check			Standard operational checks
	Inner handle reachability at max open angle (5th %ile female/95th %ile male)	SAE J826/SAE J833		Proper door handle
Seals	Minimum radii on profile P-P1 check	ECE R26		Standard sealing perimeter checks
	Nodes co-molding dimension check			Standard sealing perimeter checks
	External and internal window-scraper dimension check			Standard sealing perimeter checks
	Side mirror triangle seal selection check			Standard sealing perimeter checks
	Approach angle compression			Standard sealing perimeter checks
	External belt sealing section			Standard sealing perimeter checks
	A-B flange sealing section			Standard sealing perimeter checks

Section / Component	Feasibility check	Applicable standard	Status	Justification (from FMEA)
	Anti-rustle door-seal presence			Standard sealing perimeter checks
	Compatibility with typical sections			Standard sealing perimeter checks
	External mirror base and door upper profile presence			Standard sealing perimeter checks
	Door low dust protection seals presence	ISO 20653		Standard sealing perimeter checks
	External and internal door belt-line seal presence			Standard sealing perimeter checks
	Installation dust cover seal check			Standard sealing perimeter checks
	Water dumping DMU assessment (upward opening)			Prevent water dumping inside the cabin
	Roof drip gutter continuity and drainage check			Proper water drainage flow
	Door-roof interface aero seal lift-off check			Prevent wind noise at the door-roof interface
	Long travel seal wear and friction check			Prevent seal wear from long-travel rotation
Installation mirror	Position of the fixings side mirror base on side mirror triangle check			Standard external component packaging
	Space for electrical-cable routing check			Standard external component packaging
	Painting division mirror base check			Standard external component packaging
PHASE 2				
PH1 CHECKS UPDATE				
Hemming	Min radii and paths for hemming			Standard sheet metal joining and aesthetic finishing constraints
	Chaulking angles and main flange hemming check			Standard sheet metal joining and aesthetic finishing constraints
	Min radii and corner edges finishing (rat holes)			Standard sheet metal joining and aesthetic finishing constraints
Internal reinforcements	Roof-mounted hinge reinforcements and center spine/T-bar stiffness check	FMVSS 216a		Roof fixing points must resist high concentrated load to prevent deformations
	Definition lock reinforcements	ECE R11/FMVSS 206		Standard structural and packaging checks
	Beltline exterior beam definition	ECE R95/FMVSS 214		Standard structural and packaging checks
	Compatibility with inner reinforcements assembly and welding			Standard structural and packaging checks
	Inner structure antiintrusion bar line reinforcements definition	ECE R95/FMVSS 214		Standard structural and packaging checks
	Compatibility with lamella bag and fixing accessibility	FMVSS 226/ECE R135		Standard structural and packaging checks
	Mirror installation reinforcements	ECE R46/ECE R26		Standard structural and packaging checks
	Coupling between reinforcements of different materials check			Standard structural and packaging checks (crucial for galvanic corrosion)
	Gas strut mounting hardpoint reinforcement definition			Needed to balance door mass
	Large panel deflection and torsional rigidity check			No sagging or twisting over time
Chassis structure	Moments of inertia on main sections check			Standard structural calculations, manufacturing, packaging checks
	3D door structure definition with radii			Standard structural calculations, manufacturing, packaging checks
	Spot-welding tool access for welded reinforcements check			Standard structural calculations, manufacturing, packaging checks
	Mounting sequence of the components check			Standard structural calculations, manufacturing, packaging checks
	Water shelter membrane compatibility check			Standard structural calculations, manufacturing, packaging checks
	Holes 3D definition following weight and structure CAE analysis			Standard structural calculations, manufacturing, packaging checks
	Roof water drainage paths and pooling check			Standard structural calculations, manufacturing, packaging checks
	Compatibility with B.I.W. A-B flange			Standard structural calculations, manufacturing, packaging checks

Section / Component	Feasibility check	Applicable standard	Status	Justification (from FMEA)
	Compatibility with dropping guides			Standard structural calculations, manufacturing, packaging checks
	Compatibility with rear reflector	ECE R3/FMVSS 108		Standard structural calculations, manufacturing, packaging checks
	Compatibility with step light			Standard structural calculations, manufacturing, packaging checks
	Compatibility with rocker trim section			Standard structural calculations, manufacturing, packaging checks
	Compatibility with double sealing			Standard structural calculations, manufacturing, packaging checks
	Spaces for installation lateral defrosting vents check	ECE R122/FMVSS 103		Standard structural calculations, manufacturing, packaging checks
	Roof node concentrated load and fatigue check (CAE)			No fatigue failure
	Hinge-roof joint crash integrity check (CAE)	ECE R11/FMVSS 206		No joint detachment during impact
	Post crash rescue/rollover jamming check (CAE)	ECE R94/ECE R95 ISO 17840		Post crash rescue
External protrusions	Minimum radii external protrusions check	ECE R26		Standard pedestrian safety and manufacturing tolerance checks
	Edges correction for coupling tolerances			Standard pedestrian safety and manufacturing tolerance checks
Door rods	Definition of door rod with multi-point latch synchronization check	ECE R11/FMVSS 206		Keep correct preload
	Definition of door rod between lock and door latch	ECE R11/FMVSS 206		Standard mechanism linkages

Bibliography

[1] RM Sotheby's. *Everything You Need to Know about the Mercedes-Benz 300 SL Gullwing*. 2024. URL: https://www.sothebys.com/en/articles/everything-you-need-to-know-about-the-mercedes-benz-300-sl-gullwing-1 (cit. on p. 15).

[2] Sagar Kapgate and A. R. Pawar. «Design and Analysis of an EV Skateboard Chassis with Integrated Battery System». In: *International Journal for Multidisciplinary Research (IJFMR)* 8.3 (2026), pp. 1–11. ISSN: 2582-2160. URL: https://www.ijfmr.com/papers/2026/3/78759.pdf (cit. on p. 16).

[3] National Highway Traffic Safety Administration. *Traffic Safety Facts: Passenger Vehicles – 2023 Data*. Tech. rep. DOT HS 813 723. U.S. Department of Transportation, May 2025. URL: https://crashstats.nhtsa.dot.gov/Api/Public/ViewPublication/813723.pdf (cit. on p. 17).

[4] Mercedes-Benz. *Rescue Information: Mercedes-AMG SLS Coupé*. Rescue documentation for emergency services. Mercedes-Benz AG. URL: https://rk.mb-qr.com/ (visited on 09/14/2026) (cit. on pp. 17, 28, 31–33).

[5] Autoliv Inc. *Product Sheets: Pin Pusher, Pin Puller*. 2025. URL: https://www.autoliv.com/sites/autoliv/files/2025-01/Product%20sheets%20pin%20pusher%20pin%20puller_2.pdf (cit. on pp. 17, 31, 32, 63).

[6] SAE International. *Motor vehicle dimensions*. 2009. URL: https://www.sae.org/standards/j1100_200911-motor-vehicle-dimensions (cit. on p. 23).

[7] SAE International. *Devices for Use in Defining and Measuring Vehicle Seating Accommodation*. 2021. URL: https://www.sae.org/standards/j826-devices-use-defining-measuring-vehicle-seating-accommodation (cit. on p. 23).

[8] 49 CFR Part 571. *Standard No. 216; Roof crush resistance*. 2025. URL: https://www.federalregister.gov/documents/2025/05/30/2025-09744/federal-motor-vehicle-safety-standard-no-216-roof-crush-resistance-federal-motor-vehicle-safety (cit. on pp. 23, 26).

[9] UNECE. *Regulation No 95 of the Economic Commission for Europe of the United Nations (UNECE) — Uniform provisions concerning the approval of vehicles with regard to the protection of the occupants in the event of a lateral collision [2015/1093]*. 2015. URL: https://eur-lex.europa.eu/eli/reg/2015/95/oj (cit. on p. 24).

[10] 49 CFR 571.214. *Standard No. 214; Side impact protection*. 2026. URL: https://www.ecfr.gov/current/title-49/subtitle-B/chapter-V/part-571/subpart-B/section-571.214 (cit. on pp. 24, 26).

[11] James George Gobart, William L. Gobart, and Edward Aloysius Jedrzejczak. «Bi-fold Gull Wing Vehicle Door». 5992918. Nov. 1999 (cit. on p. 25).

[12] Kopp, Moritz. *Tesla Model X Gullwing Doors: All the Pros and Cons*. 2023. URL: https://teslabs.de/en/blogs/tesla-must-know/tesla-model-x-wing-doors-pros-disadvantages (cit. on pp. 25, 27).

[13] Cenizo, Sebastian. *Pagani Huayra Carbon Edition (2012)*. 2012. URL: https://carbuzz.com/cars/pagani/huayra/2012/ (cit. on p. 25).

[14] Amanda Jacob. «Built in Italy: the Lamborghini Avendator». In: *Reinforced Plastics* 57.5 (2013), pp. 29–31. DOI: 10.1016/S0034-3617(13)70153-X (cit. on p. 25).

[15] Baumann, Karl-Heinz. *Roof structure of a body of a motor vehicle*. 2009. URL: https://patents.google.com/patent/WO2009077065A1/en (cit. on pp. 25, 27).

[16] Stabilus. *Gas springs and dampers, Solutions for industrial applications*. 2023. URL: https://www.stabilus.com/media/default/STABILUS/PDF/Stabilus_Gas_Springs_Dampers_Brochure_EN_2023.pdf (cit. on pp. 26, 50).

[17] Tahaney, Ed. *2018 Pininfarina HK GT Concept Bows in Geneva*. 2018. URL: https://www.motortrend.com/news/2018-pininfarina-hk-gt-concept-bows-in-geneva (cit. on p. 26).

[18] Evans, Nigel. *The SLS AMG's Exploding Hinges Made gullwing Door Safe For The Modern Era*. 2025. URL: https://carbuzz.com/how-mercedes-amg-made-modern-gullwing-doors-safe/ (cit. on p. 28).

[19] Seung-Gyo Jang, Hyo-Nam Lee, and Jong-Yun Oh. «Performance Modeling of a Pyrotechnically Actuated Pin Puller». In: *International Journal of Aeronautical and Space Sciences* 15.1 (2014), pp. 102–111. DOI: 10.5139/IJASS.2014.15.1.102 (cit. on p. 31).

[20] Dangerous goods advisor. *Safety devices electrically initiated*. 2026. URL: https://www.gmspomsds.com/viewdocument.aspx?gdk=MTA2NDM1fDQwMnw (cit. on p. 33).

[21] Glenair, Inc. *Hold Down and Release Mechanism*. 2025. URL: https://www.glenair.com/space-mechanisms/hold-down-release-mechanisms/pdf/technology-overview.pdf (cit. on p. 33).

[22] Juho Lee and Jae-Hung Han. «Separation and Release Devices for Aeronautical and Astronautical Systems: A Review». In: *International Journal of Aeronautical and Space Sciences* 26.1 (2025), pp. 131–161. DOI: 10.1007/s42405-024-00802-9 (cit. on p. 33).

[23] ARQUIMEA. *HDRM: Hold Down & Release Mechanisms*. URL: https://www.arquimea.com/products/space-release-mechanisms-hdrm-react/ (cit. on p. 34).

[24] Alizee Malavart, Mark Ferris, and Nigel Philips. «A Novel Hold Down and Release Mechanism Using Hook and Loop Technology for Small Deployable Arrays». In: *Proceedings of the 17th European Space Mechanisms and Tribology Symposium (ESMATS)*. Hatfield, United Kingdom, Sept. 2017 (cit. on p. 34).

[25] M. Al-Dweikat, J. Cui, S. Sun, M. Yang, G. Zhang, and Y. Geng. «A Review on Thomson Coil Actuators in Fast Mechanical Switching». In: *Actuators* 11.6 (2022), p. 154. DOI: 10.3390/act11060154 (cit. on pp. 34, 35, 53, 54, 57, 65).

[26] Min-Seob Sim, Syed Sabir Hussain Bukhari, and Jong-Suk Ro. «Analysis and Design of a Thomson Coil Actuator System for an HVDC Circuit Breaker». In: *IEEE Access* 10 (2022), pp. 58354–58359. DOI: 10.1109/ACCESS.2022.3178724 (cit. on p. 34).

[27] ASM Aerospace Specification Metals Inc. *Aluminium 7075-T6, 7075-T651*. 2023. URL: https://www.aerospacemetals.com/wp-content/uploads/2023/06/Aluminum-7075-T6-7075-T651.pdf (cit. on pp. 42, 47, 48).

[28] Cecil H. Lewis. «Gooseneck Hinge for Vehicle Deck Lid». 5419012. Assignee: Midway Products Group, Inc., Monroe, MI. May 1995 (cit. on p. 43).

[29] Walter D. Pilkey, Deborah F. Pilkey, and Zhuming Bi. *Peterson's Stress Concentration Factors*. John Wiley & Sons, 2019 (cit. on p. 44).

[30] Allegheny Technologies Incorporated. *ATI 17-4 Technical Data Sheet*. 2014. URL: https://www.atimaterials.com/Products/Documents/datasheets/stainless-specialty-steel/precipitationhardening/ati_17-4_tds_en_v2.pdf (cit. on pp. 45, 47, 48).

[31] Richard G. Budynas and J. Keith Nisbett. *Shigley's Mechanical Engineering Design*. McGraw-Hill Education, 2015 (cit. on p. 46).

[32] Hydro Extrusions. *EN AW-6060: Technical Datasheet*. 2019. URL: https://www.hydro.com/globalassets/08-about-hydro/hydro-worldwide/france/puget/2025_en-aw-6060-t66--ce-v4-6.pdf (cit. on p. 47).

[33] *Technical Data Sheet: uD3PP-6 (Doc. D3-1-13)*. Data Sheet. Deployables Cubed GmbH. 2022. URL: https://www.cubesatshop.com/wp-content/uploads/2022/12/D3-1-13-TDS-DataSheet_uD3PP-6.pdf (cit. on p. 48).

[34] Ganter Norm. *DIN 71802 Angled Ball Joints*. 2023. URL: https://live-katalog.ganternorm.com/pdf/ganter/EN/71802.pdf (cit. on p. 50).

[35] Dong-Kuk Lim, Dong-Kyun Woo, Il-Woo Kim, Dong-Kyu Shin, Jong-Suk Ro, Tae-Kyung Chung, and Hyun-Kyo Jung. «Characteristic Analysis and Design of a Thomson Coil Actuator Using an Analytic Method and a Numerical Method». In: (2013). DOI: 10.1109/TMAG.2013.2272561 (cit. on p. 54).

[36] Ara Bissal, Jesper Magnusson, Ener Salinas, Göran Engdahl, and Anders Eriksson. «On the Design of Ultra-Fast Electromechanical Actuators: A Comprehensive Multi-Physical Simulation Model». In: (2012). DOI: 10.1109/ICEF.2012.6310320 (cit. on p. 54).

[37] D. S. Vilchis-Rodriguez, R. Shuttleworth, and M. Barnes. «Double-sided Thomson Coil Based Actuator: Finite Element Design and Performance Analysis». In: (2016). DOI: 10.1049/cp.2016.0201 (cit. on p. 54).

[38] TDK Electronics AG. *Aluminum Electrolytic Capacitors*. 2019. URL: https://www.tdk-electronics.tdk.com/inf/20/30/db/aec/B43705_B43725.pdf (cit. on pp. 55, 56).

[39] ISO. *Road vehicles – Functional safety*. 2018. URL: https://cdn.standards.iteh.ai/samples/68383/4e26ddadc54a4198bed652afe2969fa/ISO-26262-1-2018.pdf (cit. on pp. 56, 77).

[40] Littelfuse, Inc., Integrated Circuits Division. *MOSFET/IGBT Drivers: Theory and Applications*. URL: https://www.littelfuse.com/assetdocs/littelfuse-mosfetigbt-drivers-theory-and-applications-application-note?assetguid=bfc6331c-8a66-4e0c-82e8-ee191cef27c5 (cit. on p. 57).

[41] Ned Mohan, Tore M. Undeland, and William P. Robbins. *Power Electronics: Converters, Applications, and Design*. John Wiley & Sons, 2003 (cit. on p. 57).

[42] Infineon Technologies AG. *Data sheet T1500N*. URL: https://asenergi.com/pdf/semi/IFT/T1500N.pdf (cit. on p. 57).

[43] H.A. Wheeler. «Simple Inductance Formulas for Radio Coils». In: *Proceedings of the Institute of Radio Engineers* 16.10 (1928), pp. 1398–1400 (cit. on p. 57).

[44] Herbert Bristol Dwight. «Skin effect and proximity effect in tubular conductors». In: *Journal of the American Institute of Electrical Engineers* 41.3 (1922), pp. 203–209 (cit. on p. 58).

[45] ISO. *Low-voltage electrical installations – Part 4-43: Protection for safety – Protection against overcurrent*. 2023. URL: https://cdn.standards.iteh.ai/samples/23683/86789a8844914f84861c12928d57bdc3/IEC-60364-4-43-2023.pdf (cit. on p. 59).

[46] International Electrotechnical Commission. *IEC 60228:2023 – Conductors of insulated cables*. IEC. 2023. URL: https://webstore.iec.ch/en/publication/71891 (cit. on p. 59).

[47] ISO. *Road vehicles — Automotive cables*. 2019. URL: https://cdn.standards.iteh.ai/samples/66307/d23b2cdfe1e94d3882b5649c745c771f/ISO-19642-9-2019.pdf (cit. on p. 59).

[48] IEEE SA. *IEEE Standard Method for Measuring the Effectiveness of Electromagnetic Shielding Enclosures*. 2006. URL: https://standards.ieee.org/ieee/299/3090/ (cit. on p. 59).

[49] Marek Bajtos, Roman Radil, Ladislav Janoušek, and Nhat Dang. «Numerical Simulations of Static Magnetic Fields with Mu-metal Cage Shielding». In: *2023 24th International Conference on Computational Problems of Electrical Engineering (CPEE)*. 2023, pp. 1–4 (cit. on p. 59).

[50] C. Peng, I. Husain, A. Q. Huang, B. Lequesne, and R. Briggs. «A Fast Mechanical Switch for Medium-Voltage Hybrid DC and AC Circuit Breakers». In: *IEEE Transactions on Industry Applications* 52.4 (2016), pp. 2911–2918 (cit. on p. 67).

[51] B. Lequesne, T. Holp, S. C. Schmalz, R. M. Slepian, and H. Wang. «Frequency-Domain Analysis and Design of Thomson-Coil Actuators». In: *IEEE Transactions on Industry Applications* 59.2 (2023), pp. 1765–1774 (cit. on p. 67).

[52] Leandro Vargas-Meléndez, Beatriz L. Boada, María Jesús L. Boada, Antonio Gauchía, and Vicente Díaz. «A Sensor Fusion Method Based on an Integrated Neural Network and Kalman Filter for Vehicle Roll Angle Estimation». In: 16.9 (2016), p. 1400. DOI: 10.3390/s16091400 (cit. on p. 78).

[53] ISO. *Electrically propelled road vehicles — Safety specifications — Part 3: Electrical safety*. 2021. URL: https://www.iso.org/standard/81746.html (cit. on p. 83).

[54] International Organization for Standardization. *ISO 6469-4:2015 – Electrically propelled road vehicles – Safety specifications – Part 4: Post crash electrical safety*. ISO. 2015. URL: https://www.iso.org/standard/60584.html (cit. on p. 83).

[55] VLN Sport GmbH & Co. KG. *SLS AMG GT3 meets stringent safety standards*. 2011. URL: https://www.nuerburgring-langstrecken-serie.de/language/en/2011/03/30/sls-amg-gt3-meets-stringent-safety-standards/ (cit. on p. 83).

[56] FIA. *Safety Cages for Cars of Group N, A (and Extensions) and R-GT*. 2020. URL: https://api.fia.com/sites/default/files/253_2020_chap_8_wmsc_2020.10.09.pdf (cit. on p. 83).